Published for SISSA by Springer

Received: June 28, 2022
Accepted: October 17, 2022
Published: October 28, 2022

Dijet photoproduction at low x at next-to-leading order and its back-to-back limit

Pieter Taels,[a,b] **Tolga Altinoluk,**[c] **Guillaume Beuf**[c] **and Cyrille Marquet**[a]

[a] *Centre de Physique Théorique, École polytechnique, CNRS, I.P. Paris, F-91128 Palaiseau, France*

[b] *Departement fysica, Universiteit Antwerpen, Groenenborgerlaan 171, 2020 Antwerpen, Belgium*

[c] *Theoretical Physics Division, National Centre for Nuclear Research, Pasteura 7, Warsaw 02-093, Poland*

E-mail: pieter.taels@uantwerpen.be, tolga.altinoluk@ncbj.gov.pl, guillaume.beuf@ncbj.gov.pl, cyrille.marquet@polytechnique.edu

Abstract: We compute the cross section for the inclusive photoproduction of a pair of jets at next-to-leading order accuracy in the Color Glass Condensate (CGC) effective theory. The aim is to study the back-to-back limit, to investigate whether transverse momentum dependent (TMD) factorization can be recovered at this perturbative order. In particular, we focus on large Sudakov double logarithms, which are dominant terms in the TMD evolution kernel. Interestingly, the kinematical improvement of the low-x resummation scheme turns out to play a crucial role in our analysis.

Keywords: Deep Inelastic Scattering or Small-x Physics, Effective Field Theories of QCD, Higher-Order Perturbative Calculations, Resummation

ArXiv ePrint: 2204.11650

https://doi.org/10.1007/JHEP10(2022)184

JHEP10(2022)184

Contents

JHEP10(2022)184

1 Introduction

A key factor in the success of perturbative Quantum Chromodynamics (pQCD) is the resummation of large logarithms that would otherwise spoil the perturbative expansion. Generally speaking, such logarithms are sensitive to the available phase space for gluon radiation. In one of the most common approaches, known as collinear factorization, the cross section is, up to power corrections, written as a convolution of perturbative hard parts and nonperturbative parton distribution functions (PDFs), and large logarithms in $\ln(\mu^2/\Lambda^2_{\rm QCD})$ are absorbed into the latter with the help of the Dokshitzer-Gribov-Lipatov-Altarelli-Parisi (DGLAP) [1–3] evolution equations. A hard scale μ^2 is required to be present in a particle collision for pQCD to be applicable, and is typically provided by the photon virtuality in deep-inelastic scattering (DIS) or by the mass of the produced boson in proton-proton collisions.

In collinear factorization, it is tacitly assumed that the center-of-mass energy $\sqrt{s}$ is of the same order as the hard scale. At very high energies, or equivalently very small parton longitudinal momentum fractions x, this approximation breaks down, and large 'rapidity' logarithms in $\ln(s/\mu^2) \sim \ln(1/x)$ become equally or even more important than the collinear ones. Their resummation is often performed using the Balitsky-Fadin-Kuraev-Lipatov (BFKL) evolution equations [4, 5], which are embedded in another factorization framework known as k_T- or High-Energy Factorization (HEF) [6–8]. BFKL predicts a steep rise of the unintegrated or k_T-dependent gluon density which eventually violates unitarity [9]. However, below a dynamically generated saturation scale $Q_s(x)$, nonlinear gluon recombination effects will counteract this unphysical exponential growth [10]. At this point, High-Energy Factorization needs to be generalized to include nonlinear low-x evolution. This is done by the Color Glass Condensate (CGC) effective theory [11–21] employed in this paper. In the CGC, the highly dense gluon distribution is treated as a large semiclassical field sharply localized on the light cone (a 'shockwave'), whose rapidity evolution of the gluon distribution is governed by the Balitsky-Kovchegov/Jalilian-Marian-Iancu-McLerran-Weigert-Leonidov-Kovner (BK-JIMWLK) evolution equations [14–25], which can be regarded as a nonlinear generalization of BFKL.

Another situation where collinear factorization breaks down is when the process is sensitive to a second scale μ_b^2 that is much smaller than the hard scale: $\mu^2 \gg \mu_b^2 \gtrsim \Lambda^2_{\rm QCD}$. Large 'Sudakov' logarithms $\ln(\mu^2/\mu_b^2)$ [26] need to be resummed in addition to the collinear ones through the Collins-Soper-Sterman (CSS) evolution equations [27, 28] and can be absorbed [29, 30] into the parton distributions, which need to be extended to transverse momentum dependent parton distributions functions (TMD PDFs [31]). Classic examples are Z-boson hadroproduction (Drell-Yan) or semi-inclusive deep-inelastic scattering (SIDIS [32]) at low transverse momenta, where the large scale is provided by the boson mass or the photon virtuality, and the small scale by the transverse momentum of the produced boson or hadron.

In kinematics with a hierarchy of scales $s \gg \mu^2 \gg \mu_b^2 \gtrsim \Lambda^2_{\rm QCD}$, the necessity arises to simultaneously treat large $\ln(s/\mu^2)$ and $\ln(\mu^2/\mu_b^2)$ logarithms. Such a combined low-x and Sudakov resummation is the subject of intensive research, some of which very recent, either

JHEP10(2022)184

based on the HEF approach [33–43], BFKL [44, 45], BK [46], the CGC [47–52], and TMD factorization [53–55].

We should stress, however, that TMD factorization goes beyond Sudakov resummation. Indeed, gluon (and quark) TMD PDFs depend on the underlying hard process through the gauge links or Wilson lines in their operator definition [56]. Moreover, they parameterize the dependence on not only the transverse momentum, but also the spin of the partons inside the proton or nucleus. The unintegrated gluon distribution in the HEF and BFKL frameworks, on the other hand, does not contain this Wilson-line dependence and, because of the particular 'nonsense' polarization tensor used, always encodes maximally linearly polarized gluons [57, 58]. The HEF and BFKL frameworks are, therefore, only applicable at large transverse momenta $k_T \sim \mu_b \sim \mu$, since for $k_T \ll \mu$ the unintegrated gluon distribution cannot be matched to the full structure of the TMD PDFs.

It turns out that the CGC not only generalizes BFKL, but at leading order (LO) in perturbation theory also encompasses TMD factorization. Therefore, one might hope that the CGC provides a unified framework for both TMD factorization and (non)linear low-x evolution. Even at leading order this is not trivial, because a generic CGC cross section involves a complicated intertwining of perturbative coefficients with nonperturbative correlators of semiclassical fields. In the seminal papers [59, 60] it was demonstrated that, for a large class of $2 \to 2$ processes, the CGC and TMD LO calculations do result in the same cross sections, given a proper identification of the correlators of semiclassical gluon fields and gluon TMD PDFs [56, 61, 62]. This triggered a series of studies, demonstrating the sensitivity to the linearly polarized gluon TMD PDF when masses are included [57, 63, 64], applying JIMWLK evolution to gluon TMDs [65–67], and extending the CGC-TMD correspondence to $2 \to 3$ processes [68–70]. In parallel, the so-called small-x improved transverse momentum dependent (ITMD) factorization framework [71, 72] was developed to extend the applicability region of low-x TMD factorization to $\mu_b \sim \mu$ by resumming the kinematic twist corrections in powers of μ_b/μ, using off-shell matrix elements as in HEF factorization [7, 34]. Including, on top of this, the genuine saturation corrections in the ratio of Q_s/μ, eventually the results from the full CGG are recovered [58, 73–77].

The aim of this paper is twofold. First, we contribute to the effort to bring CGC calculations to higher perturbative accuracy by calculating the full NLO cross section of inclusive dijet photoproduction, i.e. the process $\gamma + A \to \text{dijet} + X$, using light-cone perturbation theory (LCPT) [78–80]. This process could be measured at low photon virtualities in the future Electron-Ion Collider [81], the proposed LHeC [82], or in ultraperipheral lead-proton collisions at the LHC. Moreover, our calculation provides an important cross-check of the $\gamma_T^* + A \to \text{dijet} + X$ impact factor recently obtained in [83] using the covariant formulation of the CGC. Second, we want to address the important open question whether the compatibility of the CGC with TMD factorization is preserved beyond leading order. To do so, we study the limit in which the dijets are back-to-back in the transverse plane, thus creating a scale hierarchy $s \gg \mathbf{P}_\perp^2 \gg \mathbf{k}_\perp^2$, where $\mathbf{P}_\perp$ is the typical large transverse momentum of each jet and $\mathbf{k}_\perp$ is their small momentum imbalance. We can reproduce the large Sudakov double logarithms that are essential ingredients in the CSS evolution of the gluon TMD, obtaining the same result as what was predicted in refs. [48, 49, 84, 85]. However, we show

JHEP10(2022)184

that the usual subtraction of low-x logarithms and their absorption into JIMWLK leads to an oversubtraction incompatible with the extraction of the Sudakov logarithms performed in [48, 49], and demonstrate that one must rather employ the kinematically-improved JIMWLK equation, similar to what has been known since a long time in the context of k_T-factorization [86–89] and the BK equation [90–94]. Finally, we observe that, at least at first sight, a class of virtual diagrams which contribute to the finite NLO corrections seem to break factorization. The analysis of these contributions and thus the answer to whether the CGC-TMD correspondence holds at full NLO accuracy is left for future work.

Note that the central role of the large semiclassical gluon field, as well as the non-linearity of the evolution equations, introduce additional complications into CGC computations. Therefore, we are still far away from the next-to-next-to-leading-order precision reached for some collinear observables. In the last decade, however, a huge effort has been made to bring CGC calculations to NLO accuracy. Prominent examples are the cross sections for inclusive hadron production in proton-nucleus collisions [95, 96], inclusive deep-inelastic-scattering (DIS) [97–102], DIS with massive quarks [103–105], exclusive vector meson production in DIS [106–108], photon+dijet production in DIS [109], diffractive dijet production in DIS [110] and very recently inclusive dijet production in DIS [83]. Moreover, the next-to-leading logarithmic extension of the BK-JIMWLK equations was studied in refs. [111–114].

The paper is organized as follows. In section 3, we use light-cone perturbation theory to calculate the loop corrections to $\gamma + A \to q + \bar{q} + X$. One set of diagrams: the initial-state loop corrections, were already calculated in ref. [100] and are not recomputed here. In section 3.2, we revisit the calculation of the real NLO corrections, i.e. the process $\gamma + A \to q + \bar{q} + g + X$, which was calculated earlier in [69].

As in any NLO calculation, individual diagrams can be plagued by ultraviolet (UV) divergences, while squared diagrams or interferences might exhibit soft and collinear divergences. We demonstrate their cancellation in sections 4, 5, and 8, respectively. Large rapidity logarithms are absorbed in the JIMWLK equation for the LO cross section, as is shown in section 6. The full NLO cross section is then presented in section 9, after which we investigate the back-to-back or 'correlation' limit in section 10.

2 Leading-order calculation

Throughout this work, we will work in LCPT in the conventions of Bjorken-Kogut-Soper [78, 79]. In this picture, the dynamics of the 'projectile', i.e. the photon splitting into the quark-antiquark pair (with, at next-to-leading order, a gluon), take place on a much longer timescale than the partonic dynamics of the 'target' proton or nucleus [115, 116]. The Color Glass Condensate effective theory then asserts that the target effectively behaves as a localized 'shockwave' of semiclassical gluon fields, which may be described by an external potential built from Wilson lines.

Taking the incoming photon to travel along the + light-cone (LC) direction, colliding head on with the hadronic target which travels along the − LC direction, the differential

JHEP10(2022)184

cross section for the process $\gamma A \to q\bar{q}X$ (see figure 1) is given by:

$$\mathrm{d}\sigma = \frac{1}{2q^+}\frac{\mathrm{d}p_1^+\mathrm{d}^{D-2}\mathbf{p}_1\theta(p_1^+)}{(2\pi)^{D-1}2p_1^+}\frac{\mathrm{d}p_2^+\mathrm{d}^{D-2}\mathbf{p}_2\theta(p_2^+)}{(2\pi)^{D-1}2p_2^+}2\pi\delta(q^+-p_1^+-p_2^+)\frac{1}{D-2}\left|\mathcal{M}\right|^2 . \tag{2.1}$$

The vectors $\vec{p}_1 \equiv (p_1^+, \mathbf{p}_1)$ and $\vec{p}_2 \equiv (p_2^+, \mathbf{p}_2)$ describe the + and transverse components of the quark and antiquark, respectively, and q^+ is the photon + momentum. The total + momentum is conserved, as encoded in the delta function. Note that the factor $1/(D-2)$ accounts for the averaging over the photon polarization, and that we work for the moment in D dimensions.

In the above formula, the amplitude $\mathcal{M}$ is defined as:

$$_f\langle(\mathbf{q})[\vec{p}_1]_{s_1};(\bar{\mathbf{q}})[\vec{p}_2]_{s_2}|\hat{F}-1|(\boldsymbol{\gamma})[\vec{q}]_\lambda\rangle_i = 2\pi\delta(q^+-p_1^+-p_2^+)\mathcal{M} . \tag{2.2}$$

In the l.h.s., the operator $\hat{F}$, which describes the interaction with the shockwave, acts on the Fock states of the incoming (i) photon and outgoing (f) quark-antiquark pair. Since these Fock states are asymptotic, their evolution to and from $x^+ = 0$: the light-cone time when the scattering takes place, should be calculated up to a given perturbative order:

$$\begin{aligned} &_f\langle(\mathbf{q})[\vec{p}_1]_{s_1};(\bar{\mathbf{q}})[\vec{p}_2]_{s_2}|\hat{F}-1|(\boldsymbol{\gamma})[\vec{q}]_\lambda\rangle_i \\ &\quad = \langle(\mathbf{q})[\vec{p}_1]_{s_1};(\bar{\mathbf{q}})[\vec{p}_2]_{s_2}|\mathcal{U}(+\infty,0)(\hat{F}-1)\mathcal{U}(0,-\infty)|(\boldsymbol{\gamma})[\vec{q}]_\lambda\rangle , \end{aligned} \tag{2.3}$$

where $\mathcal{U}$ is the LC-time evolution operator. At lowest non-trivial order, the photon splits into a quark-antiquark pair before the scattering off the shockwave, while the outgoing quark pair evolves to the asymptotic states without perturbative modifications. We thus have from the LCPT Feynman rules [69, 79, 100]:

$$\begin{aligned} \langle(\mathbf{q})[\vec{p}_1]_{s_1};(\bar{\mathbf{q}})[\vec{p}_2]_{s_2}|\mathcal{U}(+\infty,0) &= \langle(\mathbf{q})[\vec{p}_1]_{s_1};(\bar{\mathbf{q}})[\vec{p}_2]_{s_2}| + \mathcal{O}(g_e,g_s) , \\ \mathcal{U}(0,-\infty)|(\boldsymbol{\gamma})[\vec{q}]_\lambda\rangle &= |(\boldsymbol{\gamma})[\vec{q}]_\lambda\rangle + \int \mathrm{PS}(\vec{p}_1',\vec{p}_2')(2\pi)^{D-1}\delta^{(D-1)}(\vec{q}-\vec{p}_1'-\vec{p}_2') \\ &\quad \times g_e e_f \frac{\bar{u}^{s_1}(\vec{p}_1')\not{\epsilon}_\lambda(\vec{q})u^{s_2}(\vec{p}_2')}{q^- - p_1'^- - p_2'^-}|(\mathbf{q})[\vec{p}_1'];(\bar{\mathbf{q}})[\vec{p}_2']\rangle + \mathcal{O}(g_s) . \end{aligned} \tag{2.4}$$

In the above, we introduced the notation PS for the measure of the phase space integrations:

$$\int \mathrm{PS}(\vec{q}) = \mu^{4-D}\int\frac{\mathrm{d}^{D-1}\vec{q}\,\theta(q^+)}{(2\pi)^{D-1}2q^+} , \tag{2.5}$$

where $\vec{q} \equiv (q^+, \mathbf{q})$ and where θ is the Heaviside step function defined as $\theta(x \geq 0) = 1$ and $\theta(x < 0) = 0$. Combining eqs. (2.3) and (2.4), we can reshuffle the terms in the following form:

$$\begin{aligned} &_f\langle(\mathbf{q})[\vec{p}_1]_{s_1};(\bar{\mathbf{q}})[\vec{p}_2]_{s_2}|\hat{F}-1|(\boldsymbol{\gamma})[\vec{q}]_\lambda\rangle_i \\ &\quad = g_e e_f \int \mathrm{PS}(\vec{p}_1',\vec{p}_2')\times(2\pi)^{D-1}\delta^{(D-1)}(\vec{q}-\vec{p}_1'-\vec{p}_2') \\ &\qquad \times \frac{\bar{u}^{s_1}(\vec{p}_1')\not{\epsilon}_\lambda(\vec{q})u^{s_2}(\vec{p}_2')}{q^- - p_1'^- - p_2'^-} \times \langle(\mathbf{q})[\vec{p}_1];(\bar{\mathbf{q}})[\vec{p}_2]|\hat{F}-1|(\mathbf{q})[\vec{p}_1'];(\bar{\mathbf{q}})[\vec{p}_2']\rangle . \end{aligned} \tag{2.6}$$

JHEP10(2022)184

The last term in the above expression encodes the scattering of the 'bare' $q\bar{q}$ state off the target. In the eikonal approximation, it can be written as:

$$\begin{aligned}
&\langle(\mathbf{q})[\vec{p}_1];(\bar{\mathbf{q}})[\vec{p}_2]|\hat{F}-1|(\mathbf{q})[\vec{p}\,'_1];(\bar{\mathbf{q}})[\vec{p}\,'_2]\rangle \\
&\quad= 2p_1^+ 2\pi\delta(p_1'^+ - p_1^+) 2p_2^+ 2\pi\delta(p_2'^+ - p_2^+) \\
&\qquad\times\Big[\tilde{U}(\mathbf{p}'_1-\mathbf{p}_1)\tilde{U}^\dagger(\mathbf{p}'_2-\mathbf{p}_2) - (2\pi)^{2(D-2)}\delta^{D-2}(\mathbf{p}'_1-\mathbf{p}_1)\delta^{D-2}(\mathbf{p}'_2-\mathbf{p}_2)\Big]\,, \\
&\quad= 4p_1^+p_2^+ 2\pi\delta(p_1'^+ - p_1^+) 2\pi\delta(p_2'^+ - p_2^+) \\
&\qquad\times\int_{\mathbf{x}_1,\mathbf{x}_2} e^{-i\mathbf{x}_1\cdot(\mathbf{p}_1-\mathbf{p}'_1)} e^{-i\mathbf{x}_2\cdot(\mathbf{p}_2-\mathbf{p}'_2)}\Big[U_{\mathbf{x}_1}U^\dagger_{\mathbf{x}_2}-1\Big]\,,
\end{aligned} \tag{2.7}$$

where we introduced the short-hand notation $\int_{\mathbf{x}} = \mu^{D-4}\int \mathrm{d}^{D-2}\mathbf{x}$, and where

$$U_{\mathbf{x}} = \mathcal{P}\exp\left(ig_s\int \mathrm{d}x^+ A_a^-(x^+,0^-,\mathbf{x})t^a\right) \tag{2.8}$$

denotes a Wilson line (and $\tilde{U}$ its Fourier transform) in the fundamental representation going from $x^+=-\infty$ to $x^+=+\infty$ with $x^-=0$ and transverse position $\mathbf{x}$. We will use the notation $W_{\mathbf{x}}$ for Wilson lines in the adjoint representation, and suppress the fundamental color indices. Note that in the eikonal approximation, there is no exchange of spin nor + momentum between the projectile and the target.

Collecting the delta functions in eqs. (2.6) and (2.7), the phase space integration can be written as follows:

$$\begin{aligned}
&\int \mathrm{PS}(\vec{p}\,'_1,\vec{p}\,'_2)(2\pi)^{D-1}\delta^{(D-1)}(\vec{q}-\vec{p}\,'_1-\vec{p}\,'_2)2\pi\delta(p_1'^+-p_1^+)2\pi\delta(p_2'^+-p_2^+) \\
&\qquad= \frac{2\pi\delta(q^+-p_1^+-p_2^+)}{4p_1^+p_2^+}\int_{\mathbf{p}'_1}\,,
\end{aligned} \tag{2.9}$$

with the convention $\int_{\mathbf{q}} = \mu^{4-D}\int \mathrm{d}^{D-2}\mathbf{q}/(2\pi)^{D-2}$ (note the factor $(2\pi)^{D-2}$ which is not present in the integrations over transverse coordinate space).

Suppressing the spinor indices, the Dirac structure in eq. (2.6) can be rewritten in function of 'good' spinors [100] with the help of the following intermediary result:

$$\begin{aligned}
&\bar{u}(\vec{p}_1)\not{\epsilon}_\lambda(\vec{q})v(\vec{p}_2) \\
&\qquad= \bar{u}_G(p_1^+)\gamma^+\left[\delta^{\lambda\bar{\lambda}}\left(\frac{q^{\bar{\lambda}}}{q^+}-\frac{p_2^{\bar{\lambda}}}{2p_2^+}-\frac{p_1^{\bar{\lambda}}}{2p_1^+}\right)-i\sigma^{\lambda\bar{\lambda}}\left(\frac{p_2^{\bar{\lambda}}}{2p_2^+}-\frac{p_1^{\bar{\lambda}}}{2p_1^+}\right)\right]v_G(p_2^+)\,,
\end{aligned} \tag{2.10}$$

which holds irregardless of whether we work with quark or antiquark spinors (since we consider only massless quarks in this work). A very useful feature of the above formula is that the good spinors only depend on the + component of the momenta, which means that they are not affected by the shockwave. Note as well that, to arrive at eq. (2.10), we choose linear polarization vectors $\epsilon^i_\lambda = \delta^{i\lambda}$. Using the identity (2.10) and taking the delta functions in (2.9) into account, the Dirac structure in eq. (2.6) eventually becomes:

$$\bar{u}(\vec{p}\,'_1)\not{\epsilon}_\lambda(\vec{q})v(\vec{p}\,'_2) = -\frac{q^+\mathbf{p}'^{\bar{\lambda}}_1}{2p_1^+p_2^+}\bar{u}^{s_1}_G(p_1^+)\gamma^+\left[(1-2z)\delta^{\lambda\bar{\lambda}}-i\sigma^{\lambda\bar{\lambda}}\right]v^{s_2}_G(p_2^+)\,, \tag{2.11}$$

JHEP10(2022)184

where we defined $z \equiv p_1^+/q^+$ and $\sigma^{ij} \equiv \frac{i}{2}[\gamma^i, \gamma^j]$. Note that, in our frame, the photon does not have any transverse momentum.

On the other hand, the energy denominator in (2.6) gives:

$$q^- - p_1'^- - p_2'^- = \frac{-q^+}{2p_1^+ p_2^+}\mathbf{p}_1'^2 \,. \tag{2.12}$$

Putting everything together, we obtain the intermediary result (using the short-hand $\mathbf{x}_{12} \equiv \mathbf{x}_1 - \mathbf{x}_2$):

$$\mathcal{M}_{\mathrm{LO}} = g_e e_f \int_{\mathbf{x}_1,\mathbf{x}_2} e^{-i\mathbf{p}_1\cdot\mathbf{x}_1} e^{-i\mathbf{p}_2\cdot\mathbf{x}_2} \mathrm{Dirac}_{\mathrm{LO}}^{\bar{\lambda}} \int_{\mathbf{p}_1'} e^{i\mathbf{p}_1'\cdot\mathbf{x}_{12}} \frac{\mathbf{p}_1'^{\bar{\lambda}}}{\mathbf{p}_1'^2}\Big[U_{\mathbf{x}_1}U_{\mathbf{x}_2}^\dagger - 1\Big] \,, \tag{2.13}$$

with:

$$\mathrm{Dirac}_{\mathrm{LO}}^{\bar{\lambda}} \equiv \bar{u}_G^{s_1}(p_1^+)\gamma^+[(1-2z)\delta^{\lambda\bar{\lambda}} - i\sigma^{\lambda\bar{\lambda}}]v_G^{s_2}(p_2^+) \,. \tag{2.14}$$

Finally, we can perform the integration over $\mathbf{p}_1'$, which gives:

$$\int_{\mathbf{p}_1'} e^{i\mathbf{p}_1'\cdot\mathbf{x}_{12}} \frac{\mathbf{p}_1'^{\bar{\lambda}}}{\mathbf{p}_1'^2} = -iA^{\bar{\lambda}}(\mathbf{x}_{12}) \,, \tag{2.15}$$

where the Weizsäcker-Williams field $A^i(\mathbf{x})$ in $D-2$ dimensions is defined as:

$$iA^i(\mathbf{x}) \equiv \int_{\mathbf{k}} e^{-i\mathbf{k}\cdot\mathbf{x}} \frac{k^i}{\mathbf{k}^2} = \frac{-i\mu^{4-D}}{2\pi^{\frac{D}{2}-1}} \frac{x^i}{(\mathbf{x}^2)^{\frac{D}{2}-1}} \Gamma\left(\frac{D}{2}-1\right) \overset{D\to 4}{=} \frac{-i}{2\pi}\frac{x^i}{\mathbf{x}^2} \,. \tag{2.16}$$

We eventually arrive at the following result for the LO scattering amplitude:

$$\mathcal{M}_{\mathrm{LO}} = -ig_e e_f \mathrm{Dirac}_{\mathrm{LO}}^{\bar{\lambda}} \int_{\mathbf{x}_1,\mathbf{x}_2} e^{-i\mathbf{p}_1\cdot\mathbf{x}_1} e^{-i\mathbf{p}_2\cdot\mathbf{x}_2} A^{\bar{\lambda}}(\mathbf{x}_{12})\Big[U_{\mathbf{x}_1}U_{\mathbf{x}_2}^\dagger - 1\Big] \,, \tag{2.17}$$

and obtain after multiplying with its complex conjugate

$$\begin{aligned} \left|\mathcal{M}_{\mathrm{LO}}\right|^2 = {} & 4\pi\alpha_{\mathrm{em}} e_f^2 \mathrm{Tr}\Big(\mathrm{Dirac}_{\mathrm{LO}}^{\lambda'\dagger}\mathrm{Dirac}_{\mathrm{LO}}^{\bar{\lambda}}\Big) \\ & \times \int_{\mathbf{x}_1,\mathbf{x}_2,\mathbf{x}_{1'},\mathbf{x}_{2'}} e^{-i\mathbf{p}_1\cdot\mathbf{x}_{11'}} e^{-i\mathbf{p}_2\cdot\mathbf{x}_{22'}} A^{\bar{\lambda}}(\mathbf{x}_{12}) A^{\lambda'}(\mathbf{x}_{1'2'}) \\ & \times \Big\langle \mathrm{Tr}\big[U_{\mathbf{x}_{2'}}U_{\mathbf{x}_{1'}}^\dagger - 1\big]\big[U_{\mathbf{x}_1}U_{\mathbf{x}_2}^\dagger - 1\big]\Big\rangle \,, \end{aligned} \tag{2.18}$$

where the brackets $\langle\rangle$ denote the average of the semiclassical gluon fields in the target (see also section 6.1).

The Dirac trace is performed as follows:

$$\begin{aligned} \mathrm{Tr}\Big(\mathrm{Dirac}_{\mathrm{LO}}^{\lambda'\dagger}\mathrm{Dirac}_{\mathrm{LO}}^{\bar{\lambda}}\Big) = {} & \mathrm{Tr}\Big(\bar{v}_G^{s_2}(p_2^+)\gamma^+[(1-2z)\delta^{\lambda\lambda'} + i\sigma^{\lambda\lambda'}]u_G^{s_1}(p_1^+) \\ & \times \bar{u}_G^{s_1}(p_1^+)\gamma^+[(1-2z)\delta^{\lambda\bar{\lambda}} - i\sigma^{\lambda\bar{\lambda}}]v_G^{s_2}(p_2^+)\Big) \,, \\ = {} & 4p_1^+p_2^+\mathrm{Tr}\Big(\mathcal{P}_G[(1-2z)\delta^{\lambda\lambda'} + i\sigma^{\lambda\lambda'}]\mathcal{P}_G[(1-2z)\delta^{\lambda\bar{\lambda}} - i\sigma^{\lambda\bar{\lambda}}]\Big) \,, \end{aligned} \tag{2.19}$$

where we used the completeness relations for good spinors [100]:

$$\sum_s u_G(p^+)\bar{u}_G(p^+)\gamma^+ = 2p^+\mathcal{P}_G \,, \tag{2.20}$$

JHEP10(2022)184

with the same relation holding for antiquark spinors v_G, and with $\mathcal{P}_G = \gamma^-\gamma^+/2$ the projector on the good components of the spinor field.

Since $\mathcal{P}_G$ commutes with all transverse gamma matrices and since $\mathcal{P}_G\mathcal{P}_G = \mathcal{P}_G$, we get:

$$\begin{aligned}&\mathrm{Tr}\Big(\mathrm{Dirac}_{\mathrm{LO}}^{\lambda'\dagger}\mathrm{Dirac}_{\mathrm{LO}}^{\bar{\lambda}}\Big)\\&\quad= 4p_1^+p_2^+\Big((1-2z)^2\delta^{\lambda'\bar{\lambda}}\mathrm{Tr}\{\mathcal{P}_G\} + 2i(1-2z)\mathrm{Tr}\{\mathcal{P}_G\sigma^{\bar{\lambda}\lambda'}\} + \mathrm{Tr}\{\mathcal{P}_G\sigma^{\lambda\lambda'}\sigma^{\lambda\bar{\lambda}}\}\Big)\,.\end{aligned} \tag{2.21}$$

We finally obtain, using the identities (A.5) and (A.7):

$$\mathrm{Tr}\Big(\mathrm{Dirac}_{\mathrm{LO}}^{\lambda'\dagger}\mathrm{Dirac}_{\mathrm{LO}}^{\bar{\lambda}}\Big) = 16p_1^+p_2^+\delta^{\lambda'\bar{\lambda}}\left(z^2+\bar{z}^2+\frac{D-4}{2}\right), \tag{2.22}$$

where we defined $\bar{z}\equiv 1-z = p_2^+/q^+$. Our final result for the LO amplitude squared is then:

$$\begin{aligned}\left|\mathcal{M}_{\mathrm{LO}}\right|^2 &= 64\pi\alpha_{\mathrm{em}}e_f^2N_cp_1^+p_2^+\left(z^2+\bar{z}^2+\frac{D-4}{2}\right)\\&\quad\times\int_{\mathbf{x}_1,\mathbf{x}_2,\mathbf{x}_{1'},\mathbf{x}_{2'}} e^{-i\mathbf{p}_1\cdot\mathbf{x}_{11'}}e^{-i\mathbf{p}_2\cdot\mathbf{x}_{22'}}A^{\bar{\lambda}}(\mathbf{x}_{12})A^{\bar{\lambda}}(\mathbf{x}_{1'2'})\\&\quad\times\Big\langle Q_{122'1'}-s_{12}-s_{2'1'}+1\Big\rangle\,,\end{aligned} \tag{2.23}$$

which leads to the following cross section[1] in $D=4$ dimensions:

$$\begin{aligned}\frac{\mathrm{d}\sigma_{\mathrm{LO}}}{\mathrm{d}p_1^+\mathrm{d}p_2^+\mathrm{d}^2\mathbf{p}_1\mathrm{d}^2\mathbf{p}_2} &= \frac{2\alpha_{\mathrm{em}}e_f^2N_c}{(2\pi)^4}\frac{\delta(1-z-\bar{z})}{(q^+)^2}(z^2+\bar{z}^2)\\&\quad\times\int_{\mathbf{x}_1,\mathbf{x}_2,\mathbf{x}_{1'},\mathbf{x}_{2'}} e^{-i\mathbf{p}_1\cdot\mathbf{x}_{11'}}e^{-i\mathbf{p}_2\cdot\mathbf{x}_{22'}}A^{\bar{\lambda}}(\mathbf{x}_{12})A^{\bar{\lambda}}(\mathbf{x}_{1'2'})\\&\quad\times\Big\langle Q_{122'1'}-s_{12}-s_{2'1'}+1\Big\rangle\,.\end{aligned} \tag{2.24}$$

In the above two expressions, we introduced the following compact notations for the dipole and quadrupole color operators:

$$\begin{aligned}s_{12} &\equiv \frac{1}{N_c}\mathrm{Tr}(U_{\mathbf{x}_1}U^\dagger_{\mathbf{x}_2})\,,\\Q_{122'1'} &\equiv \frac{1}{N_c}\mathrm{Tr}(U_{\mathbf{x}_1}U^\dagger_{\mathbf{x}_2}U_{\mathbf{x}_{2'}}U^\dagger_{\mathbf{x}_{1'}})\,.\end{aligned} \tag{2.25}$$

3 Next-to-leading order diagrams

The calculation of the next-to-leading order amplitudes follows largely the same method as the leading-order case. We will therefore not reproduce all the intermediate steps but rather give the result for each Feynman diagram, depicted in figures 1 and 3. Of course, all diagrams have a counterpart in which the quark and antiquark are reversed. We will denote these contributions with an overline: for example, $\overline{\mathrm{GE}}\mathrm{SW}$ is the graph in which the gluon is radiated by the quark and, after scattering off the shockwave, absorbed by the antiquark. These '$q\leftrightarrow\bar{q}$ conjugate' amplitudes can be obtained in a straightforward way from their counterparts applying the following steps:

[1]For ease of notation, in this work we suppress the overall summation over light quark flavors in the cross section.

JHEP10(2022)184

	Real NLO			
	$\lvert\mathcal{M}_{\mathrm{QSF}}\rvert^2$ & $\lvert\mathcal{M}_{\overline{\mathrm{Q}}\mathrm{SF}}\rvert^2$	$\mathcal{M}^{\dagger}_{\overline{\mathrm{Q}}\mathrm{SF}}\mathcal{M}_{\mathrm{QSF}}$ & c.c.	$\lvert\mathcal{M}_{\mathrm{QSW}}\rvert^2$ & $\lvert\mathcal{M}_{\overline{\mathrm{Q}}\mathrm{SW}}\rvert^2$	cross
JIMWLK	✓	✓	✓	✓
collinear	✓			
soft	?	✓		
Sudakov	leading N_c			

Table 1. Overview of the divergencies and large logarithms encountered in our calculation, for the different real NLO contributions to the cross section. In the column 'cross', all cross terms are meant between the gluon emissions before and after the shockwave, from the quark or from the antiquark, i.e. the interference between $\mathcal{M}_{\mathrm{QFS}}$, $\mathcal{M}_{\overline{\mathrm{Q}}\mathrm{FS}}$, $\mathcal{M}_{\mathrm{QSW}}$, $\mathcal{M}_{\overline{\mathrm{Q}}\mathrm{SW}}$. Terms involving a real instantaneous gluon emission are strictly finite and do not contribute to the Sudakov logarithms at our accuracy. In this work, we do not attempt to analyze the Sudakov double logarithms beyond the large-N_c limit. Moreover, in our regularization scheme, it is not always possible to unambiguously distinguish soft from rapidity divergences. The question mark indicates this is the case for $\lvert\mathcal{M}_{\mathrm{QSF}}\rvert^2$ and $\lvert\mathcal{M}_{\overline{\mathrm{Q}}\mathrm{SF}}\rvert^2$. The only certainty is that these two diagrams combine with FSIR (table 2) into a contribution to the cross section that has rapidity divergences only, see also section 8.

1. Interchange *all* the indices 1 and 2 except in the Wilson lines and in the spinors $\bar{u}_G(p_1^+)$ and $v_G(p_2^+)$.

2. Take the complex conjugate of the part of the Dirac structures sandwiched between the spinors $\bar{u}_G(p_1^+)$ and $v_G(p_2^+)$.

3. In LCPT, the vertex for the emission or absorption of a gluon from the antiquark has an overall minus sign. Add it to the diagrams $\overline{\mathrm{I}}$SW, $\overline{\mathrm{Q}}$SW and $\overline{\mathrm{Q}}$SF.

4. Calculate the Wilson line structure separately, there is no simple rule here.

In tables 1 and 2, we list all NLO contributions to the cross section and their possible contribution to ultraviolet or infrared divergencies. Their regularization and either cancellation or renormalization will be the subject of sections 4 to 8.

3.1 Virtual corrections

ISW: instantaneous gluon traversing shockwave. The amplitude for the instantaneous production of a quark, antiquark, and gluon from the photon, where the gluon

JHEP10(2022)184

	Virtual NLO						
	SESW, sub	GESW	GEFS + IFS	SESW, UV	IS	FSIR	FSUV
ultraviolet				✓	✓		✓
JIMWLK	✓	✓	✓	?	?	✓	?
collinear						✓	
soft			✓	?	?	?	?

Table 2. Overview of the possible divergencies or large logarithms encountered in our calculation, for the different virtual NLO contributions to the cross section. IS stands for all the initial-state virtual corrections, which were already obtained in ref. [100] and are not recalculated here. FSIR and FSUV, related to the self-energy corrections in the final state, are not calculated in section 3 neither, but are introduced in section 4. Just like the real contributions involving an instantaneously created gluon (RI, $\overline{\text{RI}}$ and interferences), the virtual diagram ISW with an instantaneously emitted gluon does not exhibit any singularity or large logarithm, and hence merely contributes to the finite part of the cross section. Note that all contributions in the above table, except for IS, FSIR, and FSUV, have a $q \leftrightarrow \bar{q}$ counterpart with the same singularity structure. The contributions SESW, UV, IS, and FSUV exhibit soft- or rapidity singularities, between which we cannot make a distinction, although their combination is finite (see section 4).

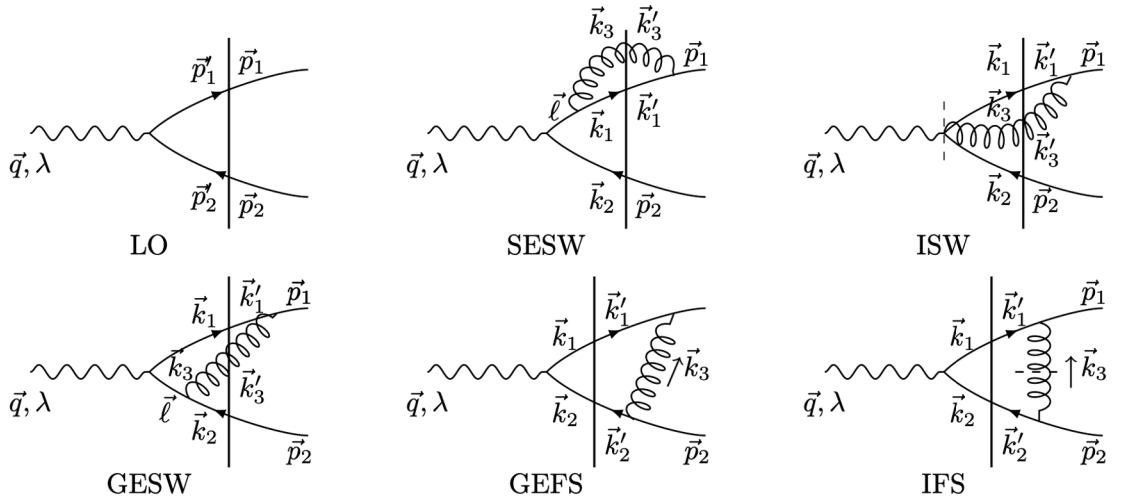

Figure 1. LO: the leading-order Feynman diagram. The shockwave of semiclassical gluon fields from the hadron target is depicted by the full vertical line. SESW: self-energy correction traversing the shockwave. ISW: instantaneous gluon emission crossing the shockwave. GESW: gluon exchange crossing the shockwave. GEFS: gluon exchange in the final state. IFS: instantaneous gluon exchange in the final state. Virtual corrections before the shockwave are not explicitly calculated in this work and not shown here, and neither are the self-energy corrections on the asymptotic final states.

JHEP10(2022)184

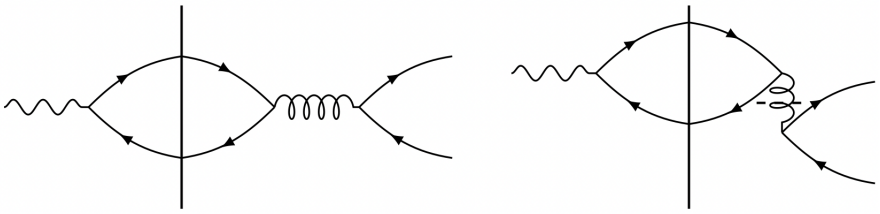

Figure 2. Two diagrams with a virtual (left) and instantaneous (right) gluon in the s-channel after the shockwave. As explained in the main text, these diagrams disappear when considering only the three lightest quarks.

crosses the shockwave and is absorbed by the outgoing quark (figure 1), is found to be:

$$\begin{aligned}\mathcal{M}_{\text{ISW}} = i\frac{g_e e_f g_s^2}{2}\int_0^{p_1^+}\frac{\mathrm{d}k_3^+}{2\pi}\frac{p_1^+-k_3^+}{p_1^+k_3^+(p_2^+-p_1^++k_3^+)}\left(\frac{k_3^+}{p_1^+}\right)^{D-2}(p_2^+-p_1^++k_3^+)\text{Dirac}^{\eta'}_{\text{ISW}}(k_3^+)\\ \times\int_{\mathbf{x}_1,\mathbf{x}_2,\mathbf{x}_3} e^{-i\mathbf{p}_1\cdot\left(\frac{p_1^+-k_3^+}{p_1^+}\mathbf{x}_1+\frac{k_3^+}{p_1^+}\mathbf{x}_3\right)}e^{-i\mathbf{p}_2\cdot\mathbf{x}_2}\\ \times A^{\eta'}(\mathbf{x}_{31})\mathcal{C}\left(\frac{k_3^+}{p_1^+}\mathbf{x}_{13}+\mathbf{x}_{21},\frac{k_3^+}{p_1^+}\mathbf{x}_{13};\frac{q^+(p_1^+-k_3^+)}{p_2^+k_3^+}\right)\\ \times\left[t^cU_{\mathbf{x}_1}t^dU^\dagger_{\mathbf{x}_2}W^{cd}_{\mathbf{x}_3}-C_F\right],\end{aligned} \tag{3.1}$$

with

$$\begin{aligned}\text{Dirac}^{\eta'}_{\text{ISW}}(k_3^+) = \bar{u}_G^{s_1}(p_1^+)\Bigg\{\left[\left(2\frac{p_1^+}{k_3^+}-1\right)-(D-3)\left(\frac{q^++k_3^+}{p_2^+-p_1^++k_3^+}\right)\right]\delta^{\lambda\eta'}\\ +i\sigma^{\lambda\eta'}\left[1-\left(2\frac{p_1^+}{k_3^+}-D+3\right)\left(\frac{q^++k_3^+}{p_2^+-p_1^++k_3^+}\right)\right]\Bigg\}\gamma^+v_G^{s_2}(p_2^+),\end{aligned} \tag{3.2}$$

and where we introduced the generalization of the Coulomb field (see [69]) to $D-4$ dimensions, defined as:

$$\begin{aligned}\mathcal{C}(\mathbf{x},\mathbf{y},c) &\equiv \int_{\mathbf{k},\mathbf{p}} e^{i\mathbf{p}\cdot\mathbf{x}}e^{i\mathbf{k}\cdot\mathbf{y}}\frac{1}{\mathbf{k}^2+c\mathbf{p}^2}\\ &= \mu^{2(4-D)}\frac{\Gamma(D-3)}{4\pi^{D-2}}\frac{c^{\frac{D}{2}-2}}{(\mathbf{x}^2+c\mathbf{y}^2)^{D-3}}\overset{D\to4}{=}\frac{1}{(2\pi)^2}\frac{1}{\mathbf{x}^2+c\mathbf{y}^2}.\end{aligned} \tag{3.3}$$

Note that eq. (3.1) involves a Wilson line in the adjoint representation, as does any amplitude in which a real or virtual gluon from the projectile interacts with the shockwave. Throughout this work, all such Wilson lines will eventually be written as fundamental ones using the Fierz identity:

$$t^bW^{ab}_{\mathbf{x}} = U^\dagger_{\mathbf{x}}t^aU_{\mathbf{x}}\,. \tag{3.4}$$

GESW: gluon exchange traversing shockwave. The amplitude for gluon exchange interacting with the shockwave (figure 1) is found to be:

$$\begin{aligned}\mathcal{M}_{\text{GESW}} = &-\frac{ig_e e_f g_s^2}{2}\int_0^{p_1^+}\frac{\mathrm{d}k_3^+}{2\pi}\frac{k_3^+}{p_1^+(p_2^+ + k_3^+)}\text{Dirac}^{\bar\lambda\bar\eta\eta'}_{\bar q\to q}(k_3^+)\\ &\times\int_{\mathbf{x}_1,\mathbf{x}_2,\mathbf{x}_3} e^{-i\frac{p_1^+-k_3^+}{p_1^+}\mathbf{p}_1\cdot\mathbf{x}_1}e^{-i\mathbf{p}_2\cdot\mathbf{x}_2}e^{-i\frac{k_3^+}{p_1^+}\mathbf{p}_1\cdot\mathbf{x}_3}\\ &\times A^{\eta'}(\mathbf{x}_{31})A^{\bar\eta}(\mathbf{x}_{32})\mathcal{A}^{\bar\lambda}\left(\frac{p_2^+\mathbf{x}_{12}+k_3^+\mathbf{x}_{13}}{p_2^+ + k_3^+},\frac{k_3^+}{p_2^+ + k_3^+}\mathbf{x}_{32};\frac{q^+p_2^+}{k_3^+(p_1^+ - k_3^+)}\right)\\ &\times\left[t^c U_{\mathbf{x}_1}t^d U^\dagger_{\mathbf{x}_2}W^{dc}_{\mathbf{x}_3} - C_F\right].\end{aligned} \tag{3.5}$$

To arrive at the above expression, we made use of the intermediary result:

$$\int_{\mathbf{K},\mathbf{P}}\frac{P^i}{P^2}\frac{K^j}{K^2+cP^2}e^{i\mathbf{K}\cdot\mathbf{r}'}e^{i\mathbf{P}\cdot\mathbf{r}} = -A^j(r')\mathcal{A}^i(r,r',c)\,, \tag{3.6}$$

where $\mathcal{A}$ is the modified Weizsäcker-Williams field[2] defined as:

$$\begin{aligned}\mathcal{A}^i(\mathbf{r},\mathbf{r}',\mathcal{C}) \equiv \frac{-\mu^{4-D}}{64\pi^{D/2}}\frac{r^i}{(\mathbf{r}^2)^{D/2-1}}\Bigg\{&32\pi\,\Gamma\left(\frac{D}{2}-1\right) - 2^D\sqrt{\pi}\mathcal{C}^{\frac{D}{2}-2}\left(\frac{\mathbf{r}'^2}{\mathbf{r}^2}\right)^{\frac{D}{2}-2}\Gamma\left(\frac{D}{2}-\frac{3}{2}\right)\\ &\times\Big[(\mathbf{r}^2)^{D-4}(\mathcal{C}\mathbf{r}'^2-\mathbf{r}^2)(\mathcal{C}\mathbf{r}'^2+\mathbf{r}^2)^{3-D}\\ &+F_{2,1}\left(\frac{D}{2}-2,D-4,\frac{D}{2}-1,-\mathcal{C}\frac{\mathbf{r}'^2}{\mathbf{r}^2}\right)\Big]\Bigg\}.\end{aligned} \tag{3.7}$$

Luckily, it turns out that we will only need to evaluate $\mathcal{A}$ in finite contributions to the cross section, where we can work in $D=4$ dimensions for which its expression reduces to:

$$\mathcal{A}^i(\mathbf{r},\mathbf{r}',\mathcal{C}) = \frac{-1}{2\pi}\frac{r^i}{\mathbf{r}^2+\mathcal{C}\mathbf{r}'^2}\,. \tag{3.8}$$

The spinor structure in (3.5) has the following form:

$$\begin{aligned}\text{Dirac}^{\bar\lambda\bar\eta\eta'}_{\bar q\to q}(k_3^+) &= \bar u_G^{s_1}(p_1^+)\left[\left(2\frac{p_1^+}{k_3^+}-1\right)\delta^{\eta\eta'}+i\sigma^{\eta\eta'}\right]\left[\left(1-2\frac{p_2^+ + k_3^+}{q^+}\right)\delta^{\lambda\bar\lambda}+i\sigma^{\lambda\bar\lambda}\right]\\ &\quad\times\left[\left(1+2\frac{p_2^+}{k_3^+}\right)\delta^{\eta\bar\eta}+i\sigma^{\eta\bar\eta}\right]\gamma^+ v_G^{s_2}(p_2^+)\,,\\ &= \text{Dirac}^{\bar\lambda\bar\eta\eta'}_{\bar q\to q,(i)} + \text{Dirac}^{\bar\lambda\bar\eta\eta'}_{\bar q\to q,(ii)}\,,\end{aligned} \tag{3.9}$$

where we defined:

$$\text{Dirac}^{\bar\lambda\bar\eta\eta'}_{\bar q\to q,(ii)} = 4\frac{p_1^+p_2^+}{(k_3^+)^2}\delta^{\bar\eta\eta'}\bar u_G^{s_1}(p_1^+)\left[\left(1-2\frac{p_2^+ + k_3^+}{q^+}\right)\delta^{\lambda\bar\lambda}+i\sigma^{\lambda\bar\lambda}\right]\gamma^+ v_G^{s_2}(p_2^+)\,, \tag{3.10}$$

which is the most singular part of the Dirac structure, scaling like $1/(k_3^+)^2$.

[2]Note that we use a slight redefinition of this field with respect to earlier work [69].

JHEP10(2022)184

SESW: self-energy correction traversing shockwave. For the self-energy corrections crossing the shockwave (figure 1), we obtain:

$$\begin{aligned}\mathcal{M}_{\text{SESW}} = i\frac{g_e e_f g_s^2}{2}\int_0^{p_1^+}\frac{\mathrm{d}k_3^+}{2\pi}\frac{k_3^+}{(p_1^+)^2}\left[\left(2\frac{p_1^+}{k_3^+}-1\right)^2+(D-3)\right]\text{Dirac}^{\bar\lambda}_{\text{LO}}\\ \times\int_{\mathbf{x}_1,\mathbf{x}_2,\mathbf{x}_3} e^{-i\mathbf{p}_1\cdot\mathbf{x}_1}e^{-i\mathbf{p}_2\cdot\mathbf{x}_2}e^{i\frac{k_3^+}{p_1^+}\mathbf{p}_1\cdot\mathbf{x}_{13}}A^{\bar\eta}(\mathbf{x}_{13})A^{\bar\eta}(\mathbf{x}_{13})\\ \times\mathcal{A}^{\bar\lambda}\left(\frac{k_3^+}{p_1^+}\mathbf{x}_{13}+\mathbf{x}_{21},\frac{k_3^+}{p_1^+}\mathbf{x}_{13};\frac{q^+(p_1^+-k_3^+)}{k_3^+p_2^+}\right)\left[t^cU_{\mathbf{x}_1}t^dU^\dagger_{\mathbf{x}_2}W^{dc}_{\mathbf{x}_3}-C_F\right].\end{aligned} \tag{3.11}$$

The above amplitude contains an ultraviolet divergence in the limit where $\mathbf{x}_3\to\mathbf{x}_1$. Following ref. [100], we construct a counterterm $\mathcal{M}_{\text{SESW,UV}}$ by taking the $\mathbf{x}_3\to\mathbf{x}_1$ limit in $\mathcal{M}_{\text{SESW}}$ except in the singular part, and by subtracting an infrared (IR) divergent contribution $\propto A^{\bar\eta}(\mathbf{x}_{13})A^{\bar\eta}(\mathbf{x}_{23})$ as follows:

$$\begin{aligned}\mathcal{M}_{\text{SESW,UV}} = i\frac{g_e e_f g_s^2}{2}C_F\int_0^{p_1^+}\frac{\mathrm{d}k_3^+}{2\pi}\frac{k_3^+}{(p_1^+)^2}\left[\left(2\frac{p_1^+}{k_3^+}-1\right)^2+(D-3)\right]\text{Dirac}^{\bar\lambda}_{\text{LO}}\\ \times\int_{\mathbf{x}_1,\mathbf{x}_2,\mathbf{x}_3} e^{-i\mathbf{p}_1\cdot\mathbf{x}_1}e^{-i\mathbf{p}_2\cdot\mathbf{x}_2}A^{\bar\eta}(\mathbf{x}_{13})\left[A^{\bar\eta}(\mathbf{x}_{13})-A^{\bar\eta}(\mathbf{x}_{23})\right]A^{\bar\lambda}(\mathbf{x}_{21})\\ \times\left[U_{\mathbf{x}_1}U^\dagger_{\mathbf{x}_2}-1\right],\end{aligned} \tag{3.12}$$

where we used that, even in D dimensions:

$$\mathcal{A}^i(\mathbf{r},0,\mathcal{C}) = A^i(\mathbf{r})\,. \tag{3.13}$$

By construction, the counterterm $\mathcal{M}_{\text{SESW,UV}}$ has the same UV pole as $\mathcal{M}_{\text{SESW}}$ while not possessing any other divergences. To show this is the case, let us explicitly evaluate the $\mathbf{x}_3$ integration in eq. (3.12). We have that:

$$\int_{\mathbf{x}_3}A^i(\mathbf{x}_{13})A^i(\mathbf{x}_{13}) = \mu^{4-D}\frac{\Gamma(\frac{D}{2}-1)^2}{4\pi^{D-2}}\int\frac{\mathrm{d}^{D-2}\mathbf{x}_3}{(\mathbf{x}_{13}^2)^{D-3}} = 0\,, \tag{3.14}$$

since scaleless integrals disappear in dimensional regularization. This is equivalent to the statement that the above integral contains two divergences, an UV ($\mathbf{x}_3\to\mathbf{x}_1$) and an IR ($\mathbf{x}_3\to\infty$) one, which cancel each other.

The second integration in eq. (3.12) reads:

$$\begin{aligned}\int_{\mathbf{x}_3}A^i(\mathbf{x}_{13})A^i(\mathbf{x}_{23}) &= \mu^{4-D}\frac{\Gamma(\frac{D}{2}-1)^2}{4\pi^{D-2}}\frac{\pi^{D/2-1}}{(\frac{D}{2}-2)\Gamma(\frac{D}{2}-1)}\frac{1}{(\mathbf{x}_{12}^2)^{\frac{D}{2}-2}}\,,\\ &= \mu^{4-D}\frac{\Gamma(\frac{D}{2}-1)}{4\pi^{D/2-1}}\frac{1}{(\frac{D}{2}-2)}\frac{1}{(\mathbf{x}_{12}^2)^{\frac{D}{2}-2}}\,,\end{aligned} \tag{3.15}$$

which is divergent in the infrared. Combining eqs. (3.14) and (3.15), the IR pole of the latter cancels the one hidden in the former, and the overall divergence of $\mathcal{M}_{\text{SESW,UV}}$ can be interpreted as an UV one.

JHEP10(2022)184

Since $\mathcal{M}_{\text{SESW,sub}} \equiv \mathcal{M}_{\text{SESW}} - \mathcal{M}_{\text{SESW,UV}}$ is now free from UV divergences, we can evaluate it in $D = 4$ dimensions:

$$\begin{aligned}\mathcal{M}_{\text{SESW,sub}} = i\frac{g_e e_f g_s^2}{2}\int_0^{p_1^+}\frac{\mathrm{d}k_3^+}{2\pi}\frac{k_3^+}{(p_1^+)^2}\left[\left(2\frac{p_1^+}{k_3^+}-1\right)^2+1\right]\text{Dirac}_{\text{LO}}^{\bar\lambda}\\ \times\int_{\mathbf{x}_1,\mathbf{x}_2,\mathbf{x}_3} e^{-i\mathbf{p}_1\cdot\mathbf{x}_1}e^{-i\mathbf{p}_2\cdot\mathbf{x}_2}A^{\bar\eta}(\mathbf{x}_{13})\\ \times\left\{e^{i\frac{k_3^+}{p_1^+}\mathbf{p}_1\cdot\mathbf{x}_{13}}A^{\bar\eta}(\mathbf{x}_{13})\mathcal{A}^{\bar\lambda}\left(\frac{k_3^+}{p_1^+}\mathbf{x}_{13}+\mathbf{x}_{21},\frac{k_3^+}{p_1^+}\mathbf{x}_{13};\frac{q^+(p_1^+-k_3^+)}{k_3^+p_2^+}\right)\right.\\ \left.\times\left[t^cU_{\mathbf{x}_1}t^dU_{\mathbf{x}_2}^\dagger W_{\mathbf{x}_3}^{dc}-C_F\right]-\left[A^{\bar\eta}(\mathbf{x}_{13})-A^{\bar\eta}(\mathbf{x}_{23})\right]A^{\bar\lambda}(\mathbf{x}_{21})C_F\left[U_{\mathbf{x}_1}U_{\mathbf{x}_2}^\dagger-1\right]\right\}.\end{aligned} \tag{3.16}$$

GEFS: gluon exchange in final state. We find for the amplitude where, after passing through the shockwave, the antiquark emits a gluon which is absorbed by the quark (figure 1):

$$\begin{aligned}\mathcal{M}_{\text{GEFS}} = -i\frac{g_e e_f g_s^2}{2}\int_0^{p_1^+}\frac{\mathrm{d}k_3^+}{2\pi}\frac{p_1^+-k_3^+}{q^+p_1^+}\text{Dirac}_{\bar q\to q}^{\bar\lambda\bar\eta\eta'}(k_3^+)\\ \times\int_{\mathbf{x}_1,\mathbf{x}_2} e^{-i\mathbf{p}_1\cdot\left(\frac{p_1^+-k_3^+}{p_1^+}\mathbf{x}_1+\frac{k_3^+}{p_1^+}\mathbf{x}_2\right)}e^{-i\mathbf{p}_2\cdot\mathbf{x}_2}\\ \times A^{\bar\lambda}(\mathbf{x}_{12})J^{\eta'\bar\eta}(k_3,\mathbf{x}_{12})\times\left[t^cU_{\mathbf{x}_1}U_{\mathbf{x}_2}^\dagger t^c-C_F\right],\end{aligned} \tag{3.17}$$

with:

$$J^{\eta'\bar\eta}(k_3^+,\mathbf{x}_{12}) = \int_{\mathbf{K}} e^{-i\mathbf{K}\cdot\mathbf{x}_{12}}\frac{\mathbf{K}^{\eta'}}{\mathbf{K}^2-i\epsilon}\frac{\mathbf{K}^{\bar\eta}-\frac{k_3^+q^+}{p_1^+p_2^+}\mathbf{P}_\perp^{\bar\eta}}{\left(\mathbf{K}+\frac{p_1^+-k_3^+}{p_1^+}\mathbf{P}_\perp\right)^2-\frac{p_2^++k_3^+}{p_2^+}\frac{p_1^+-k_3^+}{p_1^+}\mathbf{P}_\perp^2-i\epsilon}. \tag{3.18}$$

In the above expression, $\mathbf{P}_\perp$ is a transverse vector defined as:

$$\mathbf{P}_\perp \equiv \frac{p_2^+}{q^+}\mathbf{p}_1-\frac{p_1^+}{q^+}\mathbf{p}_2, \tag{3.19}$$

while the loop momentum $\mathbf{K}$ is related to the virtual gluon transverse momentum through $p_1^+\mathbf{K} \equiv p_1^+\mathbf{k}_3 - k_3^+\mathbf{p}_1$.

IFS: instantaneous gluon exchange in final state. In the case of an instantaneous $q\bar q \to q\bar q$ final-state interaction mediated by an instantaneous gluon (figure 1) we obtain:

$$\begin{aligned}\mathcal{M}_{\text{IFS}} = ig_e e_f g_s^2\int_0^{p_1^+}\frac{\mathrm{d}k_3^+}{2\pi}\frac{1}{(k_3^+)^2}\frac{2(p_2^++k_3^+)(p_1^+-k_3^+)}{q^+}\\ \times\bar u_G^{s_1}(p_1^+)\gamma^+\left[\left(1-2\frac{p_2^++k_3^+}{q^+}\right)\delta^{\lambda\bar\lambda}+i\sigma^{\lambda\bar\lambda}\right]v_G^{s_2}(p_2^+)\\ \times\int_{\mathbf{x}_1,\mathbf{x}_2} e^{-i\mathbf{p}_1\cdot\left(\frac{p_1^+-k_3^+}{p_1^+}\mathbf{x}_1+\frac{k_3^+}{p_1^+}\mathbf{x}_2\right)}e^{-i\mathbf{p}_2\cdot\mathbf{x}_2}A^{\bar\lambda}(\mathbf{x}_{12})\\ \times\int_{\mathbf{K}}\frac{e^{-i\mathbf{K}\cdot\mathbf{x}_{12}}}{\left(\mathbf{K}+\frac{p_1^+-k_3^+}{p_1^+}\mathbf{P}_\perp\right)^2-\frac{(p_2^++k_3^+)(p_1^+-k_3^+)}{p_1^+p_2^+}\mathbf{P}_\perp^2-i\epsilon}\times\left[t^cU_{\mathbf{x}_1}U_{\mathbf{x}_2}^\dagger t^c-C_F\right],\end{aligned} \tag{3.20}$$

where the loop momentum is again defined as $p_1^+\mathbf{K} \equiv p_1^+\mathbf{k}_3 - k_3^+\mathbf{p}_1$.

JHEP10(2022)184

Combining diagrams GEFS and IFS. The amplitudes (3.17) and (3.20) both exhibit an unphysical $(1/k_3^+)^2$ power divergence, which cancels when summing them. In diagram GEFS, this divergence stems from the Dirac structure $\mathrm{Dirac}^{\bar{\lambda}\bar{\eta}\eta'}_{\bar{q}\to q,(ii)}$. The subamplitude corresponding to this part of the Dirac structure, which we denote by $\mathcal{M}_{\mathrm{GEFS},(ii)}$, reads:

$$\begin{aligned}\mathcal{M}_{\mathrm{GEFS},(ii)} = -ig_e e_f g_s^2 \int_0^{p_1^+} \frac{\mathrm{d}k_3^+}{2\pi} \frac{2(p_1^+ - k_3^+)}{q^+ p_1^+} \frac{p_1^+ p_2^+}{(k_3^+)^2} \\ \times \bar{u}_G^{s_1}(p_1^+) \left[\left(1 - 2\frac{p_2^+ + k_3^+}{q^+}\right)\delta^{\lambda\bar{\lambda}} + i\sigma^{\lambda\bar{\lambda}} \right] \gamma^+ v_G^{s_2}(p_2^+) \\ \times \int_{\mathbf{x}_1,\mathbf{x}_2} e^{-i\mathbf{p}_1\cdot\left(\frac{p_1^+ - k_3^+}{p_1^+}\mathbf{x}_1 + \frac{k_3^+}{p_1^+}\mathbf{x}_2\right)} e^{-i\mathbf{p}_2\cdot\mathbf{x}_2} A^{\bar{\lambda}}(\mathbf{x}_{12}) J^{\eta'\eta'}(k_3, \mathbf{x}_{12}) \\ \times \left[t^c U_{\mathbf{x}_1} U^\dagger_{\mathbf{x}_2} t^c - C_F\right] ,\end{aligned} \tag{3.21}$$

and is clearly divergent $\propto 1/(k_3^+)^2$ in the $k_3^+ \to 0$ limit. The situation changes when the above (sub)amplitude is summed with the IFS amplitude (3.20):

$$\begin{aligned}\mathcal{M}_{\mathrm{GEFS},(ii)+\mathrm{IFS}} = i\frac{g_e e_f g_s^2}{\pi} \int_0^{p_1^+} \frac{\mathrm{d}k_3^+}{k_3^+} \frac{p_1^+ - k_3^+}{q^+} \\ \times \bar{u}_G^{s_1}(p_1^+) \gamma^+ \left[\left(1 - 2\frac{p_2^+ + k_3^+}{q^+}\right)\delta^{\lambda\bar{\lambda}} + i\sigma^{\lambda\bar{\lambda}} \right] v_G^{s_2}(p_2^+) \\ \times \int_{\mathbf{x}_1,\mathbf{x}_2} e^{-i\mathbf{p}_1\cdot\left(\frac{p_1^+ - k_3^+}{p_1^+}\mathbf{x}_1 + \frac{k_3^+}{p_1^+}\mathbf{x}_2\right)} e^{-i\mathbf{p}_2\cdot\mathbf{x}_2} A^{\bar{\lambda}}(\mathbf{x}_{12}) \\ \times \int_{\mathbf{K}} \left(1 + \frac{q^+}{p_1^+}\frac{\mathbf{K}\cdot\mathbf{P}_\perp}{\mathbf{K}^2}\right) \frac{e^{-i\mathbf{K}\cdot\mathbf{x}_{12}}}{\left(\mathbf{K} + \frac{p_1^+ - k_3^+}{p_1^+}\mathbf{P}_\perp\right)^2 - \frac{(p_2^+ + k_3^+)(p_1^+ - k_3^+)}{p_1^+ p_2^+}\mathbf{P}_\perp^2 - i\epsilon} \\ \times \left[t^c U_{\mathbf{x}_1} U^\dagger_{\mathbf{x}_2} t^c - C_F\right] ,\end{aligned} \tag{3.22}$$

and we are left with a logarithmic $k^+ \to 0$ divergence, which will contribute to JIMWLK.

Final state with gluon in *s*-channel. Finally, in figure 2, two virtual diagrams are depicted in which, after the scattering off the shockwave, the quark-antiquark pair annihilates and a new pair is created. This process either takes place through an s-channel gluon or as an instantaneous $q\bar{q} \to q\bar{q}$ vertex mediated by a fictitious instantaneous gluon. When multiplied with the conjugate leading-order amplitude, these two diagrams contribute to the cross section with a coupling:

$$\left(\sum_f e_f g_e\right)^2 g_s^2 . \tag{3.23}$$

In the above, the summation over quark flavors takes place for the two quark lines separately, since at the level of the cross section the two fermion loops are distinct and only connected by a gluon. This is a unique feature of the two diagrams under consideration;

JHEP10(2022)184

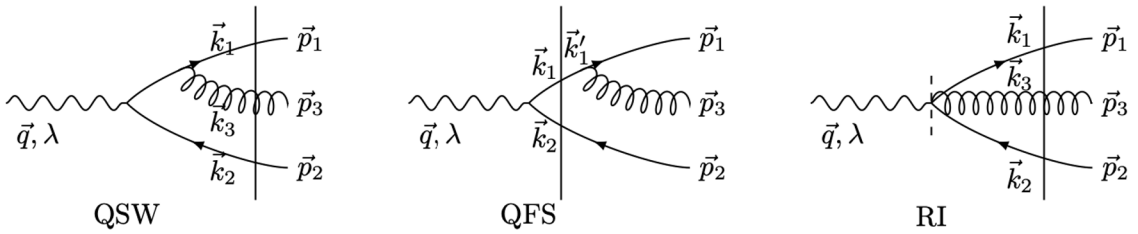

Figure 3. QSW: real gluon emission from the quark, scattering off the shockwave (vertical full line). QFS: gluon radiated from the quark in the final state. RI: instantaneously created real gluon scatters off shockwave.

all other contributions to the NLO dijet photoproduction cross section have a coupling $\sum_f e_f^2 g_e^2 g_s^2$. In particular, since we only consider the three lightest quarks in this work:

$$\left(\sum_{f=u,d,s} e_f g_e\right)^2 g_s^2 = (e_u + e_d + e_s)^2 g_e^2 g_s^2 = \left(\frac{2}{3} - \frac{1}{3} - \frac{1}{3}\right)^2 g_e^2 g_s^2 = 0\,, \tag{3.24}$$

hence these diagrams can be disregarded.

3.2 Real corrections

QSW: real gluon scatters off shockwave. For the diagram where the gluon is emitted from the quark and then interacts with the shockwave (figure 3), we obtain:

$$\begin{aligned}\mathcal{M}_{\mathrm{QSW}} = &-g_e e_f g_s \mathrm{Dirac}^{\bar\eta\bar\lambda}_{\mathrm{QSW}} \frac{p_3^+}{p_1^+ + p_3^+} \\ &\times \int_{\mathbf{x}_1,\mathbf{x}_2,\mathbf{x}_3,\mathbf{v}} e^{-i\mathbf{p}_1\cdot\mathbf{x}_1} e^{-i\mathbf{p}_2\cdot\mathbf{x}_2} e^{-i\mathbf{p}_3\cdot\mathbf{x}_3} \delta^{(D-2)}\left(\mathbf{v} - \frac{p_1^+}{p_1^+ + p_3^+}\mathbf{x}_1 - \frac{p_3^+}{p_1^+ + p_3^+}\mathbf{x}_3\right) \\ &\times A^{\bar\eta}(\mathbf{x}_{13}) \mathcal{A}^{\bar\lambda}(\mathbf{v} - \mathbf{x}_2, \mathbf{x}_{31}, \frac{p_1^+ p_3^+ q^+}{p_2^+ (p_1^+ + p_3^+)^2}) \left[U_{\mathbf{x}_1} U^\dagger_{\mathbf{x}_3} t^d U_{\mathbf{x}_3} U^\dagger_{\mathbf{x}_2} - t^d\right],\end{aligned} \tag{3.25}$$

with the Dirac structure:

$$\begin{aligned}\mathrm{Dirac}^{\bar\eta\bar\lambda}_{\mathrm{QSW}} = \bar u_G(p_1^+) &\left[\left(1 + 2\frac{p_1^+}{p_3^+}\right)\delta^{\eta\bar\eta} - i\sigma^{\eta\bar\eta}\right] \\ &\times \left[\left(1 - 2\frac{p_1^+ + p_3^+}{q^+}\right)\delta^{\lambda\bar\lambda} - i\sigma^{\lambda\bar\lambda}\right]\gamma^+ v_G(p_2^+)\,.\end{aligned} \tag{3.26}$$

QFS: gluon emitted from quark in final state. The amplitude corresponding to a final-state gluon emission from the quark (figure 3) reads:

$$\begin{aligned}\mathcal{M}_{\mathrm{QFS}} = &\, i g_e e_f g_s p_3^+ \mathrm{Dirac}^{\bar\eta\bar\lambda}_{\mathrm{QSW}} \int_{\mathbf{x}_1,\mathbf{x}_2} e^{-i(\mathbf{p}_1+\mathbf{p}_3)\cdot\mathbf{x}_1} e^{-i\mathbf{p}_2\cdot\mathbf{x}_2} \\ &\times A^{\bar\lambda}(\mathbf{x}_{12}) \frac{(p_3^+\mathbf{p}_1 - p_1^+\mathbf{p}_3)^{\bar\eta}}{\left(p_3^+\mathbf{p}_1 - p_1^+\mathbf{p}_3\right)^2}\left[t^d U_{\mathbf{x}_1} U^\dagger_{\mathbf{x}_2} - t^d\right],\end{aligned} \tag{3.27}$$

JHEP10(2022)184

which can be written as:

$$\begin{aligned}\mathcal{M}_{\rm QFS} = g_e e_f g_s \frac{p_3^+}{p_1^+ + p_3^+} \mathrm{Dirac}^{\bar\eta\bar\lambda}_{\rm QSW} \\ \times \int_{\mathbf{x}_1,\mathbf{x}_2,\mathbf{x}_3,\mathbf{v}} e^{-i\mathbf{p}_1\cdot\mathbf{x}_1} e^{-i\mathbf{p}_2\cdot\mathbf{x}_2} e^{-i\mathbf{p}_3\cdot\mathbf{x}_3} \delta^{(D-2)}\left(\mathbf{v} - \frac{p_1^+}{p_1^+ + p_3^+}\mathbf{x}_1 - \frac{p_3^+}{p_1^+ + p_3^+}\mathbf{x}_3\right) \\ \times A^{\bar\lambda}(\mathbf{v}-\mathbf{x}_2) A^{\bar\eta}(\mathbf{x}_{13}) \left[t^d U_{\mathbf{v}} U^\dagger_{\mathbf{x}_2} - t^d\right] .\end{aligned} \tag{3.28}$$

RI: real gluon created instantaneously before shockwave. Finally, the real gluon can be radiated instantaneously from the photon in addition to the quark-antiquark pair (figure 3), yielding the amplitude:

$$\begin{aligned}\mathcal{M}_{\rm RI} = g_e e_f g_s \frac{p_1^+ p_3^+ (p_1^+ + p_3^+)}{(q^+)^3} \mathrm{Dirac}_{\rm RI} \\ \times \int_{\mathbf{x}_1,\mathbf{x}_2,\mathbf{x}_3} e^{-i\mathbf{p}_1\cdot\mathbf{x}_1} e^{-i\mathbf{p}_2\cdot\mathbf{x}_2} e^{-i\mathbf{p}_3\cdot\mathbf{x}_3} \mathcal{C}\left(\frac{p_1^+}{q^+}\mathbf{x}_{21} + \frac{p_3^+}{q^+}\mathbf{x}_{23}, \mathbf{x}_{31}, \frac{p_1^+ p_3^+}{q^+ p_2^+}\right) \\ \times \left[U_{\mathbf{x}_1} t^c U^\dagger_{\mathbf{x}_2} W^{cd}_{\mathbf{x}_3} - t^d\right] ,\end{aligned} \tag{3.29}$$

where

$$\mathrm{Dirac}_{\rm RI} = \bar u_G(p_1^+) \left[\frac{q^+(p_1^+ - p_2^+)}{(p_1^+ + p_3^+)(p_2^+ + p_3^+)}\delta^{\lambda\eta} + \frac{q^+(p_1^+ + p_2^+ + 2p_3^+)}{(p_1^+ + p_3^+)(p_2^+ + p_3^+)} i\sigma^{\lambda\eta}\right]\gamma^+ v_G(p_2^+) . \tag{3.30}$$

4 UV safety

The diagrams SESW and $\overline{\rm SE}$SW, i.e. the quark- and antiquark self-energy corrections where the gluon crosses the shockwave, are UV divergent and need to be regularized by adding a counterterm, as we demonstrated in eqs. (3.11)–(3.16). These are the only diagrams we calculated that exhibit a UV singularity. There are, however, virtual contributions that we did not explicitly compute but whose UV poles will cancel with the one in our counterterms, resulting in a UV-finite total NLO amplitude. This is what we will now demonstrate.

First, comparing expression (3.12) for the UV counterterm with the LO amplitude (2.17), we can write:

$$\begin{aligned}\mathcal{M}_{\rm LO} + \mathcal{M}_{\rm SESW,UV} &= -i g_e e_f \mathrm{Dirac}^{\bar\lambda}_{\rm LO} \int_{\mathbf{x}_1,\mathbf{x}_2} e^{-i\mathbf{p}_1\cdot\mathbf{x}_1} e^{-i\mathbf{p}_2\cdot\mathbf{x}_2} A^{\bar\lambda}(\mathbf{x}_{12}) \\ &\quad \times \left(1 + \frac{\alpha_s C_F}{2\pi}\mathcal{V}_{\rm SESW,UV}\right)\left[U_{\mathbf{x}_1} U^\dagger_{\mathbf{x}_2} - 1\right] , \\ &= \mathcal{M}_{\rm LO}\left(1 + \frac{\alpha_s C_F}{2\pi}\mathcal{V}_{\rm SESW,UV}\right) ,\end{aligned} \tag{4.1}$$

where, in the last line, for future convenience we introduced a slight abuse of notation since

JHEP10(2022)184

the factorization of the term $\mathcal{V}_{\text{SESW,UV}}$ is really on the integrand level. This term reads:

$$\begin{aligned}\mathcal{V}_{\text{SESW,UV}} &= 2\pi \int_{k^+_{\text{min}}}^{p_1^+} \mathrm{d}k_3^+ \frac{k_3^+}{(p_1^+)^2}\left[\left(2\frac{p_1^+}{k_3^+}-1\right)^2+(D-3)\right] \\ &\quad\times \int_{\mathbf{x}_3} A^{\bar{\eta}}(\mathbf{x}_{13})\Big[A^{\bar{\eta}}(\mathbf{x}_{13})-A^{\bar{\eta}}(\mathbf{x}_{23})\Big]\,, \\ &= -E_{\text{gluon}}(p_1^+,k^+_{\text{min}})\frac{\Gamma(\frac{D}{2}-1)}{2\pi^{D/2-2}}\frac{1}{(\frac{D}{2}-2)}\frac{\mu^{4-D}}{(\mathbf{x}_{12}^2)^{\frac{D}{2}-2}}\,.\end{aligned} \tag{4.2}$$

To arrive at the above expression, we made use of eqs. (3.14) and (3.15) and introduced the following phase space integral over the gluon + momentum:

$$E_{\text{gluon}}(p_1^+,k^+_{\text{min}}) = \int_{k^+_{\text{min}}}^{p_1^+} \mathrm{d}k_3^+ \frac{k_3^+}{(p_1^+)^2}\left[\left(2\frac{p_1^+}{k_3^+}-1\right)^2+(D-3)\right]\,, \tag{4.3}$$

where k^+_{min} is a regulator which will be further specified in subsection (6.1). Writing $D = 4-2\epsilon_{\text{UV}}$, one can calculate further to obtain:

$$\frac{\Gamma(\frac{D}{2}-1)}{2\pi^{D/2-2}}\frac{1}{(\frac{D}{2}-2)}\frac{1}{(\mu^2\mathbf{x}_{12}^2)^{\frac{D}{2}-2}} = \frac{-1}{2}\left[\frac{1}{\epsilon_{\text{UV}}}+\gamma_E+\ln(\pi\mu^2\mathbf{x}_{12}^2)\right]+\mathcal{O}(\epsilon_{\text{UV}})\,, \tag{4.4}$$

and:

$$E_{\text{gluon}}(p_1^+,k^+_{\text{min}}) = -4\left(\ln\frac{k^+_{\text{min}}}{p_1^+}+\frac{3+\epsilon_{\text{UV}}}{4}\right)\,, \tag{4.5}$$

such that:

$$\mathcal{V}_{\text{SESW,UV}} = -2\left[\frac{1}{\epsilon_{\text{UV}}}+\gamma_E+\ln(\pi\mu^2\mathbf{x}_{12}^2)\right]\left(\ln\frac{k^+_{\text{min}}}{p_1^+}+\frac{3}{4}\right)-\frac{1}{2}\,. \tag{4.6}$$

There is a similar term stemming from when the antiquark self-energy loop scatters off the shockwave, which gives:

$$\mathcal{V}_{\overline{\text{SE}}\text{SW,UV}} = -2\left[\frac{1}{\epsilon_{\text{UV}}}+\gamma_E+\ln(\pi\mu^2\mathbf{x}_{12}^2)\right]\left(\ln\frac{k^+_{\text{min}}}{p_2^+}+\frac{3}{4}\right)-\frac{1}{2}\,, \tag{4.7}$$

hence in total:

$$\begin{aligned}\mathcal{V}_{\text{UV}} &= \mathcal{V}_{\text{SESW,UV}}+\mathcal{V}_{\overline{\text{SE}}\text{SW,UV}} \\ &= -2\left[\frac{1}{\epsilon_{\text{UV}}}+\gamma_E+\ln(\pi\mu^2\mathbf{x}_{12}^2)\right]\left[\frac{3}{2}+\ln\frac{k^+_{\text{min}}}{p_1^+}+\ln\frac{k^+_{\text{min}}}{p_2^+}\right]-1\,.\end{aligned} \tag{4.8}$$

In ref. [100] (see eq. 144 therein), it was demonstrated that the loop corrections to the initial state, which we did not explicitly calculate in this work, can be cast into a similar form factor $\mathcal{V}_{\text{IS}}$ as the one that appears in (4.1):

$$\mathcal{V}_{\text{IS}} = \left[\frac{1}{\epsilon_{\text{UV}}}+\gamma_E+\ln(\pi\mu^2\mathbf{x}_{12}^2)\right]\left[\frac{3}{2}+\ln\frac{k^+_{\text{min}}}{p_1^+}+\ln\frac{k^+_{\text{min}}}{p_2^+}\right]+\frac{1}{2}\ln^2\frac{p_1^+}{p_2^+}-\frac{\pi^2}{6}+3\,. \tag{4.9}$$

JHEP10(2022)184

Adding eqs. (4.8) and (4.9) gives:

$$\begin{aligned}\mathcal{V}_{\rm UV}+\mathcal{V}_{\rm IS} = &-\left[\frac{1}{\epsilon_{\rm UV}}+\gamma_E+\ln(\pi\mu^2\mathbf{x}_{12}^2)\right]\left[\frac{3}{2}+\ln\frac{k^+_{\rm min}}{p_1^+}+\ln\frac{k^+_{\rm min}}{p_2^+}\right]\\ &+\frac{1}{2}\ln^2\frac{p_1^+}{p_2^+}-\frac{\pi^2}{6}+2\,.\end{aligned} \tag{4.10}$$

Clearly, the initial-state loop corrections are not sufficient to fully cancel the UV poles from the SESW counterterms. A final ingredient is provided by the self-energy corrections to the quark and antiquark in the final state. We did not compute these diagrams explicitly, since they are simply zero. This is because in dimensional regularization the UV and IR contributions to a scaleless integral — such as self-energy loops on an asymptotic massless state — exactly cancel (cfr. eq. (3.14)). This property can, however, be exploited to construct the missing piece for the UV cancellation in (4.10), writing the total contribution of the asymptotic (anti)quark leg corrections as $\mathcal{V}_{\rm FS}=\mathcal{V}_{\rm FSUV}+\mathcal{V}_{\rm FSIR}=0$ with:

$$\begin{aligned}\mathcal{V}_{\rm FSUV} &= \left[\frac{1}{\epsilon_{\rm UV}}+\gamma_E+\ln(\pi\mu^2\mathbf{x}_{12}^2)\right]\left[\frac{3}{2}+\ln\frac{k^+_{\rm min}}{p_1^+}+\ln\frac{k^+_{\rm min}}{p_2^+}\right],\\ \mathcal{V}_{\rm FSIR} &= -\left[\frac{1}{\epsilon_{\rm IR}}+\gamma_E+\ln(\pi\mu^2\mathbf{x}_{12}^2)\right]\left[\frac{3}{2}+\ln\frac{k^+_{\rm min}}{p_1^+}+\ln\frac{k^+_{\rm min}}{p_2^+}\right],\end{aligned} \tag{4.11}$$

where we added subscripts to distinguish between positive infinitesimal numbers parameterizing the UV resp. IR pole.

Therefore, the sum of the leading-order diagram, the initial state loop corrections (4.9), the UV counterterms from the SESW and $\overline{\rm SE}$SW diagrams (4.8), and the UV-divergent part of the final-state corrections (4.11), is UV-finite:

$$\begin{aligned}\mathcal{M}_{\rm LO+IS+UV+FSUV} &\equiv \mathcal{M}_{\rm LO}+\mathcal{M}_{\rm SESW,UV}+\mathcal{M}_{\overline{\rm SE}{\rm SW,UV}}+\mathcal{M}_{\rm IS}+\mathcal{M}_{\rm FSUV}\\ &= \mathcal{M}_{\rm LO}\left(1+\frac{\alpha_s C_F}{2\pi}\mathcal{V}_{\rm UV}+\frac{\alpha_s C_F}{2\pi}\mathcal{V}_{\rm IS}+\frac{\alpha_s C_F}{2\pi}\mathcal{V}_{\rm FSUV}\right),\\ &= \mathcal{M}_{\rm LO}\left(1+\frac{\alpha_s C_F}{2\pi}\left(\frac{1}{2}\ln^2\frac{p_1^+}{p_2^+}-\frac{\pi^2}{6}+2\right)\right).\end{aligned} \tag{4.12}$$

After this procedure, all that is left from the cancellation of UV divergencies is the finite term above, together with a new contribution to the virtual diagrams which stems from the IR-divergent part of the asymptotic leg corrections (4.11):

$$\mathcal{M}_{\rm FSIR}=\mathcal{M}_{\rm LO}\,\frac{\alpha_s C_F}{2\pi}\mathcal{V}_{\rm FSIR}\,. \tag{4.13}$$

The above contribution will eventually cancel with the IR poles from the real NLO corrections (see section 8).

5 Soft safety in gluon exchange and interferences

A second type of infinities present in our calculation are soft divergences, which show up when the gluon momentum $\vec{k}_3=(k_3^+,\mathbf{k}_3)\to 0$. In this section, we show how they appear

JHEP10(2022)184

in virtual diagrams with a gluon exchange after the shockwave, or in the interference between diagrams with quark- or antiquark induced real final-state gluon radiation. We will demonstrate how they completely disappear from the final cross section, without any leftover large logarithms. There are, however, additional soft divergences that appear together with collinear ones, and which will be discussed in section 8.

It should be noted that soft divergences are distinct from the so-called rapidity divergences associated with $k_3^+ \to 0$ but where $\mathbf{k}_3$ stays finite. The latter will be regulated with a cutoff $k_{\min}^+$ and the remaining logarithms resummed by the JIMWLK equation (see section 6).

5.1 Virtual contributions

When computing the virtual diagrams in section 3.1, we have performed the integration over the transverse loop momentum $\mathbf{k}_3$. Therefore, the information on possible soft singularities has been lost. To investigate whether a diagram contains a soft divergence, one needs to rescale the gluon transverse momentum with its + momentum: $\mathbf{k}_3 \to \tilde{\mathbf{k}}_3 = (k_3^+/p_1^+)\mathbf{k}_3$ and then take the $k_3^+ \to 0$ limit. The only virtual diagrams with a soft singularity are the ones with a gluon exchange in the final state: GEFS and IFS (and their $q \leftrightarrow \bar{q}$ counterparts).

Let us start with the GEFS amplitude, (3.17), and perform a rescaling $\mathbf{K} = \chi\boldsymbol{\ell}/z$ with $\chi = k_3^+/p_2^+$ (remember the definitions $z = p_1^+/q^+$ and $\bar{z} = p_2^+/q^+$) in the transverse integral J (3.18):

$$\begin{aligned} J^{\eta'\bar{\eta}}(k_3^+, \mathbf{x}_{12}) = \frac{\chi^2}{z^2}\int_{\boldsymbol{\ell}} e^{-i\chi\boldsymbol{\ell}\cdot\mathbf{x}_{12}} \frac{(\chi/z)\boldsymbol{\ell}^{\eta'}}{(\chi/z)^2\boldsymbol{\ell}^2} \\ \times \frac{(\chi/z)\boldsymbol{\ell}^{\bar{\eta}} - (\chi/z)\mathbf{P}_\perp^{\bar{\eta}}}{\left((\chi/z)\boldsymbol{\ell} + (1-\frac{\bar{z}}{z}\chi)\mathbf{P}_\perp\right)^2 - (1+\chi)(1-\frac{\bar{z}}{z}\chi)\mathbf{P}_\perp^2 - i\epsilon} \,. \end{aligned} \tag{5.1}$$

The denominator tends to zero when $\chi \to 0$. Hence, after a first-order Taylor expansion, one obtains in the limit:

$$\lim_{k_3^+\to 0} J^{\eta'\bar{\eta}}(k_3^+, \mathbf{x}_{12}) = \frac{k_3^+ q^+}{p_1^+ p_2^+}\int_{\boldsymbol{\ell}} \frac{\boldsymbol{\ell}^{\eta'}}{\boldsymbol{\ell}^2} \frac{\boldsymbol{\ell}^{\bar{\eta}} - \mathbf{P}_\perp^{\bar{\eta}}}{2\boldsymbol{\ell}\cdot\mathbf{P}_\perp - \mathbf{P}_\perp^2 - i\epsilon} \,. \tag{5.2}$$

The only other source of powers $1/k_3^+$ in $\mathcal{M}_{\mathrm{GEFS}}$ is the Dirac structure, which needs to scale as $1/(k_3^+)^2$ in order to combine with the above integral to give a singularity. We can therefore pick up only the simple contribution $\mathrm{Dirac}^{\bar{\lambda}\bar{\eta}\eta'}_{\bar{q}\to q,(ii)}$ to the full Dirac structure (3.10), which gives:

$$\begin{aligned} \lim_{\text{soft}} \mathcal{M}_{\mathrm{GEFS}} = -i\frac{g_e e_f g_s^2}{\pi}\int_0^{p_1^+} \frac{\mathrm{d}k_3^+}{(k_3^+)^2}\frac{p_1^+ p_2^+}{q^+}\mathrm{Dirac}^{\bar{\lambda}}_{\mathrm{LO}} \\ \times \int_{\mathbf{x}_1,\mathbf{x}_2} e^{-i\mathbf{p}_1\cdot\mathbf{x}_1} e^{-i\mathbf{p}_2\cdot\mathbf{x}_2} A^{\bar{\lambda}}(\mathbf{x}_{12}) \lim_{k_3^+\to 0} J^{\eta'\eta'}(k_3^+, \mathbf{x}_{12}) \\ \times \left[t^c U_{\mathbf{x}_1} U^\dagger_{\mathbf{x}_2} t^c - C_F\right] \,. \end{aligned} \tag{5.3}$$

In the above expression, $\mathrm{Dirac}^{\bar{\lambda}}_{\mathrm{LO}}$ is the $q \leftrightarrow \bar{q}$ conjugate of the leading-order Dirac structure eq. (2.14)), obtained by interchanging $1 \leftrightarrow 2$ and taking the complex conjugate of the

JHEP10(2022)184

structure between the spinors (cfr. the algorithm in the beginning of section 3):

$$\text{Dirac}^{\bar{\lambda}}_{\text{LO}} \equiv \bar{u}^{s_1}_G(p_1^+)\gamma^+\left[(1-2\bar{z})\delta^{\lambda\bar{\lambda}} + i\sigma^{\lambda\bar{\lambda}}\right]v^{s_2}_G(p_2^+)\,. \tag{5.4}$$

Combined with the Kronecker delta from the Dirac structure, the soft limit of the integral J in (5.2) is thus reduced to two integrals which both can be analytically solved in dimensional regularization:

$$\begin{aligned} I_1 &= \int_\ell \frac{-1}{\mathbf{P}_\perp^2 - 2\boldsymbol{\ell}\cdot\mathbf{P}_\perp + i\epsilon}\,, \\ I_2 &= \int_\ell \frac{1}{\boldsymbol{\ell}^2}\frac{\boldsymbol{\ell}\cdot\mathbf{P}_\perp}{\mathbf{P}_\perp^2 - 2\boldsymbol{\ell}\cdot\mathbf{P}_\perp + i\epsilon}\,. \end{aligned} \tag{5.5}$$

Let us start with the integral I_2. Applying the 'real' resp. 'complex' Schwinger trick to the first and the second denominator:

$$\int_0^{+\infty}\mathrm{d}\alpha\, e^{-\alpha\Delta} = \frac{1}{\Delta}\,, \qquad \int_0^{+\infty}\mathrm{d}\beta\, e^{i\beta\Delta} = \frac{i}{\Delta+i\epsilon}\,, \tag{5.6}$$

we obtain

$$\begin{aligned} I_2 &= i\int_\ell\int_0^{+\infty}\mathrm{d}\alpha\mathrm{d}\beta\,\boldsymbol{\ell}\cdot\mathbf{P}_\perp e^{-\alpha\boldsymbol{\ell}^2}e^{i\beta\left(-2\mathbf{P}_\perp\cdot\boldsymbol{\ell}+\mathbf{P}_\perp^2\right)} \\ &\overset{\boldsymbol{\ell}\to\boldsymbol{\ell}+i\frac{\beta}{\alpha}\mathbf{P}_\perp}{=} i\int_\ell\int_0^{+\infty}\mathrm{d}\alpha\mathrm{d}\beta\left(\boldsymbol{\ell}-i\frac{\beta}{\alpha}\mathbf{P}_\perp\right)\cdot\mathbf{P}_\perp e^{-\alpha\boldsymbol{\ell}^2}e^{-\frac{\beta}{\alpha}(\beta-i\alpha)\mathbf{P}_\perp^2} \\ &= \frac{\mu^{4-D}\mathbf{P}_\perp^2}{(4\pi)^{\frac{D-2}{2}}}\int_0^{+\infty}\mathrm{d}\alpha\mathrm{d}\beta\,\frac{\beta}{\alpha^{D/2}}e^{-\frac{\beta}{\alpha}(\beta-i\alpha)\mathbf{P}_\perp^2}\,. \end{aligned} \tag{5.7}$$

Evaluating the integral over α, one finds:

$$I_2 = \frac{\mu^{4-D}(\mathbf{P}_\perp^2)^{2-\frac{D}{2}}}{(4\pi)^{\frac{D-2}{2}}}\Gamma\left(\frac{D}{2}-1\right)\int_0^{+\infty}\mathrm{d}\beta\,\beta^{3-D}e^{i\beta\mathbf{P}_\perp^2}\,. \tag{5.8}$$

Using the integral representation of the gamma function:

$$\frac{\Gamma(\alpha)}{A^\alpha} = \int_0^\infty \mathrm{d}t\, t^{\alpha-1}e^{-tA}\,, \tag{5.9}$$

we end up with:

$$I_2 = \frac{(-i)^{D-4}\mu^{4-D}(\mathbf{P}_\perp^2)^{\frac{D}{2}-2}}{(4\pi)^{\frac{D-2}{2}}}\Gamma\left(\frac{D}{2}-1\right)\Gamma(4-D)\,. \tag{5.10}$$

Writing $-i = e^{i(-\frac{\pi}{2}+2n\pi)}$ and $D = 4-2\epsilon_{\text{IR}}$:

$$I_2 = \frac{1}{8\pi}\left(\frac{1}{\epsilon_{\text{IR}}} - \gamma_E - \ln\left(\frac{\mathbf{P}_\perp^2}{4\pi\mu^2}\right) - 2i\pi\left(2n-\frac{1}{2}\right)\right) + \mathcal{O}(\epsilon_{\text{IR}})\,. \tag{5.11}$$

Likewise, applying (5.6) to the (finite) integral I_1 yields:

$$I_1 = -i\int_\ell\int_0^{+\infty}\mathrm{d}\beta\, e^{i\beta\left(-2\mathbf{P}_\perp\cdot\boldsymbol{\ell}+\mathbf{P}_\perp^2\right)}\,. \tag{5.12}$$

JHEP10(2022)184

The next step is to rewrite the $D-2$ dimensional $\boldsymbol{\ell}$-integration as follows:

$$\begin{aligned}\int_{\boldsymbol{\ell}} &= \frac{\mu^{4-D}}{(2\pi)^{D-2}} \int \mathrm{d}\Omega_{D-3} \int \mathrm{d}\cos\theta \int \mathrm{d}\ell\, \ell^{D-3}\,, \\ &= \frac{\mu^{4-D}}{(2\pi)^{D-2}} \frac{2\pi^{\frac{D-3}{2}}}{\Gamma(\frac{D-3}{2})} \int \mathrm{d}\cos\theta \int \mathrm{d}\ell\, \ell^{D-3}\,.\end{aligned} \tag{5.13}$$

The I_1 integral can then be evaluated starting with the integration over $\cos\theta$, followed by the β integral:

$$\begin{aligned} I_1 &= -2i \frac{\mu^{4-D}}{(4\pi)^{\frac{D-3}{2}}} \frac{1}{\Gamma(\frac{D-3}{2})} \int \mathrm{d}\ell\, \ell^{D-3} \int_0^{+\infty} \mathrm{d}\beta J_0(2\beta\ell|\mathbf{P}_\perp|) e^{i\beta\mathbf{P}_\perp^2}\,, \\ &= \frac{2\mu^{4-D}}{(4\pi)^{\frac{D-3}{2}}} \frac{1}{\Gamma(\frac{D-3}{2})} \frac{1}{\mathbf{P}_\perp^2} \int \mathrm{d}\ell\, \ell^{D-3} \frac{1}{\sqrt{1-4\ell^2/\mathbf{P}_\perp^2}}\,, \\ &= \frac{2\mu^{4-D}}{(4\pi)^{\frac{D-3}{2}}} \frac{1}{\Gamma(\frac{D-3}{2})} \frac{1}{\mathbf{P}_\perp^2} \frac{i 2^{1-D}}{\sqrt{\pi}} \Big(-\frac{1}{\mathbf{P}_\perp^2}\Big)^{1-D/2} \Gamma\Big(\frac{3-D}{2}\Big)\Gamma\Big(\frac{D-2}{2}\Big) \overset{D\to 4}{=} \frac{i}{4\pi}\,. \end{aligned} \tag{5.14}$$

We finally obtain:

$$\lim_{k_3^+\to 0} J^{\eta'\eta'}(k_3^+, \mathbf{x}_{12}) = \frac{k_3^+ q^+}{p_1^+ p_2^+} \frac{1}{8\pi} \left(\frac{1}{\epsilon_{\mathrm{IR}}} - \gamma_E - \ln\left(\frac{\mathbf{P}_\perp^2}{4\pi\mu^2}\right) - 2i\pi\left(2n - \frac{1}{2}\right) + 2i \right). \tag{5.15}$$

The soft limit of diagram IFS can be extracted in a similar way. Rescaling $\mathbf{k}_3 = \frac{k_3^+ q^+}{p_1^+ p_2^+}\boldsymbol{\ell} - \frac{k_3^+}{p_1^+}\mathbf{P}_\perp - \frac{k_3^+}{q^+}\mathbf{k}_\perp$ in eq. (3.20)):

$$\begin{aligned} &\int_{\mathbf{k}_3} \frac{e^{-i\mathbf{k}_3\cdot\mathbf{x}_{12}}}{\Big(\mathbf{k}_3 + \mathbf{P}_\perp + \frac{k_3^+}{q^+}\mathbf{k}_\perp\Big)^2 - \frac{(p_2^+ + k_3^+)(p_1^+ - k_3^+)}{p_1^+ p_2^+}\mathbf{P}_\perp^2 - i\epsilon} \\ &\qquad = \Big(\frac{k_3^+ q^+}{p_1^+ p_2^+}\Big)^2 \int_{\boldsymbol{\ell}} \frac{e^{-i\left(\frac{k_3^+ q^+}{p_1^+ p_2^+}\boldsymbol{\ell} - \frac{k_3^+}{p_1^+}\mathbf{P}_\perp - \frac{k_3^+}{q^+}\mathbf{k}_\perp\right)\cdot\mathbf{x}_{12}}}{\Big(\frac{k_3^+ q^+}{p_1^+ p_2^+}\boldsymbol{\ell} + \bar{\xi}\mathbf{P}_\perp\Big)^2 - \frac{(p_2^+ + k_3^+)(p_1^+ - k_3^+)}{p_1^+ p_2^+}\mathbf{P}_\perp^2 - i\epsilon}\,, \\ &\qquad \overset{\lim k_3^+\to 0}{\simeq} \Big(\frac{k_3^+ q^+}{p_1^+ p_2^+}\Big) \int_{\boldsymbol{\ell}} \frac{1}{2\boldsymbol{\ell}\cdot\mathbf{P}_\perp - \mathbf{P}_\perp^2 - i\epsilon} = \Big(\frac{k_3^+ q^+}{p_1^+ p_2^+}\Big) I_1\,. \end{aligned} \tag{5.16}$$

Combining this with eqs. (3.20), (5.3), and (5.15) yields (writing $\xi = k_3^+/p_1^+$):

$$\begin{aligned} \lim_{\text{soft}} (\mathcal{M}_{\mathrm{GEFS}} + \mathcal{M}_{\mathrm{IFS}}) = -i\frac{g_e e_f g_s^2}{\pi} \int \frac{\mathrm{d}\xi}{\xi} \mathrm{Dirac}_{\overline{\mathrm{LO}}} \int_{\mathbf{x}_1,\mathbf{x}_2} e^{-i\mathbf{p}_1\cdot\mathbf{x}_1} e^{-i\mathbf{p}_2\cdot\mathbf{x}_2} A^{\bar{\lambda}}(\mathbf{x}_{12}) \\ \times \frac{1}{8\pi}\left(\frac{1}{\epsilon_{\mathrm{IR}}} - \gamma_E - \ln\left(\frac{\mathbf{P}_\perp^2}{4\pi\mu^2}\right) - 2i\pi\left(2n - \frac{1}{2}\right)\right) \\ \times \left[t^c U_{\mathbf{x}_1} U_{\mathbf{x}_2}^\dagger t^c - C_F\right]. \end{aligned} \tag{5.17}$$

The IR pole will be canceled with certain real NLO corrections, as will be shown in the next subsection. This cancellation takes place on the level of the amplitude squared, obtained

JHEP10(2022)184

by multiplying with $\mathcal{M}^\dagger_{\rm LO}$. Adding as well the $q \leftrightarrow \bar{q}$ diagrams and the complex conjugate (c.c.), we obtain:

$$\begin{aligned}
&\lim_{\rm soft} \mathcal{M}^\dagger_{\rm LO}(\mathcal{M}_{\rm GEFS} + \mathcal{M}_{\rm IFS} + \mathcal{M}_{\overline{\rm GEFS}} + \mathcal{M}_{\overline{\rm IFS}}) + \text{c.c.} \\
&\quad = 64\alpha_{\rm em} e_f^2 \alpha_s N_c^2 p_1^+ p_2^+ (z^2 + \bar{z}^2) \int \frac{\mathrm{d}\xi}{\xi} \\
&\qquad \times \int_{\mathbf{x}_1, \mathbf{x}_2} e^{-i\mathbf{p}_1\cdot\mathbf{x}_{11'}} e^{-i\mathbf{p}_2\cdot\mathbf{x}_{22'}} A^{\bar{\lambda}}(\mathbf{x}_{12}) A^{\bar{\lambda}}(\mathbf{x}_{1'2'}) \times \left[\frac{1}{\epsilon_{\rm IR}} - \gamma_E - \ln\left(\frac{\mathbf{P}_\perp^2}{4\pi\mu^2}\right)\right] \\
&\qquad \times \left\langle s_{12}s_{2'1'} - s_{12} - s_{2'1'} + 1 - \frac{1}{N_c^2}\Big(Q_{122'1'} - s_{12} - s_{2'1'} + 1\Big)\right\rangle ,
\end{aligned} \tag{5.18}$$

where we made use of the spinor trace (2.22) with $D = 4$, as well as:

$$\mathrm{Tr}\Big(\mathrm{Dirac}^{\lambda'\dagger}_{\rm LO}\mathrm{Dirac}^{\bar{\lambda}}_{\rm LO}\Big) = -16 p_1^+ p_2^+ \delta^{\bar{\lambda}\lambda'}(z^2 + \bar{z}^2) \,. \tag{5.19}$$

5.2 Real contributions

The IR pole found in the previous subsection stems from a soft virtual gluon exchange in the final state. It will cancel with real contributions that have the same topology, i.e. a soft final-state gluon radiated from the quark in the amplitude (3.27) and from the antiquark in the complex conjugate amplitude, or vice versa. The corresponding contribution to the cross section is:

$$\begin{aligned}
&\int \mathrm{PS}(\vec{p}_3)\mathcal{M}^\dagger_{\overline{\rm QFS}}\mathcal{M}_{\rm QFS} = \int \frac{\mathrm{d}p_3^+}{4\pi p_3^+} g_e e_f^2 g_s^2 (p_3^+)^2 \frac{N_c^2}{2} \mathrm{Tr}\Big(\mathrm{Dirac}^{\eta'\lambda'\dagger}_{\overline{\rm QSW}}\mathrm{Dirac}^{\bar{\eta}\bar{\lambda}}_{\rm QSW}\Big) \\
&\times \int_{\mathbf{x}_{1'},\mathbf{x}_{2'},\mathbf{x}_1,\mathbf{x}_2} e^{-i\mathbf{p}_1\cdot\mathbf{x}_{11'}} e^{-i\mathbf{p}_2\cdot\mathbf{x}_{22'}} e^{-i\mathbf{p}_3\cdot\mathbf{x}_{12'}} A^{\lambda'}(\mathbf{x}_{1'2'}) A^{\bar{\lambda}}(\mathbf{x}_{12}) \\
&\times \int_{\mathbf{p}_3} \frac{(p_3^+\mathbf{p}_1 - p_1^+\mathbf{p}_3)^{\bar{\eta}}}{\big(p_3^+\mathbf{p}_1 - p_1^+\mathbf{p}_3\big)^2} \frac{(p_3^+\mathbf{p}_2 - p_2^+\mathbf{p}_3)^{\eta'}}{\big(p_3^+\mathbf{p}_2 - p_2^+\mathbf{p}_3\big)^2} \\
&\times \left\langle s_{12}s_{2'1'} - s_{12} - s_{2'1'} + 1 - \frac{1}{N_c^2}\Big(Q_{122'1'} - s_{12} - s_{2'1'} + 1\Big)\right\rangle .
\end{aligned} \tag{5.20}$$

Introducing $\mathbf{p}_3 = \frac{p_3^+}{p_1^+}\boldsymbol{\ell}$ and taking the $p_3^+ \to 0$ limit, the above equation becomes:

$$\begin{aligned}
&\int \mathrm{PS}(\vec{p}_3)\mathcal{M}^\dagger_{\overline{\rm QFS}}\mathcal{M}_{\rm QFS} = 64(2\pi)\alpha_{\rm em} e_f^2 \alpha_s N_c^2 p_1^+ (p_2^+)^2 (z^2 + \bar{z}^2) \int \frac{\mathrm{d}\xi}{\xi} \\
&\times \int_{\mathbf{x}_{1'},\mathbf{x}_{2'},\mathbf{x}_1,\mathbf{x}_2} e^{-i\mathbf{p}_1\cdot\mathbf{x}_{11'}} e^{-i\mathbf{p}_2\cdot\mathbf{x}_{22'}} A^{\bar{\lambda}}(\mathbf{x}_{1'2'}) A^{\bar{\lambda}}(\mathbf{x}_{12}) \int_{\boldsymbol{\ell}} \frac{(\boldsymbol{\ell} - \mathbf{p}_1)\cdot(p_1^+\mathbf{p}_2 - p_2^+\boldsymbol{\ell})}{(\boldsymbol{\ell} - \mathbf{p}_1)^2\left(p_1^+\mathbf{p}_2 - p_2^+\boldsymbol{\ell}\right)^2} \\
&\times \left\langle s_{12}s_{2'1'} - s_{12} - s_{2'1'} + 1 - \frac{1}{N_c^2}\Big(Q_{122'1'} - s_{12} - s_{2'1'} + 1\Big)\right\rangle ,
\end{aligned} \tag{5.21}$$

where we wrote $\mathrm{d}p_3^+/p_3^+ \to \mathrm{d}\xi/\xi$ and extracted the leading-power of the Dirac structure:

$$\lim_{p_3^+ \to 0} \mathrm{Dirac}^{\bar{\eta}\bar{\lambda}}_{\rm QSW} = 2\frac{p_1^+}{p_3^+}\delta^{\eta\bar{\eta}}\mathrm{Dirac}^{\bar{\lambda}}_{\rm LO} + \mathcal{O}((p_3^+)^0) \,, \tag{5.22}$$

JHEP10(2022)184

which leads to:

$$\lim_{p_3^+\to 0} \mathrm{Dirac}^{\eta'\lambda'\dagger}_{\mathrm{QSW}} \mathrm{Dirac}^{\bar{\eta}\bar{\lambda}}_{\overline{\mathrm{QSW}}} = -64\left(\frac{p_1^+ p_2^+}{p_3^+}\right)^2 (z^2+\bar{z}^2)\delta^{\bar{\lambda}\lambda'}\delta^{\eta'\bar{\eta}} + \mathcal{O}((p_3^+)^0)\,. \tag{5.23}$$

The integral over transverse momentum can be cast into the following form (where $\mathbf{P}_\perp$ is again the momentum vector defined in (3.19)):

$$\int_\ell \frac{(\boldsymbol{\ell}-\mathbf{p}_1)\cdot(p_1^+\mathbf{p}_2 - p_2^+\boldsymbol{\ell})}{(\boldsymbol{\ell}-\mathbf{p}_1)^2\left(p_1^+\mathbf{p}_2 - p_2^+\boldsymbol{\ell}\right)^2} = -\frac{\bar{z}}{q^+}\int_\ell \frac{1}{(\mathbf{P}_\perp+\bar{z}\boldsymbol{\ell})^2} - \frac{1}{q^+}\int_\ell \frac{\boldsymbol{\ell}\cdot\mathbf{P}_\perp}{\boldsymbol{\ell}^2(\mathbf{P}_\perp+\bar{z}\boldsymbol{\ell})^2}\,. \tag{5.24}$$

The first integral disappears in dimensional regularization because it is scaleless. The second one can be computed by applying the real Schwinger trick (5.6) twice:

$$\begin{aligned}
-\int_\ell \frac{\boldsymbol{\ell}\cdot\mathbf{P}_\perp}{q^+\boldsymbol{\ell}^2(\mathbf{P}_\perp+\bar{z}\boldsymbol{\ell})^2} &= -\frac{1}{p_2^+}\int_\ell \frac{\boldsymbol{\ell}\cdot\mathbf{p}}{\boldsymbol{\ell}^2(\boldsymbol{\ell}+\mathbf{p})^2} \\
&= \frac{1}{p_2^+}\frac{\mathbf{P}_\perp^2\mu^{4-D}}{(4\pi)^{\frac{D-2}{2}}}\frac{1}{2}(1+e^{i\pi D})(-1)^{-D/2}(\mathbf{P}_\perp^2)^{D/2-3}\Gamma(5-D)\Gamma\left(\frac{D}{2}-2\right), \\
&= -\frac{1}{p_2^+}\frac{1}{4\pi}\left[\frac{1}{\epsilon_{\mathrm{IR}}} - \gamma_E + 2in\pi - \ln\left(\frac{\mathbf{P}_\perp^2}{4\pi\mu^2}\right)\right],
\end{aligned} \tag{5.25}$$

where we wrote $-1 = e^{i(\pi+2n\pi)}$. Combining the above result with eq. (5.21) and adding the complex conjugate, we finally obtain:

$$\begin{aligned}
&\int \mathrm{PS}(\vec{p}_3)\mathcal{M}^\dagger_{\overline{\mathrm{QFS}}}\mathcal{M}_{\mathrm{QFS}} + \mathrm{c.c.} = -64\alpha_{\mathrm{em}}e_f^2\alpha_s N_c^2 p_1^+ p_2^+(z^2+\bar{z}^2)\int\frac{\mathrm{d}\xi}{\xi} \\
&\times \int_{\mathbf{x}_{1'},\mathbf{x}_{2'},\mathbf{x}_1,\mathbf{x}_2} e^{-i\mathbf{p}_1\cdot\mathbf{x}_{11'}}e^{-i\mathbf{p}_2\cdot\mathbf{x}_{22'}}A^{\bar{\lambda}}(\mathbf{x}_{1'2'})A^{\bar{\lambda}}(\mathbf{x}_{12})\left[\frac{1}{\epsilon_{\mathrm{IR}}} - \gamma_E - \ln\left(\frac{\mathbf{P}_\perp^2}{4\pi\mu^2}\right)\right] \\
&\times \left\langle s_{12}s_{2'1'} - s_{12} - s_{2'1'} + 1 - \frac{1}{N_c^2}\left(Q_{122'1'} - s_{12} - s_{2'1'} + 1\right)\right\rangle = -(9.3)\,.
\end{aligned} \tag{5.26}$$

The above result is exactly the opposite of the soft limit of the virtual contributions, eq. (5.18). Therefore, the total cross section is free from soft divergences from contributions with final-state gluon exchange topology (including interferences of real final-state gluon emission from the quark or the antiquark).

6 JIMWLK

6.1 Kinematics

So far, among the virtual NLO corrections to the dijet cross section that we have calculated, many have a logarithmically divergent integral over the + momentum k_3^+ of the virtual gluon stemming from the $k_3^+ \to 0$ regime. In some cases, like the SESW, UV contribution (3.12) or the IS contribution (4.9), in which the transverse loop integration can be performed explicitly, one could have used dimensional regularization to deal with these divergences. But in other cases, like the GESW contribution (3.5) or the SESW, sub contribution (3.16), the integration over the transverse position of the gluon $\mathbf{x}_3$ cannot be

JHEP10(2022)184

performed explicitly due to the presence of a Wilson line at $\mathbf{x}_3$. In such cases, dimensional regularization cannot handle the $k_3^+ \to 0$ singularities. For this reason, we regularize all divergent k_3^+ loop integrals in this work with a lower cutoff $k_{\min}^+$. Similarly, one encounters divergences in the real NLO corrections (at the cross section level) from the $p_3^+ \to 0$ regime in the integration over the real gluon + momentum p_3^+ (either inside or outside the measured jets, as we will see in sections 7 and 8), which we regularize with the same cutoff $k_{\min}^+$.

Part of these $k_3^+ \to 0$ or $p_3^+ \to 0$ divergences are genuine soft divergences which cancel at the dijet cross section level, as we have seen in the previous section 5. However, others are rapidity divergences which survive in the form of single logs of $k_{\min}^+$ after regularization. These large logs of $k_{\min}^+$ are high-energy leading logs, which can be extracted from the NLO correction to the cross section, and resummed into the LO term via the JIMWLK evolution of the target-averaged color- or Wilson-line operators, as we will now explain.

In the LO cross section (2.24), the target-averaged color operator is unevolved and should not yet include high-energy logarithms. We can, therefore, use the notation:

$$\Big\langle Q_{122'1'} - s_{12} - s_{2'1'} + 1 \Big\rangle_0 \,. \tag{6.1}$$

In the simplest scheme for the JIMWLK evolution, which we will use in most of the present study, JIMWLK is viewed as an evolution equation along the k^+ axis in logarithmic scale. In this scheme, one defines

$$\Big\langle Q_{122'1'} - s_{12} - s_{2'1'} + 1 \Big\rangle_{Y_f^+} \equiv \Big\langle Q_{122'1'} - s_{12} - s_{2'1'} + 1 \Big\rangle_{\ln(k_f^+/k_{\min}^+)} \tag{6.2}$$

as the same target-averaged operator but now including the resummation of high-energy leading logs associated with gluons with light-cone momentum k^+ between the cutoff $k_{\min}^+$ and the factorization scale k_f^+, in the notations of ref. [91]. The evolution with the factorization scale k_f^+, or equivalently with $Y_f^+ \equiv \ln(k_f^+/k_{\min}^+)$, is given by the JIMWLK equation for the LO operator:

$$\partial_{Y_f^+} \Big\langle Q_{122'1'} - s_{12} - s_{2'1'} + 1 \Big\rangle_{Y_f^+} = \Big\langle \hat{H}_{\text{JIMWLK}} (Q_{122'1'} - s_{12} - s_{2'1'} + 1) \Big\rangle_{Y_f^+} \,. \tag{6.3}$$

A more explicit version of this equation, with the action of the JIMWLK Hamiltonian $\hat{H}_{\text{JIMWLK}}$ fully worked out, can be found in ref. [117]. Integrating eq. (6.3), one finds

$$\begin{aligned} \Big\langle Q_{122'1'} - s_{12} - s_{2'1'} + 1 \Big\rangle_{Y_f^+} &= \Big\langle Q_{122'1'} - s_{12} - s_{2'1'} + 1 \Big\rangle_0 \\ &\quad + \int_0^{Y_f^+} \mathrm{d}Y^+ \Big\langle \hat{H}_{\text{JIMWLK}} (Q_{122'1'} - s_{12} - s_{2'1'} + 1) \Big\rangle_{Y^+} \,. \end{aligned} \tag{6.4}$$

The JIMWLK Hamiltonian is of order α_s. Hence, the dependence of a target-averaged operator on Y^+ is an effect suppressed by one extra power of α_s in fixed-order perturbation theory. Therefore, expanding eq. (6.4) in powers of α_s and reshuffling the terms, we can write:

$$\begin{aligned} \Big\langle Q_{122'1'} - s_{12} - s_{2'1'} + 1 \Big\rangle_0 &= \Big\langle Q_{122'1'} - s_{12} - s_{2'1'} + 1 \Big\rangle_{\ln(k_f^+/k_{\min}^+)} \\ &\quad - \ln(k_f^+/k_{\min}^+) \Big\langle \hat{H}_{\text{JIMWLK}} (Q_{122'1'} - s_{12} - s_{2'1'} + 1) \Big\rangle + \mathcal{O}(\alpha_s^2) \,, \end{aligned} \tag{6.5}$$

JHEP10(2022)184

with the scale unspecified for the operator in the second line, since it is not under control at this perturbative order. Hence, inserting eq. (6.5) into the LO cross section (2.24), one substitutes the unevolved target-averaged operator with its evolved (up to the factorization scale k_f^+) version, generating an extra NLO term which involves the JIMWLK Hamiltonian. This new NLO term will subtract the logarithmic dependence on the cutoff $k_{\min}^+$ found in the NLO cross section due to rapidity divergences at $k_3^+ \to 0$ or $p_3^+ \to 0$. Writing formally the NLO correction to the dijet cross section found from the fixed-order calculation as

$$\mathrm{d}\sigma_{\mathrm{NLO}} = \int_{k_{\min}^+}^{+\infty} \frac{\mathrm{d}p_3^+}{p_3^+} \mathrm{d}\tilde{\sigma}_{\mathrm{NLO}} \,, \tag{6.6}$$

to separate the gluon + momentum integral from the rest of the cross section (with other Heaviside or Dirac delta functions constraining p_3^+ included in $\tilde{\sigma}_{\mathrm{NLO}}$), one has:

$$\begin{aligned} \mathrm{d}\sigma_{\mathrm{NLO}} = & \int_{k_{\min}^+}^{k_f^+} \frac{\mathrm{d}p_3^+}{p_3^+} \hat{H}_{\mathrm{JIMWLK}} \mathrm{d}\sigma_{\mathrm{LO}} \\ & + \int_{k_{\min}^+}^{+\infty} \frac{\mathrm{d}p_3^+}{p_3^+} \Big[\mathrm{d}\tilde{\sigma}_{\mathrm{NLO}} - \theta(k_f^+ - p_3^+) \hat{H}_{\mathrm{JIMWLK}} \mathrm{d}\sigma_{\mathrm{LO}} \Big] \,. \end{aligned} \tag{6.7}$$

By construction, the first term in eq. (6.7), extracted from the total NLO correction, identically cancels the second term from eq. (6.5) after substituting the left hand side of eq. (6.5) into the LO cross section (2.24). Then, the statement that rapidity divergences are subtracted and resummed thanks to the JIMWLK evolution is equivalent to saying that in the second term of eq. (6.7), the cutoff $k_{\min}^+$ can be dropped, thanks to cancelations happening at low p_3^+ between the terms in the square bracket. In the rest of this section, we will check this statement, by studying the $p_3^+ \to 0$ (or $k_3^+ \to 0$) limit for each of the NLO contributions to the cross section.

Finally, we should discuss appropriate values for k_f^+ and $k_{\min}^+$ (and thus for Y_f^+) in order to resum high-energy logarithms via JIMWLK evolution. The factorization scale k_f^+ should be of the order of the + momenta of the measured jets (or at most q^+). The cutoff $k_{\min}^+$ represents the typical + momentum scale set by the valence (and other large-x) partons inside the target, before evolution. Modeling the target before low-x evolution as a collection of partons carrying a fraction of at least x_0 of the target momentum p_A^- and with a typical transverse mass Q_0, one has:

$$k_{\min}^+ = \frac{Q_0^2}{2x_0\, p_A^-} \,. \tag{6.8}$$

Moreover, we have chosen a frame in which the photon momentum $q^\mu = (q^+, 0, 0)$ lies entirely in the light-cone + direction, and the target nucleus $p_A^\mu = (p_A^+, p_A^-, 0)$ mostly in the light-cone − direction, up to $p_A^+ = M_A^2/2p_A^-$, where M_A is the target mass. Then, the total energy squared of the collision is

$$s = (q + p_A)^2 = 2q^+ p_A^- + M_A^2 \simeq 2q^+ p_A^- \tag{6.9}$$

at high energy. Hence, one can write the cutoff as

$$k_{\min}^+ \simeq \frac{q^+ Q_0^2}{x_0\, s} \,, \tag{6.10}$$

JHEP10(2022)184

and the range for JIMWLK evolution as

$$Y_f^+ = \ln\left(\frac{k_f^+}{k_{\min}^+}\right) = \ln\left(\frac{k_f^+ \, x_0 \, s}{q^+ Q_0^2}\right) \, . \tag{6.11}$$

For this reason, Y_f^+ is considered to be a high-energy logarithm. x_0 can be taken to be 0.01, or at most 0.1. Q_0 should be a scale around the transition between perturbative and non-perturbative QCD, or should be related to the initial saturation scale $Q_{s,0}$ in the case of a large enough nucleus. However, in practice, Q_0^2/x_0 can be treated as a parameter in a BK/JIMWLK global fit, together with the shape of the initial condition for the evolution.

The scheme chosen for the JIMWLK resummation, based on an evolution strictly along the p^+ axis, is particularly simple to handle. However, this scheme is not unique and, in fact, neither is it optimal as we will discuss in section 10.3, in particular for the study of Sudakov logarithms.

In the rest of this section, we start by considering the virtual NLO amplitudes and studying their $k_3^+ \to 0$ limit. After that, we bring them to the level of the cross section by multiplying them with the complex conjugate of the LO amplitude $\mathcal{M}_{\text{LO}}^\dagger$, constructing the total virtual contribution to JIMWLK. For the real NLO amplitudes the procedure is similar, as it turns out to be easiest to take the $p_3^+ \to 0$ limit at the amplitude level. Interestingly, we find that the thus obtained 'virtual' and 'real' contributions to JIMWLK are separately free of subleading-N_c terms. In the end, we demonstrate how in the $k_3^+, p_3^+ \to 0$ limit, the cross section corresponds to the JIMWLK evolution equations applied to the Wilson-line structure

$$Q_{122'1'} - s_{12} - s_{2'1'} + 1 \tag{6.12}$$

of the leading-order result, which is consistent with the resummation of high-energy logs by JIMWLK into the LO term, as presented in this section.

6.2 Virtual diagrams

GEFS+IFS. In the $k_3^+ \to 0$ limit, the subamplitude $\mathcal{M}_{\text{GEFS},(ii)+\text{IFS}}$ (3.22) becomes:

$$\begin{aligned}\lim_{k_3^+\to 0} \mathcal{M}_{\text{GEFS},(ii)+\text{IFS}} = i\frac{g_e e_f g_s^2}{\pi} \int_{k_{\min}^+}^{k_f^+} \frac{\mathrm{d}k_3^+}{k_3^+} \text{Dirac}_{\text{LO}}^{\bar\lambda} \times \left[t^c U_{\mathbf{x}_1} U_{\mathbf{x}_2}^\dagger t^c - C_F\right] \\ \times \int_{\mathbf{x}_1,\mathbf{x}_2} e^{-i\mathbf{p}_1\cdot\mathbf{x}_1} e^{-i\mathbf{p}_2\cdot\mathbf{x}_2} A^{\bar\lambda}(\mathbf{x}_{12}) \\ \times \int_{\mathbf{K}} \left(\frac{p_1^+}{q^+} + \frac{\mathbf{K}\cdot\mathbf{P}_\perp}{\mathbf{K}^2}\right) \frac{e^{-i\mathbf{K}\cdot\mathbf{x}_{12}}}{(\mathbf{K}+\mathbf{P}_\perp)^2 - \mathbf{P}_\perp^2 - i\epsilon} \, .\end{aligned} \tag{6.13}$$

There is another contribution to JIMWLK due to the $\text{Dirac}_{\bar q\to q,(i)}^{\bar\lambda\bar\eta\eta'}$ spinor structure in the amplitude $\mathcal{M}_{\text{GEFS}}$ (3.17), which yields:

$$\begin{aligned}\lim_{k_3^+\to 0} \mathcal{M}_{\text{GEFS},(i)} = -i\frac{g_e e_f g_s^2}{\pi} \int_{k_{\min}^+}^{k_f^+} \frac{\mathrm{d}k_3^+}{k_3^+} \frac{p_1^+ - p_2^+}{2q^+} \text{Dirac}_{\text{LO}}^{\bar\lambda} \times \left[t^c U_{\mathbf{x}_1} U_{\mathbf{x}_2}^\dagger t^c - C_F\right] \\ \times \int_{\mathbf{x}_1,\mathbf{x}_2} e^{-i\mathbf{p}_1\cdot\mathbf{x}_1} e^{-i\mathbf{p}_2\cdot\mathbf{x}_2} A^{\bar\lambda}(\mathbf{x}_{12}) \int_{\mathbf{K}} \frac{e^{-i\mathbf{K}\cdot\mathbf{x}_{12}}}{(\mathbf{K}+\mathbf{P}_\perp)^2 - \mathbf{P}_\perp^2 - i\epsilon} \, .\end{aligned} \tag{6.14}$$

JHEP10(2022)184

Subamplitudes eqs. (6.13) and (6.14) nicely combine into:

$$\begin{aligned}\lim_{k_3^+\to 0}\mathcal{M}_{\text{GEFS}} &\equiv \lim_{k_3^+\to 0}\Big(\mathcal{M}_{\text{GEFS},(ii)+\text{IFS}}+\mathcal{M}_{\text{GEFS},(i)}\Big)\\ &= i\frac{g_e e_f g_s^2}{2\pi}\int_{k_{\min}^+}^{k_f^+}\frac{\mathrm{d}k_3^+}{k_3^+}\text{Dirac}^{\bar\lambda}_{\text{LO}}\times\left[t^c U_{\mathbf{x}_1}U^\dagger_{\mathbf{x}_2}t^c-C_F\right]\\ &\quad\times\int_{\mathbf{x}_1,\mathbf{x}_2}e^{-i\mathbf{p}_1\cdot\mathbf{x}_1}e^{-i\mathbf{p}_2\cdot\mathbf{x}_2}A^{\bar\lambda}(\mathbf{x}_{12})\int_{\mathbf{K}}\frac{e^{-i\mathbf{K}\cdot\mathbf{x}_{12}}}{\mathbf{K}^2}\,.\end{aligned}\tag{6.15}$$

Finally, with the help of definition (2.16) of the Weizsäcker-Williams fields, it is easy to show that:

$$\int_{\mathbf{x}_3}A^{\eta'}(\mathbf{x}_{13})A^{\eta'}(\mathbf{x}_{23})=-\int_{\mathbf{x}_3}\int_{\boldsymbol{\ell}}\int_{\mathbf{k}}e^{-i\boldsymbol{\ell}\cdot\mathbf{x}_{13}}e^{-i\mathbf{k}\cdot\mathbf{x}_{23}}\frac{\boldsymbol{\ell}\cdot\mathbf{k}}{\boldsymbol{\ell}^2\mathbf{k}^2}=\int_{\mathbf{K}}\frac{e^{-i\mathbf{K}\cdot\mathbf{x}_{12}}}{\mathbf{K}^2}\,.\tag{6.16}$$

Multiplying with the complex conjugate of the leading-order amplitude, we finally obtain:

$$\begin{aligned}&\lim_{k_3^+\to 0}\mathcal{M}^\dagger_{\text{LO}}\mathcal{M}_{\text{GEFS}}=64\pi\alpha_{\text{em}}e_f^2\alpha_s N_c p_1^+p_2^+(z^2+\bar z^2)\int_{k_{\min}^+}^{k_f^+}\frac{\mathrm{d}k_3^+}{k_3^+}\\ &\times\int_{\mathbf{x}_{1'},\mathbf{x}_{2'},\mathbf{x}_1,\mathbf{x}_2}e^{-i\mathbf{p}_1\cdot\mathbf{x}_{11'}}e^{-i\mathbf{p}_2\cdot\mathbf{x}_{22'}}A^{\bar\lambda}(\mathbf{x}_{12})A^{\bar\lambda}(\mathbf{x}_{1'2'})\int_{\mathbf{x}_3}A^{\eta'}(\mathbf{x}_{13})A^{\eta'}(\mathbf{x}_{23})\\ &\times\left\langle s_{12}s_{2'1'}-s_{12}-s_{2'1'}+1-\frac{1}{N_c^2}\Big(Q_{122'1'}-s_{12}-s_{2'1'}+1\Big)\right\rangle\\ &=\lim_{k_3^+\to 0}\mathcal{M}^\dagger_{\text{LO}}\mathcal{M}_{\overline{\text{GE}}\text{FS}}\,.\end{aligned}\tag{6.17}$$

GESW. Since the modified Weizsäcker-Williams structure is finite in the limit $k_3^+\to 0$:

$$\lim_{k_3^+\to 0}\mathcal{A}^{\bar\lambda}\left(\frac{p_2^+\mathbf{x}_{12}+k_3^+\mathbf{x}_{13}}{p_2^++k_3^+},\frac{k_3^+}{p_2^++k_3^+}\mathbf{x}_{32};\frac{q^+p_2^+}{k_3^+(p_1^+-k_3^+)}\right)=A^{\bar\lambda}(\mathbf{x}_{12})\,,\tag{6.18}$$

the only contribution to JIMWLK from this diagram, see eq. (3.5), comes from the $\text{Dirac}_{q\to\bar q(ii)}$ term:

$$\begin{aligned}\lim_{k_3^+\to 0}\mathcal{M}_{\text{GESW}}&=-\frac{ig_e e_f g_s^2}{\pi}\int_{k_{\min}^+}^{k_f^+}\frac{\mathrm{d}k_3^+}{k_3^+}\text{Dirac}^{\bar\lambda}_{\text{LO}}\\ &\quad\times\int_{\mathbf{x}_1,\mathbf{x}_2,\mathbf{x}_3}e^{-i\mathbf{p}_1\cdot\mathbf{x}_1}e^{-i\mathbf{p}_2\cdot\mathbf{x}_2}A^{\eta'}(\mathbf{x}_{31})A^{\eta'}(\mathbf{x}_{32})A^{\bar\lambda}(\mathbf{x}_{12})\\ &\quad\times\Big[t^cU_{\mathbf{x}_1}t^dU^\dagger_{\mathbf{x}_2}W^{dc}_{\mathbf{x}_3}-C_F\Big]\,.\end{aligned}\tag{6.19}$$

After multiplying with $\mathcal{M}^\dagger_{\text{LO}}$, making use of eq. (5.19), one obtains:

$$\begin{aligned}&\lim_{k_3^+\to 0}\mathcal{M}^\dagger_{\text{LO}}\mathcal{M}_{\text{GESW}}=-128\pi\alpha_{\text{em}}e_f^2\alpha_s N_c^2 p_1^+p_2^+(z^2+\bar z^2)\int_{k_{\min}^+}^{k_f^+}\frac{\mathrm{d}k_3^+}{k_3^+}\\ &\times\int_{\mathbf{x}_{1'},\mathbf{x}_{2'},\mathbf{x}_1,\mathbf{x}_2,\mathbf{x}_3}e^{-i\mathbf{p}_1\cdot\mathbf{x}_{11'}}e^{-i\mathbf{p}_2\cdot\mathbf{x}_{22'}}A^{\bar\lambda}(\mathbf{x}_{12})A^{\bar\lambda}(\mathbf{x}_{1'2'})A^{\eta'}(\mathbf{x}_{31})A^{\eta'}(\mathbf{x}_{32})\\ &\times\left\langle Q_{322'1'}s_{13}-s_{13}s_{32}-s_{2'1'}+1-\frac{1}{N_c^2}\Big(Q_{122'1'}-s_{12}-s_{2'1'}+1\Big)\right\rangle\,.\end{aligned}\tag{6.20}$$

JHEP10(2022)184

It is easy to see that the $q \leftrightarrow \bar{q}$ counterpart of this diagram will give the contribution:

$$\begin{aligned}\lim_{k_3^+\to 0} \mathcal{M}_{\mathrm{LO}}^\dagger \mathcal{M}_{\overline{\mathrm{GESW}}} &= -128\pi\alpha_{\mathrm{em}} e_f^2 \alpha_s N_c^2 p_1^+ p_2^+ (z^2+\bar{z}^2) \int_{k_{\min}^+}^{k_f^+} \frac{\mathrm{d}k_3^+}{k_3^+} \\ &\times \int_{\mathbf{x}_{1'},\mathbf{x}_{2'},\mathbf{x}_1,\mathbf{x}_2,\mathbf{x}_3} e^{-i\mathbf{p}_1\cdot\mathbf{x}_{11'}} e^{-i\mathbf{p}_2\cdot\mathbf{x}_{22'}} A^{\bar{\lambda}}(\mathbf{x}_{12}) A^{\bar{\lambda}}(\mathbf{x}_{1'2'}) A^{\eta'}(\mathbf{x}_{31}) A^{\eta'}(\mathbf{x}_{32}) \\ &\times \left\langle Q_{2'1'13} s_{32} - s_{13} s_{32} - s_{2'1'} + 1 - \frac{1}{N_c^2}\Big(Q_{122'1'} - s_{12} - s_{2'1'} + 1\Big)\right\rangle .\end{aligned} \tag{6.21}$$

SESW, sub. Taking the $k_3^+ \to 0$ limit of (3.16) is trivial and yields, after multiplying with $\mathcal{M}_{\mathrm{LO}}^\dagger$:

$$\begin{aligned}\lim_{k_3^+\to 0} \mathcal{M}_{\mathrm{LO}}^\dagger \mathcal{M}_{\mathrm{SESW,sub}} &= 128\pi\alpha_{\mathrm{em}} e_f^2 \alpha_s N_c^2 p_1^+ p_2^+ (z^2+\bar{z}^2) \int_{k_{\min}^+}^{k_f^+} \frac{\mathrm{d}k_3^+}{k_3^+} \\ &\times \int_{\mathbf{x}_{1'},\mathbf{x}_{2'},\mathbf{x}_1,\mathbf{x}_2,\mathbf{x}_3} e^{-i\mathbf{p}_1\cdot\mathbf{x}_{11'}} e^{-i\mathbf{p}_2\cdot\mathbf{x}_{22'}} A^{\bar{\lambda}}(\mathbf{x}_{1'2'}) A^{\bar{\lambda}}(\mathbf{x}_{12}) A^{\eta'}(\mathbf{x}_{31}) \\ &\times \Bigg\{ A^{\eta'}(\mathbf{x}_{31}) \left\langle Q_{322'1'} s_{13} - s_{13} s_{32} - s_{2'1'} + 1 - \frac{1}{N_c^2}\Big(Q_{122'1'} - s_{12} - s_{2'1'} + 1\Big)\right\rangle \\ &\quad - \Big(A^{\eta'}(\mathbf{x}_{31}) - A^{\eta'}(\mathbf{x}_{32})\Big)\left(1 - \frac{1}{N_c^2}\right)\left\langle Q_{122'1'} - s_{12} - s_{2'1'} + 1\right\rangle \Bigg\} .\end{aligned} \tag{6.22}$$

Likewise, we get for the diagram with a gluon loop on the antiquark:

$$\begin{aligned}\lim_{k_3^+\to 0} \mathcal{M}_{\mathrm{LO}}^\dagger \mathcal{M}_{\overline{\mathrm{SESW}},\mathrm{sub}} &= 128\pi\alpha_{\mathrm{em}} e_f^2 \alpha_s N_c^2 p_1^+ p_2^+ (z^2+\bar{z}^2) \int_{k_{\min}^+}^{k_f^+} \frac{\mathrm{d}k_3^+}{k_3^+} \\ &\times \int_{\mathbf{x}_{1'},\mathbf{x}_{2'},\mathbf{x}_1,\mathbf{x}_2,\mathbf{x}_3} e^{-i\mathbf{p}_1\cdot\mathbf{x}_{11'}} e^{-i\mathbf{p}_2\cdot\mathbf{x}_{22'}} A^{\bar{\lambda}}(\mathbf{x}_{1'2'}) A^{\bar{\lambda}}(\mathbf{x}_{12}) A^{\eta'}(\mathbf{x}_{32}) \\ &\times \Bigg\{ A^{\eta'}(\mathbf{x}_{32}) \left\langle Q_{132'1'} s_{32} - s_{13} s_{32} - s_{2'1'} + 1 - \frac{1}{N_c^2}\Big(Q_{122'1'} - s_{12} - s_{2'1'} + 1\Big)\right\rangle \\ &\quad - \Big(A^{\eta'}(\mathbf{x}_{32}) - A^{\eta'}(\mathbf{x}_{31})\Big)\left(1 - \frac{1}{N_c^2}\right)\left\langle Q_{122'1'} - s_{12} - s_{2'1'} + 1\right\rangle \Bigg\} .\end{aligned} \tag{6.23}$$

FSIR. The last set of virtual diagrams that exhibit a rapidity divergency and hence contribute to JIMWLK are the IR parts of the self-energy corrections to the asymptotic (anti)quark, eq. (4.13):

$$\lim_{k_3^+\to 0} \mathcal{M}_{\mathrm{FSIR}} = \mathcal{M}_{\mathrm{LO}} \times \frac{\alpha_s C_F}{2\pi} \lim_{k_3^+\to 0} \mathcal{V}_{\mathrm{FSIR}} , \tag{6.24}$$

where, from eq. (3.15):

$$\begin{aligned}\lim_{k_3^+\to 0} \mathcal{V}_{\mathrm{FSIR}} &= 2\left[\frac{1}{\epsilon_{\mathrm{IR}}} + \gamma_E + \ln(\pi\mu^2\mathbf{x}_{12}^2)\right] \int_{k_{\min}^+}^{k_f^+} \frac{\mathrm{d}k_3^+}{k_3^+} , \\ &= -8\pi \int_{\mathbf{x}_3} A^{\eta'}(\mathbf{x}_{13}) A^{\eta'}(\mathbf{x}_{23}) \int_{k_{\min}^+}^{k_f^+} \frac{\mathrm{d}k_3^+}{k_3^+} .\end{aligned} \tag{6.25}$$

JHEP10(2022)184

Multiplying with $\mathcal{M}_{\rm LO}^\dagger$:

$$\begin{aligned}
&\lim_{k_3^+\to 0}\mathcal{M}_{\rm LO}^\dagger\mathcal{M}_{\rm FSIR} = |\mathcal{M}_{\rm LO}|^2\times\frac{\alpha_s C_F}{2\pi}\lim_{k_3^+\to 0}\mathcal{V}_{\rm FSIR}\,,\\
&= -128\pi\alpha_{\rm em}e_f^2\alpha_s N_c^2 p_1^+p_2^+(z^2+\bar z^2)\int_{k_{\rm min}^+}^{k_f^+}\frac{{\rm d}k_3^+}{k_3^+}\\
&\quad\times\int_{\mathbf{x}_1,\mathbf{x}_2,\mathbf{x}_{1'},\mathbf{x}_{2'}} e^{-i\mathbf{p}_1\cdot\mathbf{x}_{11'}}e^{-i\mathbf{p}_2\cdot\mathbf{x}_{22'}}A^{\bar\lambda}(\mathbf{x}_{12})A^{\bar\lambda}(\mathbf{x}_{1'2'})\int_{\mathbf{x}_3}A^{\eta'}(\mathbf{x}_{13})A^{\eta'}(\mathbf{x}_{23})\\
&\quad\times\left(1-\frac{1}{N_c^2}\right)\Big\langle Q_{122'1'}-s_{12}-s_{2'1'}+1\Big\rangle\,.
\end{aligned}\tag{6.26}$$

Total virtual contribution to JIMWLK. Collecting all the above virtual contributions to JIMWLK, we finally obtain:

$$\begin{aligned}
&\lim_{k_3^+\to 0}\mathcal{M}_{\rm LO}^\dagger\Big(\mathcal{M}_{\rm GEFS}+\mathcal{M}_{\overline{\rm GE}\rm FS}+\mathcal{M}_{\rm GESW}+\mathcal{M}_{\overline{\rm GE}\rm SW}\\
&\qquad+\mathcal{M}_{\rm SESW,sub}+\mathcal{M}_{\overline{\rm SE}\rm SW,sub}+\mathcal{M}_{\rm FSIR}\Big)\\
&= 128\pi\alpha_{\rm em}e_f^2\alpha_s N_c^2 p_1^+p_2^+(z^2+\bar z^2)\int_{k_{\rm min}^+}^{k_f^+}\frac{{\rm d}k_3^+}{k_3^+}\\
&\quad\times\int_{\mathbf{x}_{1'},\mathbf{x}_{2'},\mathbf{x}_1,\mathbf{x}_2} e^{-i\mathbf{p}_1\cdot\mathbf{x}_{11'}}e^{-i\mathbf{p}_2\cdot\mathbf{x}_{22'}}A^{\bar\lambda}(\mathbf{x}_{12})A^{\bar\lambda}(\mathbf{x}_{1'2'})\\
&\quad\times\int_{\mathbf{x}_3}A^{\eta'}(\mathbf{x}_{13})A^{\eta'}(\mathbf{x}_{23})\Big\langle s_{12}s_{2'1'}-s_{12}-s_{2'1'}+1\Big\rangle\\
&\quad+A^{\eta'}(\mathbf{x}_{13})\Big(A^{\eta'}(\mathbf{x}_{13})-A^{\eta'}(\mathbf{x}_{23})\Big)\Big\langle Q_{322'1'}s_{13}-s_{13}s_{32}-s_{2'1'}+1\Big\rangle\\
&\quad+A^{\eta'}(\mathbf{x}_{23})\Big(A^{\eta'}(\mathbf{x}_{23})-A^{\eta'}(\mathbf{x}_{13})\Big)\Big\langle Q_{132'1'}s_{32}-s_{13}s_{32}-s_{2'1'}+1\Big\rangle\\
&\quad-\Big(A^{\eta'}(\mathbf{x}_{13})-A^{\eta'}(\mathbf{x}_{23})\Big)\Big(A^{\eta'}(\mathbf{x}_{13})-A^{\eta'}(\mathbf{x}_{23})\Big)\Big\langle Q_{122'1'}-s_{12}-s_{2'1'}+1\Big\rangle\\
&\quad-A^{\eta'}(\mathbf{x}_{13})A^{\eta'}(\mathbf{x}_{23})\Big\langle Q_{122'1'}-s_{12}-s_{2'1'}+1\Big\rangle\,.
\end{aligned}\tag{6.27}$$

An interesting feature of the above formula is that all subleading-N_c contributions have cancelled.

6.3 Real diagrams

Taking the $p_3^+\to 0$ limit of the real gluon emission amplitudes $\mathcal{M}_{\rm QSW}$ and $\mathcal{M}_{\rm QFS}$, eqs. (3.25) and (3.28), is very straightforward due to the simple leading-power behavior (5.22) of the Dirac structure:

$$\begin{aligned}
\lim_{p_3^+\to 0}\mathcal{M}_{\rm QFS} &= 2g_e e_f g_s{\rm Dirac}_{\rm LO}^{\bar\lambda}\int_{\mathbf{x}_1,\mathbf{x}_2,\mathbf{x}_3}e^{-i\mathbf{p}_1\cdot\mathbf{x}_1}e^{-i\mathbf{p}_2\cdot\mathbf{x}_2}e^{-i\mathbf{p}_3\cdot\mathbf{x}_3}\\
&\quad\times A^{\bar\lambda}(\mathbf{x}_{12})A^{\eta}(\mathbf{x}_{13})\Big[t^dU_{\mathbf{x}_1}U^\dagger_{\mathbf{x}_2}-t^d\Big]\,,
\end{aligned}\tag{6.28}$$

$$\begin{aligned}
\lim_{p_3^+\to 0}\mathcal{M}_{\rm QSW} &= -2g_e e_f g_s{\rm Dirac}_{\rm LO}^{\bar\lambda}\int_{\mathbf{x}_1,\mathbf{x}_2,\mathbf{x}_3}e^{-i\mathbf{p}_1\cdot\mathbf{x}_1}e^{-i\mathbf{p}_2\cdot\mathbf{x}_2}e^{-i\mathbf{p}_3\cdot\mathbf{x}_3}\\
&\quad\times A^{\bar\lambda}(\mathbf{x}_{12})A^{\eta}(\mathbf{x}_{13})\Big[U_{\mathbf{x}_1}U^\dagger_{\mathbf{x}_3}t^dU_{\mathbf{x}_3}U^\dagger_{\mathbf{x}_2}-t^d\Big]\,.
\end{aligned}\tag{6.29}$$

JHEP10(2022)184

Care should be taken with the amplitudes $\mathcal{M}_{\overline{\text{QFS}}}$ and $\mathcal{M}_{\overline{\text{QSW}}}$, which as we remarked in section 3, receive an additional minus sign from the LCPT Feynman rules due to the $\bar{q} \to \bar{q}g$ vertex:

$$\lim_{p_3^+ \to 0} \mathcal{M}_{\overline{\text{QFS}}} = 2 g_e e_f g_s \text{Dirac} \frac{\bar{\lambda}}{\text{LO}} \int_{\mathbf{x}_1, \mathbf{x}_2, \mathbf{x}_3} e^{-i\mathbf{p}_1 \cdot \mathbf{x}_1} e^{-i\mathbf{p}_2 \cdot \mathbf{x}_2} e^{-i\mathbf{p}_3 \cdot \mathbf{x}_3} \times A^{\bar{\lambda}}(\mathbf{x}_{12}) A^{\eta}(\mathbf{x}_{23}) \Big[U_{\mathbf{x}_1} U^{\dagger}_{\mathbf{x}_2} t^d - t^d \Big] , \tag{6.30}$$

$$\lim_{p_3^+ \to 0} \mathcal{M}_{\overline{\text{QSW}}} = -2 g_e e_f g_s \text{Dirac} \frac{\bar{\lambda}}{\text{LO}} \int_{\mathbf{x}_1, \mathbf{x}_2, \mathbf{x}_3} e^{-i\mathbf{p}_1 \cdot \mathbf{x}_1} e^{-i\mathbf{p}_2 \cdot \mathbf{x}_2} e^{-i\mathbf{p}_3 \cdot \mathbf{x}_3} \times A^{\bar{\lambda}}(\mathbf{x}_{12}) A^{\eta}(\mathbf{x}_{23}) \Big[U_{\mathbf{x}_1} U^{\dagger}_{\mathbf{x}_3} t^d U_{\mathbf{x}_3} U^{\dagger}_{\mathbf{x}_2} - t^d \Big] . \tag{6.31}$$

With the above expressions, constructing the real part of the JIMWLK equation is a trivial task, yielding:

$$\begin{aligned}
&\lim_{p_3^+ \to 0} \int \text{PS}(\vec{p}_3) \big| \mathcal{M}_{\text{QFS}} + \mathcal{M}_{\overline{\text{QFS}}} + \mathcal{M}_{\text{QSW}} + \mathcal{M}_{\overline{\text{QSW}}} \big|^2 \\
&= 128 \pi \alpha_{\text{em}} e_f^2 \alpha_s p_1^+ p_2^+ N_c^2 (z^2 + \bar{z}^2) \int_{k_{\min}^+}^{k_f^+} \frac{\mathrm{d}p_3^+}{p_3^+} \\
&\quad \times \int_{\mathbf{x}_{1'}, \mathbf{x}_{2'}, \mathbf{x}_1, \mathbf{x}_2} e^{-i\mathbf{p}_1 \cdot \mathbf{x}_{11'}} e^{-i\mathbf{p}_2 \cdot \mathbf{x}_{22'}} A^{\lambda}(\mathbf{x}_{12}) A^{\lambda}(\mathbf{x}_{1'2'}) \\
&\quad \times \int_{\mathbf{x}_3} \Big(A^{\eta}(\mathbf{x}_{13}) A^{\eta}(\mathbf{x}_{1'3}) + A^{\eta}(\mathbf{x}_{23}) A^{\eta}(\mathbf{x}_{2'3}) \Big) \Big\langle Q_{122'1'} - s_{12} - s_{2'1'} + 1 \Big\rangle \\
&\quad - \Big(A^{\eta}(\mathbf{x}_{13}) A^{\eta}(\mathbf{x}_{2'3}) + A^{\eta}(\mathbf{x}_{23}) A^{\eta}(\mathbf{x}_{1'3}) \Big) \Big\langle s_{12} s_{2'1'} - s_{12} - s_{2'1'} + 1 \Big\rangle \\
&\quad + \Big(A^{\eta}(\mathbf{x}_{13}) A^{\eta}(\mathbf{x}_{1'3}) - A^{\eta}(\mathbf{x}_{23}) A^{\eta}(\mathbf{x}_{1'3}) - A^{\eta}(\mathbf{x}_{13}) A^{\eta}(\mathbf{x}_{2'3}) + A^{\eta}(\mathbf{x}_{23}) A^{\eta}(\mathbf{x}_{2'3}) \Big) \\
&\quad \times \Big\langle s_{11'} s_{2'2} - s_{13} s_{32} - s_{2'3} s_{31'} + 1 \Big\rangle \\
&\quad - A^{\eta}(\mathbf{x}_{1'3}) \Big(A^{\eta}(\mathbf{x}_{13}) - A^{\eta}(\mathbf{x}_{23}) \Big) \Big\langle Q_{322'1'} s_{13} - s_{13} s_{32} - s_{2'1'} + 1 \Big\rangle \\
&\quad - A^{\eta}(\mathbf{x}_{13}) \Big(A^{\eta}(\mathbf{x}_{1'3}) - A^{\eta}(\mathbf{x}_{2'3}) \Big) \Big\langle Q_{122'3} s_{31'} - s_{31'} s_{2'3} - s_{12} + 1 \Big\rangle \\
&\quad + A^{\eta}(\mathbf{x}_{2'3}) \Big(A^{\eta}(\mathbf{x}_{13}) - A^{\eta}(\mathbf{x}_{23}) \Big) \Big\langle Q_{2'1'13} s_{32} - s_{13} s_{32} - s_{2'1'} + 1 \Big\rangle \\
&\quad + A^{\eta}(\mathbf{x}_{23}) \Big(A^{\eta}(\mathbf{x}_{1'3}) - A^{\eta}(\mathbf{x}_{2'3}) \Big) \Big\langle Q_{31'12} s_{2'3} - s_{31'} s_{2'3} - s_{12} + 1 \Big\rangle .
\end{aligned} \tag{6.32}$$

Just like in the case of the virtual diagrams, all subleading-N_c contributions have cancelled.

6.4 Full JIMWLK limit

Combining eq. (6.32) with eq. (6.27) and its complex conjugate, we obtain:

$$\begin{aligned}
&\lim_{p_3^+ \to 0} \int \text{PS}(\vec{p}_3) \big| \mathcal{M}_{\text{real}} \big|^2 + \lim_{k_3^+ \to 0} \big| \mathcal{M}_{\text{virtual}} \big|^2 \\
&= 64 \pi \alpha_{\text{em}} e_f^2 p_1^+ p_2^+ N_c (z^2 + \bar{z}^2) \int_{\mathbf{x}_{1'}, \mathbf{x}_{2'}, \mathbf{x}_1, \mathbf{x}_2} e^{-i\mathbf{p}_1 \cdot \mathbf{x}_{11'}} e^{-i\mathbf{p}_2 \cdot \mathbf{x}_{22'}} A^{\lambda}(\mathbf{x}_{12}) A^{\lambda}(\mathbf{x}_{1'2'})
\end{aligned}$$

JHEP10(2022)184

$$\times\left(\frac{\alpha_s N_c}{(2\pi)^2}\int_{k^+_{\min}}^{k^+_f}\frac{\mathrm{d}k^+_3}{k^+_3}\right)\int_{\mathbf{x}_3}\Big\{-\mathcal{K}_1(\mathbf{x}_1,\mathbf{x}_2,\mathbf{x}_{2'},\mathbf{x}_{1'};\mathbf{x}_3)\times\langle Q_{122'1'}\rangle \tag{6.33}$$
$$+\mathcal{A}(\mathbf{x}_1,\mathbf{x}_2,\mathbf{x}_{2'},\mathbf{x}_{1'};\mathbf{x}_3)\times\langle s_{11'}s_{2'2}\rangle+\mathcal{B}(\mathbf{x}_1,\mathbf{x}_2,\mathbf{x}_{2'},\mathbf{x}_{1'};\mathbf{x}_3)\times\langle s_{12}s_{2'1'}\rangle$$
$$+\mathcal{K}_2(\mathbf{x}_1;\mathbf{x}_2,\mathbf{x}_{1'};\mathbf{x}_3)\times\langle Q_{322'1'}s_{13}\rangle+\text{c.c.}$$
$$+\mathcal{K}_2(\mathbf{x}_2;\mathbf{x}_1,\mathbf{x}_{2'};\mathbf{x}_3)\times\langle Q_{2'1'13}s_{32}\rangle+\text{c.c.}+2\frac{\mathbf{x}_{12}^2}{\mathbf{x}_{13}^2\mathbf{x}_{23}^2}\langle s_{12}-s_{13}s_{32}\rangle+\text{c.c.}\Big\}\,.$$

The above expression is the JIMWLK equation for $|\mathcal{M}_{\mathrm{LO}}|^2$, eq. (2.23), consisting in the evolution of the quadrupole $Q_{122'1'}$ (eq. 4 in ref. [117]) and, in the last line, of the dipole s_{12} and its complex conjugate. We have, therefore, proven what we asserted in eq. (6.7), namely that the part of the cross section $\mathrm{d}\sigma$ enhanced by large logarithms $\ln(k_f^+/k_{\min}^+)$ takes the form $\hat{H}_{\mathrm{JIMWLK}}\mathrm{d}\sigma_{\mathrm{LO}}$.

The structures $\mathcal{A}$,$\mathcal{B}$,$\mathcal{K}_1$ and $\mathcal{K}_2$ in eq. (6.33) are defined according to the notation in [117], and read:

$$\begin{aligned}\mathcal{A}(\mathbf{x}_1,\mathbf{x}_2,\mathbf{x}_{2'},\mathbf{x}_{1'};\mathbf{x}_3)&=2(2\pi)^2\Big(A^\eta(\mathbf{x}_{13})A^\eta(\mathbf{x}_{1'3})-A^\eta(\mathbf{x}_{23})A^\eta(\mathbf{x}_{1'3})\\&\qquad-A^\eta(\mathbf{x}_{13})A^\eta(\mathbf{x}_{2'3})+A^\eta(\mathbf{x}_{23})A^\eta(\mathbf{x}_{2'3})\Big)\,,\\&=\frac{\mathbf{x}_{1'2}^2}{\mathbf{x}_{1'3}^2\mathbf{x}_{23}^2}+\frac{\mathbf{x}_{2'1}^2}{\mathbf{x}_{2'3}^2\mathbf{x}_{13}^2}-\frac{\mathbf{x}_{1'1}^2}{\mathbf{x}_{1'3}^2\mathbf{x}_{13}^2}-\frac{\mathbf{x}_{2'2}^2}{\mathbf{x}_{2'3}^2\mathbf{x}_{23}^2}\,,\end{aligned} \tag{6.34}$$

$$\begin{aligned}\mathcal{B}(\mathbf{x}_1,\mathbf{x}_2,\mathbf{x}_{2'},\mathbf{x}_{1'};\mathbf{x}_3)&=2(2\pi)^2\Big(A^\eta(\mathbf{x}_{13})A^\eta(\mathbf{x}_{23})+A^\eta(\mathbf{x}_{1'3})A^\eta(\mathbf{x}_{2'3})\\&\qquad-A^\eta(\mathbf{x}_{13})A^\eta(\mathbf{x}_{2'3})-A^\eta(\mathbf{x}_{23})A^\eta(\mathbf{x}_{1'3})\Big)\,,\\&=\frac{\mathbf{x}_{12'}^2}{\mathbf{x}_{13}^2\mathbf{x}_{2'3}^2}+\frac{\mathbf{x}_{1'2}^2}{\mathbf{x}_{1'3}^2\mathbf{x}_{23}^2}-\frac{\mathbf{x}_{12}^2}{\mathbf{x}_{13}^2\mathbf{x}_{23}^2}-\frac{\mathbf{x}_{1'2'}^2}{\mathbf{x}_{1'3}^2\mathbf{x}_{2'3}^2}\,,\end{aligned} \tag{6.35}$$

$$\begin{aligned}\mathcal{K}_1(\mathbf{x}_1,\mathbf{x}_2,\mathbf{x}_{2'},\mathbf{x}_{1'};\mathbf{x}_3)&=-2(2\pi)^2\Big(A^\eta(\mathbf{x}_{13})A^\eta(\mathbf{x}_{1'3})+A^\eta(\mathbf{x}_{23})A^\eta(\mathbf{x}_{2'3})\\&\quad-A^\eta(\mathbf{x}_{13})A^\eta(\mathbf{x}_{13})+A^\eta(\mathbf{x}_{13})A^\eta(\mathbf{x}_{23})-A^\eta(\mathbf{x}_{23})A^\eta(\mathbf{x}_{23})\\&\quad-A^\eta(\mathbf{x}_{1'3})A^\eta(\mathbf{x}_{1'3})+A^\eta(\mathbf{x}_{2'3})A^\eta(\mathbf{x}_{1'3})-A^\eta(\mathbf{x}_{2'3})A^\eta(\mathbf{x}_{2'3})\Big)\,,\\&=\frac{\mathbf{x}_{11'}^2}{\mathbf{x}_{13}^2\mathbf{x}_{1'3}^2}+\frac{\mathbf{x}_{12}^2}{\mathbf{x}_{13}^2\mathbf{x}_{23}^2}+\frac{\mathbf{x}_{22'}^2}{\mathbf{x}_{23}^2\mathbf{x}_{2'3}^2}+\frac{\mathbf{x}_{1'2'}^2}{\mathbf{x}_{1'3}^2\mathbf{x}_{2'3}^2}\,,\end{aligned} \tag{6.36}$$

$$\begin{aligned}\mathcal{K}_2(\mathbf{x}_1;\mathbf{x}_2,\mathbf{x}_{1'};\mathbf{x}_3)&=2(2\pi)^2\Big(A^\eta(\mathbf{x}_{13})-A^\eta(\mathbf{x}_{1'3})\Big)\Big(A^\eta(\mathbf{x}_{13})-A^\eta(\mathbf{x}_{23})\Big)\,,\\&=\frac{\mathbf{x}_{12}^2}{\mathbf{x}_{23}^2\mathbf{x}_{13}^2}+\frac{\mathbf{x}_{11'}^2}{\mathbf{x}_{13}^2\mathbf{x}_{1'3}^2}-\frac{\mathbf{x}_{21'}^2}{\mathbf{x}_{23}^2\mathbf{x}_{1'3}^2}\,.\end{aligned} \tag{6.37}$$

7 Jet definition

In the previous sections, we were always concerned with partonic scattering amplitudes, hiding any hadronic physics inside the nonperturbative CGC averages over the Wilson lines. The aim of this work, however, is to compute the NLO *dijet* photoproduction cross section, not the diquark one, which implies that at a certain point we need to quantify what we mean by a jet.

JHEP10(2022)184

At leading order, transforming the $\gamma+A\to q+\bar{q}+X$ cross section to the $\gamma+A\to\text{dijet}+X$ one is trivial and done by simply identifying the quark and antiquark partonic momenta $\vec{p}_1$ and $\vec{p}_2$ with the jet momenta $\vec{p}_{j1}$ and $\vec{p}_{j2}$. This same trivial identification can be done for the virtual NLO contributions to the cross section. It is implicitly assumed that the outgoing momenta are sufficiently separated to prevent the quark and antiquark being grouped within the same jet.

For the real NLO corrections, the situation is different. In this case, two steps are needed to go from the tree-level $\gamma+A\to q+\bar{q}+g+X$ partonic cross section to the real NLO correction to the dijet cross section. First, a jet algorithm needs to be applied in order to determine in what part of the phase space the three partons are considered to form three separate jets, and in what part two of the partons are clustered into a single jet. Second, in the case of the three jet configuration, in order to obtain the corresponding contribution to the inclusive dijet cross section at NLO, two jets should be identified with the measured jets with momenta $\vec{p}_{j1}$ and $\vec{p}_{j2}$ while the third jet should be integrated over.

The jet definition or algorithm that we use in this NLO calculation is as follows: if two partons i and j in the final state are such that

$$\frac{(p_i^+ + p_j^+)}{|\mathbf{p}_i + \mathbf{p}_j|}\left|\frac{\mathbf{p}_i}{p_i^+} - \frac{\mathbf{p}_j}{p_j^+}\right| < R\,, \tag{7.1}$$

then they are considered to be part of the same jet with momentum $(p_i^+ + p_j^+, \mathbf{p}_i + \mathbf{p}_j)$. Otherwise, the partons i and j are considered to form separate jets. This definition depends on the jet radius parameter R, satisfying $0 < R < 1$.

In the present study, for simplicity and in order to be able to perform analytic calculations as far as possible, we are using our jet definition in the narrow-jet limit, meaning that formally $R \to 0$. In practice, this means that terms in $\log(R)$ or terms independent of R are kept in the cross section, whereas terms suppressed as positive powers of R are neglected. In diagrams without a collinear divergence, one can then always identify each of the three partons with a separate jet, because the merging of two partons into one jet takes place only in a parametrically small part of the phase space, suppressed by powers of R. The only real NLO corrections that exhibit a collinear divergence are $|\mathcal{M}_{\text{QFS}}|^2$ and $|\mathcal{M}_{\overline{\text{QFS}}}|^2$. In the narrow-jet limit, these two squared amplitudes are, therefore, the only contributions to the cross section in which one needs to distinguish whether the quark (resp. antiquark) and the gluon are clustered into a single jet or not by the jet algorithm.

As a remark, when the left hand side of eq. (7.1) is much smaller than 1, one has the equivalence

$$\frac{(p_i^+ + p_j^+)}{|\mathbf{p}_i + \mathbf{p}_j|}\left|\frac{\mathbf{p}_i}{p_i^+} - \frac{\mathbf{p}_j}{p_j^+}\right| \sim \sqrt{(\Delta y_{ij})^2 + (\Delta\phi_{ij})^2}\,, \tag{7.2}$$

where Δy_{ij} and $\Delta\phi_{ij}$ are the difference in rapidity and in azimuthal angle between the two partons. For this reason, our jet algorithm and the Cambridge/Aachen algorithm (see refs. [118, 119]) become equivalent in the narrow-jet limit $R \to 0$.

Moreover, in the case of three-jet configurations, we always consider the quark jet to be the first measured jet, the antiquark jet to be the second measured jet, and the gluon

JHEP10(2022)184

jet to be the jet which is unmeasured and integrated over. Hence, the results we present correspond specifically to the flavor-tagged inclusive quark-antiquark dijet cross section at NLO. Other contributions to the full inclusive dijet cross section at NLO, for example with a gluon jet and a quark jet, do not involve any conceptual difficulty (in particular, they do not contain any divergence whatsoever), and could be obtained in a straightforward way from our intermediate results on the quark-antiquark-gluon partonic cross section.

From the $|\mathcal{M}_{\mathrm{QFS}}|^2$ contribution to the $q\bar{q}g$ partonic cross section

$$\begin{aligned}\frac{\mathrm{d}\sigma_{q\bar{q}g}^{|\mathrm{QFS}|^2}}{\mathrm{d}p_1^+\mathrm{d}^{D-2}\mathbf{p}_1\mathrm{d}p_2^+\mathrm{d}^{D-2}\mathbf{p}_2\mathrm{d}p_3^+\mathrm{d}^{D-2}\mathbf{p}_3} &= \frac{\theta(p_1^+)}{(2\pi)^{D-1}2p_1^+}\frac{\theta(p_2^+)}{(2\pi)^{D-1}2p_2^+}\frac{\theta(p_3^+)}{(2\pi)^{D-1}2p_3^+} \\ &\quad\times\frac{2\pi\delta(q^+-p_1^+-p_2^+-p_3^+)}{2q^+}\frac{1}{(D-2)}|\mathcal{M}_{\mathrm{QFS}}|^2\,,\end{aligned} \tag{7.3}$$

applying our jet definition in the narrow-jet limit, we thus obtain two contributions to the dijet cross section. The first one, in which each of the three partons is forming a jet and in which the gluon jet is integrated over, reads

$$\begin{aligned}&\frac{\mathrm{d}\sigma_{\mathrm{dijet}}^{|\mathrm{QFS}|^2;\,\mathrm{out}}}{\mathrm{d}p_{j1}^+\mathrm{d}^{D-2}\mathbf{p}_{j1}\mathrm{d}p_{j2}^+\mathrm{d}^{D-2}\mathbf{p}_{j2}} \\ &\quad=\int\mathrm{PS}(\vec{p}_3)\,\Big[1-\theta_{\mathrm{in}}(\vec{p}_{j1},\vec{p}_3)\Big]\frac{\mathrm{d}\sigma_{q\bar{q}g}^{|\mathrm{QFS}|^2}}{\mathrm{d}p_{j1}^+\mathrm{d}^{D-2}\mathbf{p}_{j1}\mathrm{d}p_{j2}^+\mathrm{d}^{D-2}\mathbf{p}_{j2}\mathrm{d}p_3^+\mathrm{d}^{D-2}\mathbf{p}_3} \\ &\quad=\frac{\theta(p_{j1}^+)}{(2\pi)^{D-1}2p_{j1}^+}\frac{\theta(p_{j2}^+)}{(2\pi)^{D-1}2p_{j2}^+}\int\mathrm{PS}(\vec{p}_3)\,\frac{2\pi\delta(q^+-p_{j1}^+-p_{j2}^+-p_3^+)}{2q^+} \\ &\qquad\times\Big[1-\theta_{\mathrm{in}}(\vec{p}_{j1},\vec{p}_3)\Big]\frac{1}{(D-2)}|\mathcal{M}_{\mathrm{QFS}}|^2\Big|_{\vec{p}_1=\vec{p}_{j1};\,\vec{p}_2=\vec{p}_{j2}}\,.\end{aligned} \tag{7.4}$$

We have excluded the region in which the quark and the gluon are merged into one jet thanks to $\theta_{\mathrm{in}}(\vec{p}_i,\vec{p}_j)$, which is defined as

$$\theta_{\mathrm{in}}(\vec{p}_i,\vec{p}_j)=\theta\bigg((\mathbf{p}_i+\mathbf{p}_j)^2R^2-(p_i^++p_j^+)^2\Big(\frac{\mathbf{p}_i}{p_i^+}-\frac{\mathbf{p}_j}{p_j^+}\Big)^2\bigg) \tag{7.5}$$

and enforces the condition (7.1). The second contribution, in which the quark and the gluon are combined into one jet of momentum $\vec{p}_{j1}=\vec{p}_1+\vec{p}_3$ whereas the antiquark forms a jet of momentum $\vec{p}_{j2}=\vec{p}_2$, reads

$$\begin{aligned}&\frac{\mathrm{d}\sigma_{\mathrm{dijet}}^{|\mathrm{QFS}|^2;\,\mathrm{in}}}{\mathrm{d}p_{j1}^+\mathrm{d}^{D-2}\mathbf{p}_{j1}\mathrm{d}p_{j2}^+\mathrm{d}^{D-2}\mathbf{p}_{j2}}=\frac{\theta(p_{j1}^+)}{(2\pi)^{D-1}2p_{j1}^+}\frac{\theta(p_{j2}^+)}{(2\pi)^{D-1}2p_{j2}^+}\frac{2\pi\delta(q^+-p_{j1}^+-p_{j2}^+)}{2q^+} \\ &\times\int\mathrm{PS}(\vec{p}_3)\theta_{\mathrm{in}}(\vec{p}_{j1}-\vec{p}_3,\vec{p}_3)\theta(p_{j1}^+-p_3^+)\frac{p_{j1}^+}{(p_{j1}^+-p_3^+)}\frac{1}{(D-2)}|\mathcal{M}_{\mathrm{QFS}}|^2\Big|_{\vec{p}_1=\vec{p}_{j1}-\vec{p}_3;\vec{p}_2=\vec{p}_{j2}}\,.\end{aligned} \tag{7.6}$$

For the $|\mathcal{M}_{\overline{\mathrm{QFS}}}|^2$ contribution, which is the square of the gluon emission by the antiquark in the final state, one obtains two contributions to the NLO dijet cross section in a

JHEP10(2022)184

similar way. Their expressions are the same as eqs. (7.4) and (7.6), up to the exchange of the role of the quark and the antiquark, meaning in particular $\vec{p}_1 \leftrightarrow \vec{p}_2$ and $\vec{p}_{j1} \leftrightarrow \vec{p}_{j2}$.

Finally, for all the contributions to the $q\bar{q}g$ partonic cross section other than $|\mathcal{M}_{\mathrm{QFS}}|^2$ and $|\mathcal{M}_{\overline{\mathrm{QFS}}}|^2$, which are collinear safe, we go from the partonic to the dijet cross section by integrating over the gluon momentum and identifying the produced quark and antiquark with the measured jets, as

$$\frac{\mathrm{d}\sigma_{\mathrm{dijet}}^{\text{NLO real; coll. safe diags.}}}{\mathrm{d}p_{j1}^+\mathrm{d}^{D-2}\mathbf{p}_{j1}\mathrm{d}p_{j2}^+\mathrm{d}^{D-2}\mathbf{p}_{j2}} = \int \mathrm{PS}(\vec{p}_3)\, \frac{\mathrm{d}\sigma_{q\bar{q}g}^{\text{coll. safe diags.}}\big|_{\vec{p}_1\to\vec{p}_{j1},\vec{p}_2\to\vec{p}_{j2}}}{\mathrm{d}p_{j1}^+\mathrm{d}^{D-2}\mathbf{p}_{j1}\mathrm{d}p_{j2}^+\mathrm{d}^{D-2}\mathbf{p}_{j2}\mathrm{d}p_3^+\mathrm{d}^{D-2}\mathbf{p}_3}\,. \tag{7.7}$$

8 Collinear and soft safety in final state fragmentation

As already mentioned in the previous section, the real contributions $|\mathrm{QFS}|^2$ and $|\overline{\mathrm{Q}}\mathrm{FS}|^2$ to the dijet cross section have collinear divergences. Such divergences come from the transverse integration, and we are handling them with dimensional regularization. In addition, these diagrams also lead to soft divergences at the dijet cross section level. In our regularization scheme, using dimensional regularization for transverse integrals and the cutoff k_{min}^+ for the p_3^+ integral, it is difficult to distinguish unambiguously between genuine soft divergences and rapidity divergences, since both arise from the $p_3^+ \to 0$ regime. In this section, after calculating the real contributions from $|\mathrm{QFS}|^2$ to the dijet cross section, we will show that the collinear and soft divergences cancel when the real corrections $|\mathrm{QFS}|^2$ and $|\overline{\mathrm{Q}}\mathrm{FS}|^2$ are added to the virtual corrections FSIR and $\mathrm{FSIR}^\dagger$. This is evident from the fact that, in the resulting sum, the only leftover singularity is the rapidity divergence associated with the JIMWLK evolution (section 6).

In order to calculate the real correction $|\mathrm{QFS}|^2$ to the dijet cross section, following the discussion in section 7, we first split it into the *in* contribution (7.6), in which the quark and the gluon belong to the same jet, and the *out* contribution (7.4), in which they form separate jets.

The amplitude for the diagram QFS is given in eq. (3.27). Squaring it and summing over the colors, helicities and the photon polarization, one finds

$$\begin{aligned}
|\mathcal{M}_{\mathrm{QFS}}|^2 = {} & (4\pi)^2\alpha_{\mathrm{em}}e_f^2\alpha_s C_F N_c 8 p_1^+ p_2^+ (p_3^+)^2 \\
& \times \left[2\left(\frac{p_1^+ + p_3^+}{q^+}\right)^2 + 2\left(\frac{p_2^+}{q^+}\right)^2 + (D-4)\right]\left[\left(1+2\frac{p_1^+}{p_3^+}\right)^2 + (D-3)\right] \\
& \times \frac{1}{(p_3^+\mathbf{p}_1 - p_1^+\mathbf{p}_3)^2}\int_{\mathbf{x}_1,\mathbf{x}_2,\mathbf{x}_{1'},\mathbf{x}_{2'}} e^{-i(\mathbf{p}_1+\mathbf{p}_3)\cdot\mathbf{x}_{11'}} e^{-i\mathbf{p}_2\cdot\mathbf{x}_{22'}} A^{\bar{\lambda}}(\mathbf{x}_{12}) A^{\bar{\lambda}}(\mathbf{x}_{1'2'}) \\
& \times \left\langle Q_{122'1'} - s_{12} - s_{2'1'} + 1\right\rangle .
\end{aligned} \tag{8.1}$$

8.1 Contribution $|\mathrm{QFS}|^2$; in

When the gluon and the quark are merged into a single jet by the jet algorithm, we have by definition $\vec{p}_1 + \vec{p}_3 = \vec{p}_{j1}$. Introducing the transverse momentum of the gluon relative to the one of jet $j1$

$$\mathbf{P}_3 \equiv \mathbf{p}_3 - \frac{p_3^+}{p_{j1}^+}\mathbf{p}_{j1}\,, \tag{8.2}$$

JHEP10(2022)184

one can rewrite the denominator of eq. (8.1) as

$$(p_3^+\mathbf{p}_1 - p_1^+\mathbf{p}_3)^2 = (p_{j1}^+)^2\mathbf{P}_3^2 \,, \tag{8.3}$$

Then, comparing with the LO squared amplitude (2.23), eq. (8.1) becomes:

$$\begin{aligned}\left|\mathcal{M}_{\text{QFS}}\right|^2\Big|_{\vec{p}_1=\vec{p}_{j1}-\vec{p}_3} &= \left|\mathcal{M}_{\text{LO}}\right|^2_{\vec{p}_{1,2}\to\vec{p}_{j1,j2}} \\ &\quad\times 4\pi\alpha_s C_F \frac{(p_3^+)^2(p_{j1}^+-p_3^+)}{(p_{j1}^+)^3\mathbf{P}_3^2}\left[\left(1+2\frac{(p_{j1}^+-p_3^+)}{p_3^+}\right)^2+(D-3)\right] .\end{aligned} \tag{8.4}$$

Moreover, with the notation (8.2),

$$\theta_{\text{in}}(\vec{p}_1,\vec{p}_3) = \theta_{\text{in}}(\vec{p}_{j1}-\vec{p}_3,\vec{p}_3) = \theta\left(\mathbf{p}_{j1}^2R^2 - \frac{(p_{j1}^+)^4}{(p_{j1}^+-p_3^+)^2\,(p_3^+)^2}\mathbf{P}_3^2\right) . \tag{8.5}$$

Inserting eqs. (8.4) and (8.5) into eq. (7.6), one finds that the inside jet radiation contribution from $|\text{QFS}|^2$ factorizes as

$$\frac{\mathrm{d}\sigma_{\text{dijet}}^{|\text{QFS}|^2;\,\text{in}}}{\mathrm{d}p_{j1}^+\mathrm{d}^{D-2}\mathbf{p}_{j1}\mathrm{d}p_{j2}^+\mathrm{d}^{D-2}\mathbf{p}_{j2}} = \frac{\mathrm{d}\sigma_{\text{LO}}^{\text{dijet}}}{\mathrm{d}p_{j1}^+\mathrm{d}^{D-2}\mathbf{p}_{j1}\mathrm{d}p_{j2}^+\mathrm{d}^{D-2}\mathbf{p}_{j2}} \times \frac{\alpha_s C_F}{2\pi}\mathcal{V}_{|\text{QFS}|^2}^{\text{in}} \,, \tag{8.6}$$

where

$$\begin{aligned}\mathcal{V}_{|\text{QFS}|^2}^{\text{in}} &= (2\pi)(4\pi)\int \text{PS}(\vec{p}_3)\,\theta(p_{j1}^+-p_3^+)\,\frac{1}{(p_{j1}^+)^2\mathbf{P}_3^2} \\ &\quad\times\theta\left(\frac{(p_{j1}^+-p_3^+)^2(p_3^+)^2}{(p_{j1}^+)^4}\mathbf{p}_{j1}^2R^2-\mathbf{P}_3^2\right)\left[(2p_{j1}^+-p_3^+)^2+(D-3)(p_3^+)^2\right] .\end{aligned} \tag{8.7}$$

In eq. (8.7), the transverse integral is straightforward to calculate in dimensional regularization, and yields

$$\begin{aligned}&4\pi\mu^{4-D}\int\frac{\mathrm{d}^{D-2}\mathbf{P}_3}{(2\pi)^{D-2}}\frac{1}{\mathbf{P}_3^2}\theta\left(\frac{(p_{j1}^+-p_3^+)^2\,(p_3^+)^2}{(p_{j1}^+)^4}\mathbf{p}_{j1}^2R^2-\mathbf{P}_3^2\right) \\ &\quad= -\frac{1}{\epsilon_{\text{coll}}}\frac{1}{\Gamma(1-\epsilon)}\left[\frac{(p_{j1}^+-p_3^+)^2(p_3^+)^2}{(p_{j1}^+)^4}\frac{\mathbf{p}_{j1}^2R^2}{4\pi\mu^2}\right]^{-\epsilon} \\ &\quad= -\frac{1}{\epsilon_{\text{coll}}}+\gamma_E+\ln\frac{\mathbf{p}_{j1}^2}{4\pi\mu^2}+2\ln R+2\ln\frac{p_3^+}{p_{j1}^+}+2\ln\left(\frac{p_{j1}^+-p_3^+}{p_{j1}^+}\right)+\mathcal{O}(\epsilon) .\end{aligned} \tag{8.8}$$

Note that we perform the $D\to 4$ expansion before taking the integration over p_3^+, since in our scheme, only transverse integrals (and thus UV and collinear divergences) are regulated with dimensional regularization, whereas p_3^+-integrals are always regulated with the lower cutoff k_{min}^+.

JHEP10(2022)184

Thus, eq. (8.7) becomes:

$$\begin{aligned}\mathcal{V}^{\text{in}}_{|\text{QFS}|^2} &= \int_{k^+_{\min}}^{p^+_{j1}} \frac{\mathrm{d}p_3^+}{2p_3^+}\,\frac{1}{(p^+_{j1})^2}\Big[4(p^+_{j1})^2 - 4p^+_{j1}p_3^+ + 2(1-\epsilon)(p_3^+)^2\Big] \\ &\quad\times\left[-\frac{1}{\epsilon_{\text{coll}}} + \gamma_E + \ln\frac{\mathbf{p}^2_{j1}}{4\pi\mu^2} + 2\ln R + 2\ln\frac{p_3^+}{p^+_{j1}} + 2\ln\left(\frac{p^+_{j1}-p_3^+}{p^+_{j1}}\right) + \mathcal{O}(\epsilon)\right] \\ &= \left(-\frac{3}{2} + 2\ln\frac{p^+_{j1}}{k^+_{\min}}\right)\left(-\frac{1}{\epsilon_{\text{coll}}} + \gamma_E + \ln\frac{\mathbf{p}^2_{j1}}{4\pi\mu^2} + 2\ln R\right) \\ &\quad - 2\left(\ln\frac{p^+_{j1}}{k^+_{\min}}\right)^2 - \frac{2\pi^2}{3} + \frac{13}{2} + \mathcal{O}(\epsilon)\,.\end{aligned} \tag{8.9}$$

As explained in section 6.1, $k^+_{\min}$ plays a double role in our calculation. On the one hand it is used as a regulator for the integrals in p_3^+ or k_3^+. On the other hand, it is used to specify the physical scale set by the target at which the low-x evolution is starting, or equivalently to encode the dependence on the total energy $\sqrt{s}$ of the collision. The JIMWLK evolution resums single high-energy logarithms, written as logarithms of $k^+_{\min}$, and unlike the jet radius parameter R does not depend on details of the process. Hence, in the result (8.9), the term in $\ln^2 k^+_{\min}$ and the term in $\ln R\,\ln k^+_{\min}$ can definitely not be subtracted and resummed by JIMWLK. Instead, these two terms in eq. (8.9) should be understood as manifestations of the standard soft-collinear double logarithmic divergence for final state gluon radiation in our hybrid regularization scheme, having nothing to do with rapidity divergences and low-x evolution. In the remainder of this section, we will see how these $\ln^2 k^+_{\min}$ and $\ln R\,\ln k^+_{\min}$ terms as well as the collinear $1/\epsilon_{\text{coll}}$ pole are canceled by other contributions, leaving only the expected single high-energy logarithm to be subtracted and resummed by JIMWLK, following section 6.

For the diagram $|\overline{\text{Q}}\text{FS}|^2$, the contribution from the regime in which the antiquark and the gluon are merged into the same jet can be calculated in the same way, leading to

$$\begin{aligned}\mathcal{V}^{\text{in}}_{|\overline{\text{Q}}\text{FS}|^2} &= \left(-\frac{3}{2} + 2\ln\frac{p^+_{j2}}{k^+_{\min}}\right)\left(-\frac{1}{\epsilon_{\text{coll}}} + \gamma_E + \ln\frac{\mathbf{p}^2_{j2}}{4\pi\mu^2} + 2\ln R\right) \\ &\quad - 2\left(\ln\frac{p^+_{j2}}{k^+_{\min}}\right)^2 - \frac{2\pi^2}{3} + \frac{13}{2} + \mathcal{O}(\epsilon)\,.\end{aligned} \tag{8.10}$$

8.2 Contribution $|\text{QFS}|^2$; out

Let us now consider the other contribution to the dijet cross section from the $|\text{QFS}|^2$ diagram, in which the quark and the gluon are forming separate jets according to our jet definition. In that case, the quark and antiquark momenta are identified with the momenta of the measured jets, as $\vec{p}_1 = \vec{p}_{j1}$ and $\vec{p}_2 = \vec{p}_{j2}$. Using again the notation (8.2), the expression (8.3) for the denominator in eq. (8.1) stays valid. By contrast, the $\mathbf{x}_{11'}$ dependent phase factor in eq. (8.1) now becomes:

$$e^{-i(\mathbf{p}_1+\mathbf{p}_3)\cdot\mathbf{x}_{11'}} = e^{-i(\mathbf{p}_{j1}+\mathbf{p}_3)\cdot\mathbf{x}_{11'}} = e^{-i\mathbf{p}_{j1}\cdot\mathbf{x}_{11'}}e^{-i\mathbf{P}_3\cdot\mathbf{x}_{11'}}e^{-i\frac{p_3^+}{p^+_{j1}}\mathbf{p}_{j1}\cdot\mathbf{x}_{11'}}\,. \tag{8.11}$$

JHEP10(2022)184

With all this, the squared amplitude $|\mathcal{M}_{\rm QFS}|^2$ from eq. (8.1) can be written in the case of three separate jets as

$$\begin{aligned}|\mathcal{M}_{\rm QFS}|^2\Big|_{\vec{p}_1=\vec{p}_{j1},\vec{p}_2=\vec{p}_{j2}} &= |\mathcal{M}_{\rm LO}|^2_{\vec{p}_{1,2}\to\vec{p}_{j1,j2}}\times 4\pi\alpha_s C_F\frac{(p_3^+)^2}{(p_{j1}^+)^2}\left[\left(1+2\frac{p_{j1}^+}{p_3^+}\right)^2+(D-3)\right]\\ &\times\frac{e^{-i\mathbf{P}_3\cdot\mathbf{x}_{11'}}e^{-i\frac{p_3^+}{p_{j1}^+}\mathbf{p}_{j1}\cdot\mathbf{x}_{11'}}}{\mathbf{P}_3^2}\frac{2\left(\frac{p_{j1}^++p_3^+}{q^+}\right)^2+2\left(\frac{p_{j2}^+}{q^+}\right)^2+D-4}{2\left(\frac{p_{j1}^+}{q^+}\right)^2+2\left(\frac{p_{j2}^+}{q^+}\right)^2+D-4},\end{aligned}\tag{8.12}$$

with $|\mathcal{M}_{\rm LO}|^2$ written as in eq. (2.23). Note that eq. (8.12) is, once again, a slight abuse of notation, since the factorization actually happens at the integrand level and the integrations over $\mathbf{x}_1$ and $\mathbf{x}_{1'}$ are hidden inside $|\mathcal{M}_{\rm LO}|^2$.

Moreover, from the definition (7.5), one has now

$$\begin{aligned}1-\theta_{\rm in}(\vec{p}_{j1},\vec{p}_3) &= \theta\left((p_{j1}^++p_3^+)^2\left(\frac{\mathbf{p}_3}{p_3^+}-\frac{\mathbf{p}_{j1}}{p_{j1}^+}\right)^2-(\mathbf{p}_{j1}+\mathbf{p}_3)^2R^2\right)\\ &= \theta\left(\mathbf{P}_3^2-\frac{(p_3^+)^2}{(p_{j1}^++p_3^+)^2}\left(\frac{(p_{j1}^++p_3^+)}{p_{j1}^+}\mathbf{p}_{j1}+\mathbf{P}_3\right)^2R^2\right).\end{aligned}\tag{8.13}$$

In the narrow jet $R\to 0$ limit, this theta function changes values from 0 to 1 at a parametrically small value of $|\mathbf{P}_3|$, which scales as R. Hence, in this limit, $\mathbf{P}_3$ is negligible compared to $\mathbf{p}_{j1}$, so that

$$1-\theta_{\rm in}(\vec{p}_{j1},\vec{p}_3)\to\theta\left(\mathbf{P}_3^2-\frac{(p_3^+)^2}{(p_{j1}^+)^2}\mathbf{p}_{j1}^2R^2\right).\tag{8.14}$$

Inserting the expressions (8.12) and (8.14) into eq. (7.4), we can write the contribution to the dijet cross section from $|\mathrm{QFS}|^2$ with three separate jets as

$$\begin{aligned}&\frac{\mathrm{d}\sigma_{\rm dijet}^{|\mathrm{QFS}|^2;\ \rm out}}{\mathrm{d}p_{j1}^+\mathrm{d}^{D-2}\mathbf{p}_{j1}\mathrm{d}p_{j2}^+\mathrm{d}^{D-2}\mathbf{p}_{j2}}\\ &=\frac{\theta(p_{j1}^+)}{(2\pi)^{D-1}2p_{j1}^+}\frac{\theta(p_{j2}^+)}{(2\pi)^{D-1}2p_{j2}^+}\frac{1}{2q^+}\frac{1}{(D-2)}|\mathcal{M}_{\rm LO}|^2_{\vec{p}_{1,2}\to\vec{p}_{j1,j2}}4\pi\alpha_sC_F\int\mathrm{PS}(\vec{p}_3)\\ &\times 2\pi\delta(q^+-p_{j1}^+-p_{j2}^+-p_3^+)\theta\left(\mathbf{P}_3^2-\frac{(p_3^+)^2}{(p_{j1}^+)^2}\mathbf{p}_{j1}^2R^2\right)\frac{1}{\mathbf{P}_3^2}e^{-i\mathbf{P}_3\cdot\mathbf{x}_{11'}}e^{-i\frac{p_3^+}{p_{j1}^+}\mathbf{p}_{j1}\cdot\mathbf{x}_{11'}}\\ &\times\frac{\left[2\left(\frac{p_{j1}^++p_3^+}{q^+}\right)^2+2\left(\frac{p_{j2}^+}{q^+}\right)^2+(D-4)\right]}{\left[2\left(\frac{p_{j1}^+}{q^+}\right)^2+2\left(\frac{p_{j2}^+}{q^+}\right)^2+(D-4)\right]}\frac{(p_3^+)^2}{(p_{j1}^+)^2}\left[\left(1+2\frac{p_{j1}^+}{p_3^+}\right)^2+(D-3)\right].\end{aligned}\tag{8.15}$$

In eq. (8.15), the integral over $\mathbf{P}_3$ is actually finite, since the phase prevents UV divergences to occur while the theta function cuts off the collinear regime, preventing the gluon to

JHEP10(2022)184

belong to the quark jet. Hence, dimensional regularization is actually not necessary here and one can take $D = 4 - 2\epsilon \to 4$. The transverse integral in eq. (8.15) can then be calculated as

$$\begin{aligned} &4\pi \int \frac{\mathrm{d}^2\mathbf{P}_3}{(2\pi)^2}\frac{1}{\mathbf{P}_3^2} e^{-i\mathbf{P}_3\cdot\mathbf{x}_{11'}}\theta\left(\mathbf{P}_3^2 - \frac{(p_3^+)^2}{(p_{j1}^+)^2}\mathbf{p}_{j1}^2 R^2\right) \\ &\quad = 2\int_0^{+\infty}\frac{\mathrm{d}|\mathbf{P}_3|}{|\mathbf{P}_3|}\mathrm{J}_0(|\mathbf{P}_3||\mathbf{x}_{11'}|)\theta\left(|\mathbf{P}_3| - \frac{p_3^+}{p_{j1}^+}|\mathbf{p}_{j1}|R\right) \\ &\quad = -2\ln R - \ln\left(\frac{\mathbf{p}_{j1}^2\mathbf{x}_{11'}^2}{c_0^2}\right) - 2\ln\frac{p_3^+}{p_{j1}^+} + \mathcal{O}(R^2)\,, \end{aligned} \tag{8.16}$$

in the narrow-jet limit $R \to 0$. In eq. (8.16), J_0 is the Bessel function of the first kind, and $c_0 \equiv 2e^{-\gamma_E}$. At this stage, eq. (8.15) becomes

$$\begin{aligned} &\frac{\mathrm{d}\sigma_{\mathrm{dijet}}^{|\mathrm{QFS}|^2;\,\mathrm{out}}}{\mathrm{d}p_{j1}^+\mathrm{d}^2\mathbf{p}_{j1}\mathrm{d}p_{j2}^+\mathrm{d}^2\mathbf{p}_{j2}} \\ &\quad = \frac{\theta(p_{j1}^+)}{(2\pi)^3 2p_{j1}^+}\frac{\theta(p_{j2}^+)}{(2\pi)^3 2p_{j2}^+}\frac{1}{2q^+}\frac{1}{2}|\mathcal{M}_{\mathrm{LO}}|^2_{\vec{p}_{1,2}\to\vec{p}_{j1,j2}}\frac{\alpha_s C_F}{2\pi}\int_{k_{\min}^+}^{+\infty}\frac{\mathrm{d}p_3^+}{p_3^+}e^{-i\frac{p_3^+}{p_{j1}^+}\mathbf{p}_{j1}\cdot\mathbf{x}_{11'}} \\ &\quad\quad \times 2\pi\delta(q^+ - p_{j1}^+ - p_{j2}^+ - p_3^+)\left[-2\ln R - \ln\left(\frac{\mathbf{p}_{j1}^2\mathbf{x}_{11'}^2}{c_0^2}\right) - 2\ln\frac{p_3^+}{p_{j1}^+}\right] \\ &\quad\quad \times \frac{[(p_{j1}^+ + p_3^+)^2 + (p_{j2}^+)^2]}{[(p_{j1}^+)^2 + (p_{j2}^+)^2]}\left[2 + 2\frac{p_3^+}{p_{j1}^+} + \frac{(p_3^+)^2}{(p_{j1}^+)^2}\right]. \end{aligned} \tag{8.17}$$

In this expression, we could simply use the delta function in order to perform the p_3^+ integration. However, the result would be proportional to $1/(q^+ - p_{j1}^+ - p_{j2}^+)$, which could diverge depending on the kinematics of the jets, unless the cutoff $k_{\min}^+$ is taken into account. In order to obtain a well-behaved result and to extract the sensitivity of the expression (8.17) on the cutoff $k_{\min}^+$, let us split it into several pieces. First, let us evaluate the integrand at $p_3^+ \to 0$, including in the delta function. The corresponding piece of eq. (8.17) can be written as

$$\frac{\mathrm{d}\sigma_{\mathrm{dijet}}^{|\mathrm{QFS}|^2;\,\mathrm{out;\,soft}}}{\mathrm{d}p_{j1}^+\mathrm{d}^2\mathbf{p}_{j1}\mathrm{d}p_{j2}^+\mathrm{d}^2\mathbf{p}_{j2}} = \frac{\mathrm{d}\sigma_{\mathrm{dijet}}^{\mathrm{LO}}}{\mathrm{d}p_{j1}^+\mathrm{d}^2\mathbf{p}_{j1}\mathrm{d}p_{j2}^+\mathrm{d}^2\mathbf{p}_{j2}} \times \frac{\alpha_s C_F}{2\pi}\mathcal{V}_{|\mathrm{QFS}|^2}^{\mathrm{out;\,soft}} \tag{8.18}$$

where

$$\begin{aligned} \mathcal{V}_{|\mathrm{QFS}|^2}^{\mathrm{out;\,soft}} &= 2\int_{k_{\min}^+}^{p_{j1}^+}\frac{\mathrm{d}p_3^+}{p_3^+}\left[-2\ln R - \ln\left(\frac{\mathbf{p}_{j1}^2\mathbf{x}_{11'}^2}{c_0^2}\right) - 2\ln\frac{p_3^+}{p_{j1}^+}\right] \\ &= 2\left(\ln\frac{p_{j1}^+}{k_{\min}^+}\right)^2 - 4\ln\left(\frac{p_{j1}^+}{k_{\min}^+}\right)\ln R - 2\ln\left(\frac{p_{j1}^+}{k_{\min}^+}\right)\ln\left(\frac{\mathbf{p}_{j1}^2\mathbf{x}_{11'}^2}{c_0^2}\right)\,, \end{aligned} \tag{8.19}$$

introducing p_{j1}^+ as an upper bound in this soft contribution. The first two terms in eq. (8.19): in $\ln^2 k_{\min}^+$ and $\ln R\,\ln k_{\min}^+$, precisely cancel the ones found in from the in-jet radiation contribution (8.9), as we will show in subsection 8.3. As discussed earlier, these

JHEP10(2022)184

terms cannot be associated with high-energy evolution but are, instead, manifestations of soft-collinear divergences in our regularization scheme. Their cancellation is a crucial requirement for the consistency of our hybrid regularization scheme in which we combine transverse dimensional regularization with a lower cutoff for p_3^+.

Subtracting the term (8.18) from (8.17) is sufficient to remove any divergence from the p_3^+ integral, or more precisely any logarithmic sensitivity on $k_{\min}^+$, so that one can remove the cutoff $k_{\min}^+$ in the leftover piece. Nevertheless, the finite p_3^+ integral can still produce a potentially large logarithm. The reason for this is that the approximation $p_3^+ \to 0$ in the integrand of eq. (8.17), in order to obtain (8.18), breaks down at small but finite $p_3^+ \ll p_{j1}^+,\ p_{j2}^+$. Indeed, in this regime, the smallness of p_3^+ compared to p_{j1}^+ can be compensated for by very large values of $|\mathbf{p}_{j1}\cdot\mathbf{x}_{11'}|$, making the phase factor in eq. (8.17) non trivial even at small p_3^+. In order to have control on this issue, let us as well extract from eq. (8.17) the following contribution:

$$\frac{\mathrm{d}\sigma_{\text{dijet}}^{|\text{QFS}|^2;\ \text{out};\ \text{phase}}}{\mathrm{d}p_{j1}^+\mathrm{d}^2\mathbf{p}_{j1}\mathrm{d}p_{j2}^+\mathrm{d}^2\mathbf{p}_{j2}} = \frac{\mathrm{d}\sigma_{\text{dijet}}^{\text{LO}}}{\mathrm{d}p_{j1}^+\mathrm{d}^2\mathbf{p}_{j1}\mathrm{d}p_{j2}^+\mathrm{d}^2\mathbf{p}_{j2}} \times \frac{\alpha_s C_F}{2\pi}\mathcal{V}_{|\text{QFS}|^2}^{\text{out};\ \text{phase}} \tag{8.20}$$

where

$$\begin{aligned}\mathcal{V}_{|\text{QFS}|^2}^{\text{out};\ \text{phase}} &= 2\int_0^{p_{j1}^+}\frac{\mathrm{d}p_3^+}{p_3^+}\left[e^{-i\frac{p_3^+}{p_{j1}^+}\mathbf{p}_{j1}\cdot\mathbf{x}_{11'}}-1\right]\left[-2\ln R-\ln\left(\frac{\mathbf{p}_{j1}^2\mathbf{x}_{11'}^2}{c_0^2}\right)-2\ln\frac{p_3^+}{p_{j1}^+}\right]\\ &= 2\int_0^1\frac{\mathrm{d}\xi}{\xi}\left[e^{-i\xi\mathbf{p}_{j1}\cdot\mathbf{x}_{11'}}-1\right]\left[-2\ln R-\ln\left(\frac{\mathbf{p}_{j1}^2\mathbf{x}_{11'}^2}{c_0^2}\right)-2\ln\xi\right],\end{aligned} \tag{8.21}$$

where we introduced once again $\xi \equiv p_3^+/p_{j1}^+$. The above expression will be further studied in section 10, in the back-to-back jets limit.

Finally, we call *regular* the leftover part of eq. (8.17) obtained after subtracting the terms (8.18) and (8.20), as

$$\mathrm{d}\sigma_{\text{dijet}}^{|\text{QFS}|^2;\ \text{out};\ \text{reg}} = \mathrm{d}\sigma_{\text{dijet}}^{|\text{QFS}|^2;\ \text{out}} - \mathrm{d}\sigma_{\text{dijet}}^{|\text{QFS}|^2;\ \text{out};\ \text{soft}} - \mathrm{d}\sigma_{\text{dijet}}^{|\text{QFS}|^2;\ \text{out};\ \text{phase}}, \tag{8.22}$$

since in this contribution, the integration over p_3^+ cannot produce a divergent result even without cutoff, and neither can it produce further large logarithms. It can be written explicitly as

$$\begin{aligned}\frac{\mathrm{d}\sigma_{\text{dijet}}^{|\text{QFS}|^2;\ \text{out};\ \text{reg}}}{\mathrm{d}p_{j1}^+\mathrm{d}^2\mathbf{p}_{j1}\mathrm{d}p_{j2}^+\mathrm{d}^2\mathbf{p}_{j2}} &= \frac{\theta(p_{j1}^+)}{(2\pi)^3 2p_{j1}^+}\frac{\theta(p_{j2}^+)}{(2\pi)^3 2p_{j2}^+}\frac{1}{2q^+}\frac{1}{2}|\mathcal{M}_{\text{LO}}|^2_{\vec{p}_{1,2}\to\vec{p}_{j1,j2}}\\ &\quad\times\frac{\alpha_s C_F}{2\pi}\int_0^{+\infty}\frac{\mathrm{d}\xi}{\xi}e^{-i\xi\mathbf{p}_{j1}\cdot\mathbf{x}_{11'}}\left[-2\ln R-\ln\left(\frac{\mathbf{p}_{j1}^2\mathbf{x}_{11'}^2}{c_0^2}\right)-2\ln\xi\right]\\ &\quad\times\left\{2\pi\delta(q^+-(1+\xi)p_{j1}^+-p_{j2}^+)\left[1+\frac{(2\xi+\xi^2)(p_{j1}^+)^2}{(p_{j1}^+)^2+(p_{j2}^+)^2}\right](1+(1+\xi)^2)\right.\\ &\quad\left.-4\pi\delta(q^+-p_{j1}^+-p_{j2}^+)\theta(1-\xi)\right\}.\end{aligned} \tag{8.23}$$

JHEP10(2022)184

For the diagram $|\overline{\mathrm{Q}}\mathrm{FS}|^2$, the contribution from the regime in which the antiquark and the gluon form two separate jets can be split into three contributions in the same way, and one obtains

$$\mathcal{V}^{\text{out; soft}}_{|\overline{\mathrm{Q}}\mathrm{FS}|^2} = \mathcal{V}^{\text{out; soft}}_{|\mathrm{QFS}|^2}(1 \leftrightarrow 2) \,, \tag{8.24}$$

$$\mathcal{V}^{\text{out; phase}}_{|\overline{\mathrm{Q}}\mathrm{FS}|^2} = \mathcal{V}^{\text{out; phase}}_{|\mathrm{QFS}|^2}(1 \leftrightarrow 2) \,, \tag{8.25}$$

and

$$\frac{\mathrm{d}\sigma^{|\overline{\mathrm{Q}}\mathrm{FS}|^2;\,\text{out; reg}}_{\text{dijet}}}{\mathrm{d}p^+_{j1}\mathrm{d}^2\mathbf{p}_{j1}\mathrm{d}p^+_{j2}\mathrm{d}^2\mathbf{p}_{j2}} = \frac{\mathrm{d}\sigma^{|\mathrm{QFS}|^2;\,\text{out; reg}}_{\text{dijet}}}{\mathrm{d}p^+_{j1}\mathrm{d}^2\mathbf{p}_{j1}\mathrm{d}p^+_{j2}\mathrm{d}^2\mathbf{p}_{j2}}(1 \leftrightarrow 2) \,. \tag{8.26}$$

8.3 Cancellation of collinear and soft divergences

As already discussed, soft and collinear divergences manifest themselves in various ways when $|\mathrm{QFS}|^2$ is calculated using transverse dimensional regularization and a cutoff $k^+_{\min}$. In addition to the $1/\epsilon_{\text{coll}}$ collinear pole in the inside jet radiation contribution (8.9), both eqs. (8.9) and (8.19) contain terms of soft-collinear origin, namely in $\ln^2 k^+_{\min}$ and in $\ln R \ln k^+_{\min}$. It is then difficult to disentangle single logarithms $\ln k^+_{\min}$ associated with either soft or rapidity divergences.

Adding eqs. (8.9) and (8.19) together, the terms in $\ln^2 k^+_{\min}$ and in $\ln R \ln k^+_{\min}$ cancel, and one obtains:

$$\begin{aligned}\mathcal{V}^{\text{in}}_{|\mathrm{QFS}|^2} + \mathcal{V}^{\text{out; soft}}_{|\mathrm{QFS}|^2} = &\left[\frac{3}{2} - 2\ln\left(\frac{p^+_{j1}}{k^+_{\min}}\right)\right]\left[\frac{1}{\epsilon_{\text{coll}}} + \gamma_E + \ln\left(\pi\mu^2\mathbf{x}^2_{11'}\right)\right] \\ &- \frac{3}{2}\ln\left(\frac{\mathbf{p}^2_{j1}\mathbf{x}^2_{11'}}{c_0^2}\right) - 3\ln R - \frac{2\pi^2}{3} + \frac{13}{2} + \mathcal{O}(\epsilon) \,.\end{aligned} \tag{8.27}$$

The other two contributions (8.21) and (8.23) from $|\mathrm{QFS}|^2$ do not contain any divergence. Similarly, for the diagram $|\overline{\mathrm{Q}}\mathrm{FS}|^2$, one finds

$$\begin{aligned}\mathcal{V}^{\text{in}}_{|\overline{\mathrm{Q}}\mathrm{FS}|^2} + \mathcal{V}^{\text{out; soft}}_{|\overline{\mathrm{Q}}\mathrm{FS}|^2} = &\left[\frac{3}{2} - 2\ln\left(\frac{p^+_{j2}}{k^+_{\min}}\right)\right]\left[\frac{1}{\epsilon_{\text{coll}}} + \gamma_E + \ln\left(\pi\mu^2\mathbf{x}^2_{22'}\right)\right] \\ &- \frac{3}{2}\ln\left(\frac{\mathbf{p}^2_{j2}\mathbf{x}^2_{22'}}{c_0^2}\right) - 3\ln R - \frac{2\pi^2}{3} + \frac{13}{2} + \mathcal{O}(\epsilon) \,.\end{aligned} \tag{8.28}$$

In the NLO virtual corrections to DIS dijets, the only contribution containing a collinear divergence is FSIR, see eq. (4.11), which factorizes as well from the LO cross section at integrand level. This contribution corresponds to the IR part of the self energy diagrams for the quark and for the antiquark in the final state. With the identification of the momenta of partons and jets, it can be written as

$$\mathcal{V}_{\text{FSIR}} = \left[\frac{1}{\epsilon_{\text{coll}}} + \gamma_E + \ln(\pi\mu^2\mathbf{x}^2_{12})\right]\left[-\frac{3}{2} + \ln\left(\frac{p^+_{j1}}{k^+_{\min}}\right) + \ln\left(\frac{p^+_{j2}}{k^+_{\min}}\right)\right] \,. \tag{8.29}$$

The above equation corresponds to a virtual correction in the amplitude. We should also consider the same virtual correction in the complex conjugate amplitude, which only differs

JHEP10(2022)184

from (8.29) in that it depends on $\mathbf{x}_{1'}$ and $\mathbf{x}_{2'}$ rather than $\mathbf{x}_1$ and $\mathbf{x}_2$:

$$\mathcal{V}_{\mathrm{FSIR}^\dagger} = \left[\frac{1}{\epsilon_{\mathrm{coll}}} + \gamma_E + \ln(\pi\mu^2\mathbf{x}_{1'2'}^2)\right]\left[-\frac{3}{2} + \ln\left(\frac{p_{j1}^+}{k_{\mathrm{min}}^+}\right) + \ln\left(\frac{p_{j2}^+}{k_{\mathrm{min}}^+}\right)\right] . \tag{8.30}$$

In the sum of the contributions (8.27), (8.28), (8.29) and (8.30), the collinear poles cancel, and one finds

$$\begin{aligned}\mathcal{V}_{\mathrm{jet}} &\equiv \mathcal{V}^{\mathrm{in}}_{|\mathrm{QFS}|^2} + \mathcal{V}^{\mathrm{out;\,soft}}_{|\mathrm{QFS}|^2} + \mathcal{V}^{\mathrm{in}}_{|\overline{\mathrm{Q}}\mathrm{FS}|^2} + \mathcal{V}^{\mathrm{out;\,soft}}_{|\overline{\mathrm{Q}}\mathrm{FS}|^2} + \mathcal{V}_{\mathrm{FSIR}} + \mathcal{V}_{\mathrm{FSIR}^\dagger} \\ &= -2\ln\left(\frac{p_{j1}^+}{k_{\mathrm{min}}^+}\right)\ln\left(\frac{\mathbf{x}_{11'}^2}{|\mathbf{x}_{12}|\,|\mathbf{x}_{1'2'}|}\right) - 2\ln\left(\frac{p_{j2}^+}{k_{\mathrm{min}}^+}\right)\ln\left(\frac{\mathbf{x}_{22'}^2}{|\mathbf{x}_{12}|\,|\mathbf{x}_{1'2'}|}\right) \\ &\quad - 3\ln\left(\frac{|\mathbf{p}_{j1}|\,|\mathbf{p}_{j2}|\,|\mathbf{x}_{12}|\,|\mathbf{x}_{1'2'}|}{c_0^2}\right) - 6\ln R - \frac{4\pi^2}{3} + 13 .\end{aligned} \tag{8.31}$$

In this expression, all soft and collinear divergences have canceled [120]. Only a single logarithmic dependence on k_{min}^+ remains, which now corresponds to high-energy evolution. This can be shown as follows: introducing the factorization scale k_f^+, one can isolate the dependence on the cutoff k_{min}^+ as

$$\begin{aligned}\mathcal{V}_{\mathrm{jet}} &= 2\ln\left(\frac{k_f^+}{k_{\mathrm{min}}^+}\right)\ln\left(\frac{\mathbf{x}_{12}^2\mathbf{x}_{1'2'}^2}{\mathbf{x}_{11'}^2\mathbf{x}_{22'}^2}\right) - 2\ln\left(\frac{p_{j1}^+}{k_f^+}\right)\ln\left(\frac{\mathbf{x}_{11'}^2}{|\mathbf{x}_{12}|\,|\mathbf{x}_{1'2'}|}\right) \\ &\quad - 2\ln\left(\frac{p_{j2}^+}{k_f^+}\right)\ln\left(\frac{\mathbf{x}_{22'}^2}{|\mathbf{x}_{12}|\,|\mathbf{x}_{1'2'}|}\right) - 3\ln\left(\frac{|\mathbf{p}_{j1}|\,|\mathbf{p}_{j2}|\,|\mathbf{x}_{12}|\,|\mathbf{x}_{1'2'}|}{c_0^2}\right) \\ &\quad - 6\ln R - \frac{4\pi^2}{3} + 13 .\end{aligned} \tag{8.32}$$

The first term in eq. (8.32) amounts to a multiplication of the LO cross section by

$$\begin{aligned}&\frac{\alpha_s C_F}{2\pi} 2\ln\left(\frac{k_f^+}{k_{\mathrm{min}}^+}\right)\ln\left(\frac{\mathbf{x}_{12}^2\mathbf{x}_{1'2'}^2}{\mathbf{x}_{11'}^2\mathbf{x}_{22'}^2}\right) \\ &\quad = 2\alpha_s N_c\left(1 - \frac{1}{N_c^2}\right)\ln\left(\frac{k_f^+}{k_{\mathrm{min}}^+}\right)\int_{\mathbf{x}_3}\Big(A^\eta(\mathbf{x}_{13})A^\eta(\mathbf{x}_{1'3}) \\ &\qquad\qquad + A^\eta(\mathbf{x}_{23})A^\eta(\mathbf{x}_{2'3}) - A^\eta(\mathbf{x}_{13})A^\eta(\mathbf{x}_{23}) - A^\eta(\mathbf{x}_{1'3})A^\eta(\mathbf{x}_{2'3})\Big) .\end{aligned} \tag{8.33}$$

This corresponds indeed to the part of the JIMWLK evolution proportional to $\alpha_s C_F$ times the LO cross section. Hence, in our resummation scheme for high-energy leading logs, the first term in eq. (8.32) is the part which is subtracted and resummed by the JIMWLK evolution.

9 Inclusive dijet cross section

In this section, we present the full differential NLO cross section for $\gamma + A \to \mathrm{dijet} + X$ in the CGC. It is given by the sum:

$$\mathrm{d}\sigma_{\mathrm{NLO}}^{\gamma A\to \mathrm{dijet}X} = \mathrm{d}\sigma_{\mathrm{LO}} + \mathrm{d}\sigma_{\mathrm{jet}} + \mathrm{d}\sigma_{\mathrm{softGE}} + \mathrm{d}\sigma_{\mathrm{real}}^{\mathrm{Sudakov}} + \mathrm{d}\sigma_{\mathrm{virtual}}^{\mathrm{finite}} + \mathrm{d}\sigma_{\mathrm{real}}^{\mathrm{finite}} , \tag{9.1}$$

JHEP10(2022)184

where it is understood that the rapidity divergences are subtracted and absorbed into JIMWLK according to eq. (6.7). The cross section is written in terms of different contributions which are each separately soft- and collinear safe. We will shortly discuss each of the terms, and provide their explicit expressions in the next subsections.

The first part of the cross section is the leading-order one, given in eq. (2.24), where the outgoing partons are identified with jets: $\vec{p}_{1,2} \to \vec{p}_{j1,j2}$.

Second, following the discussion in sections 7 and 8, the real NLO corrections due to final-state gluon emission contain soft-collinear singularities. These singularities are cured when applying the jet algorithm and summing the contributions due to gluon emission inside the jet, soft gluon emission outside the jet, and the IR part of the virtual self-energy corrections to the final state:

$$\frac{\mathrm{d}\sigma_{\mathrm{jet}}}{\mathrm{d}p_{j1}^+\mathrm{d}^2\mathbf{p}_{j1}\mathrm{d}p_{j2}^+\mathrm{d}^2\mathbf{p}_{j2}} = \frac{\mathrm{d}\sigma_{\mathrm{dijet}}^{\mathrm{LO}}}{\mathrm{d}p_{j1}^+\mathrm{d}^{D-2}\mathbf{p}_{j1}\mathrm{d}p_{j2}^+\mathrm{d}^{D-2}\mathbf{p}_{j2}} \times \frac{\alpha_s C_F}{2\pi}\mathcal{V}_{\mathrm{jet}}\,. \tag{9.2}$$

The explicit expression for $\mathcal{V}_{\mathrm{jet}}$ is given in eq. (8.32).

Third, as explained in section 5, the contribution to the cross section due to diagram GEFS, (ii) + IFS and its $q \leftrightarrow \bar{q}$ counterpart contains a soft divergence. This singularity cancels with the one found in the interference between quark- and antiquark induced real final-state emission in the amplitude resp. complex conjugate amplitude, and vice versa. Summing both virtual and real contributions, one ends up with the following finite contribution to the cross section which we might call softGE for soft final-state gluon exchange:

$$\begin{aligned}\frac{\mathrm{d}\sigma_{\mathrm{softGE}}}{\mathrm{d}p_{j1}^+\mathrm{d}^{D-2}\mathbf{p}_{j1}\mathrm{d}p_{j2}^+\mathrm{d}^{D-2}\mathbf{p}_{j2}} &= \frac{1}{2q^+}\frac{\theta(p_{j1}^+)}{(2\pi)^{D-1}2p_{j1}^+}\frac{\theta(p_{j2}^+)}{(2\pi)^{D-1}2p_{j2}^+}\\ &\times \frac{1}{D-2}\Bigg[2\pi\delta(q^+ - p_{j1}^+ - p_{j2}^+)\Big(\mathcal{M}_{\mathrm{LO}}^\dagger\mathcal{M}_{\mathrm{GEFS},(ii)+\mathrm{IFS}} + q \leftrightarrow \bar{q} + \mathrm{c.c.}\Big)_{\vec{p}_{1,2}\to\vec{p}_{j1,j2}}\\ &\quad + \int \mathrm{PS}(\vec{p}_3)2\pi\delta(q^+ - p_{j1}^+ - p_{j2}^+ - p_3^+)\Big(\mathcal{M}_{\overline{\mathrm{Q}}\mathrm{FS}}^\dagger\mathcal{M}_{\mathrm{QFS}} + \mathrm{c.c.}\Big)_{\vec{p}_{1,2}\to\vec{p}_{j1,j2}}\Bigg]\,.\end{aligned} \tag{9.3}$$

The explicit expressions for the different terms are listed in subsection 9.1.

Fourth, there are terms due to final-state gluon radiation outside the jet, that in certain kinematics will become enhanced by a large Sudakov double logarithm (see sections 8 and 10):

$$\frac{\mathrm{d}\sigma_{\mathrm{real}}^{\mathrm{Sudakov}}}{\mathrm{d}p_{j1}^+\mathrm{d}^2\mathbf{p}_{j1}\mathrm{d}p_{j2}^+\mathrm{d}^2\mathbf{p}_{j2}} = \frac{\mathrm{d}\sigma_{\mathrm{dijet}}^{\mathrm{LO}}}{\mathrm{d}p_{j1}^+\mathrm{d}^2\mathbf{p}_{j1}\mathrm{d}p_{j2}^+\mathrm{d}^2\mathbf{p}_{j2}} \times \frac{\alpha_s C_F}{2\pi}\Big(\mathcal{V}_{|\mathrm{QFS}|^2}^{\text{out; phase}} + \mathcal{V}_{|\overline{\mathrm{Q}}\mathrm{FS}|^2}^{\text{out; phase}}\Big)\,. \tag{9.4}$$

The explicit formulae for $\mathcal{V}_{|\mathrm{QFS}|^2}^{\text{out; phase}}$ and $\mathcal{V}_{|\overline{\mathrm{Q}}\mathrm{FS}|^2}^{\text{out; phase}}$ are given in eqs. (8.21) and (8.25).

JHEP10(2022)184

The final contributions to eq. (9.1) are due to purely finite virtual and real NLO corrections:

$$\begin{aligned}\frac{\mathrm{d}\sigma^{\text{finite}}_{\text{virtual}}}{\mathrm{d}p^+_{j1}\mathrm{d}^2\mathbf{p}_{j1}\mathrm{d}p^+_{j2}\mathrm{d}^2\mathbf{p}_{j2}} &= \frac{1}{2q^+}\frac{\theta(p^+_{j1})}{(2\pi)^3 2p^+_{j1}}\frac{\theta(p^+_{j2})}{(2\pi)^3 2p^+_{j2}}2\pi\delta(q^+-p^+_{j1}-p^+_{j2})\\ &\times\frac{1}{2}\Bigg[\Big(\mathcal{M}^\dagger_{\text{LO}}\mathcal{M}_{\text{SESW,sub}}+\mathcal{M}^\dagger_{\text{LO}}\mathcal{M}_{\text{GESW}}+\mathcal{M}^\dagger_{\text{LO}}\mathcal{M}_{\text{ISW}}\\ &\quad+\mathcal{M}^\dagger_{\text{LO}}\mathcal{M}_{\text{GEFS},(i)}+q\leftrightarrow\bar{q}\Big)+\mathcal{M}^\dagger_{\text{LO}}\mathcal{M}_{\text{IS+UV+FSUV}}+\text{c.c.}\Bigg]_{\vec{p}_{1,2}\to\vec{p}_{j1,j2}},\end{aligned}\tag{9.5}$$

and

$$\begin{aligned}&\frac{\mathrm{d}\sigma^{\text{finite}}_{\text{real}}}{\mathrm{d}p^+_{j1}\mathrm{d}^2\mathbf{p}_{j1}\mathrm{d}p^+_{j2}\mathrm{d}^2\mathbf{p}_{j2}}\\ &=\frac{\mathrm{d}\sigma^{|\text{QFS}|^2;\text{out;reg}}_{\text{dijet}}}{\mathrm{d}p^+_{j1}\mathrm{d}^2\mathbf{p}_{j1}\mathrm{d}p^+_{j2}\mathrm{d}^2\mathbf{p}_{j2}}+\frac{\mathrm{d}\sigma^{|\overline{\text{Q}}\text{FS}|^2;\text{out;reg}}_{\text{dijet}}}{\mathrm{d}p^+_{j1}\mathrm{d}^2\mathbf{p}_{j1}\mathrm{d}p^+_{j2}\mathrm{d}^2\mathbf{p}_{j2}}+\frac{1}{2q^+}\frac{\theta(p^+_{j1})}{(2\pi)^3 2p^+_{j1}}\frac{\theta(p^+_{j2})}{(2\pi)^3 2p^+_{j2}}\frac{1}{4p^+_3}\\ &\times\int_{\mathbf{p}_3}\Big\{|\mathcal{M}_{\text{QSW}}|^2+\mathcal{M}^\dagger_{\text{QSW}}\mathcal{M}_{\text{QFS}}+\mathcal{M}^\dagger_{\text{QFS}}\mathcal{M}_{\text{QSW}}\\ &\quad+|\mathcal{M}_{\overline{\text{Q}}\text{SW}}|^2+\mathcal{M}^\dagger_{\overline{\text{Q}}\text{SW}}\mathcal{M}_{\overline{\text{Q}}\text{FS}}+\mathcal{M}^\dagger_{\overline{\text{Q}}\text{FS}}\mathcal{M}_{\overline{\text{Q}}\text{SW}}\\ &\quad+\mathcal{M}^\dagger_{\overline{\text{Q}}\text{SW}}\mathcal{M}_{\text{QSW}}+\mathcal{M}^\dagger_{\overline{\text{Q}}\text{SW}}\mathcal{M}_{\text{QFS}}+\mathcal{M}^\dagger_{\overline{\text{Q}}\text{FS}}\mathcal{M}_{\text{QSW}}+\text{c.c.}\\ &\quad+\mathcal{M}^\dagger_{\text{RI}}\Big(\mathcal{M}_{\text{QSW}}+\mathcal{M}_{\text{QFS}}\Big)+\text{c.c.}\\ &\quad+\mathcal{M}^\dagger_{\text{RI}}\Big(\mathcal{M}_{\overline{\text{Q}}\text{FS}}+\mathcal{M}_{\overline{\text{Q}}\text{SW}}\Big)+\text{c.c.}+|\mathcal{M}_{\text{RI}}|^2\Big\}\Big|_{\vec{p}_{1,2}\to\vec{p}_{j1,j2},p^+_3=q^+-p^+_{j1}-p^+_{j2}>0}.\end{aligned}\tag{9.6}$$

The explicit expressions for all the above terms are gathered in subsections 9.2 and 9.3.

In table 3 on page 45, we provide an overview of the different Wilson-line correlators that appear in the NLO cross section. They are all build from simple dipoles and quadrupoles in the fundamental representation (2.25), and never become more complicated than a six-point function made from a quadrupole and a dipole. Remember that $1, 2, 3$, and v are short-hand notations for the positions in coordinate space of, respectively, the quark $\mathbf{x}_1$, antiquark $\mathbf{x}_2$, gluon $\mathbf{x}_3$ and quark or antiquark before a final-state emission $\mathbf{v}$.

9.1 SoftGE

As discussed in section 3, the amplitudes due to gluon exchange in the final state exhibit an unphysical power-divergence in k^+_3. This is cured by summing the problematic part of the amplitude, $\mathcal{M}_{\text{GEFS},(ii)}$, with the amplitude $\mathcal{M}_{\text{IFS}}$ corresponding to the final-state

JHEP10(2022)184

LO 2.24, jet 9.2		$Q_{122'1'}-s_{12}-s_{2'1'}+1$
Sudakov 9.4		
IS+UV+FSUV 9.25		
real terms 9.26	$\mathrm{d}\sigma_{\mathrm{dijet}}^{\lvert\mathrm{QFS}\rvert^2;\ \mathrm{out};\ \mathrm{reg}}$	
9.27	$\mathrm{d}\sigma_{\mathrm{dijet}}^{\lvert\overline{\mathrm{Q}}\mathrm{FS}\rvert^2;\ \mathrm{out};\ \mathrm{reg}}$	
finite virtual 9.12	$\mathcal{M}_{\mathrm{LO}}^{\dagger}\mathcal{M}_{\mathrm{SESW,sub}}$	
9.13	$\mathcal{M}_{\mathrm{LO}}^{\dagger}\mathcal{M}_{\overline{\mathrm{SE}}\mathrm{SW,sub}}$	
softGE 9.7	$\mathcal{M}_{\mathrm{LO}}^{\dagger}\mathcal{M}_{\mathrm{GEFS},(ii)+\mathrm{IFS}}$	$s_{2'1'}s_{12}-s_{12}-s_{2'1'}+1-\frac{1}{N_c^2}\left(Q_{2'1'12}-s_{12}-s_{2'1'}-1\right)$
9.9	$\mathcal{M}_{\mathrm{LO}}^{\dagger}\mathcal{M}_{\overline{\mathrm{GE}}\mathrm{FS},(ii)+\overline{\mathrm{I}}\mathrm{FS}}$	
finite virtual 9.22	$\mathcal{M}_{\mathrm{LO}}^{\dagger}\mathcal{M}_{\mathrm{GEFS},(i)}$	
9.24	$\mathcal{M}_{\mathrm{LO}}^{\dagger}\mathcal{M}_{\overline{\mathrm{GE}}\mathrm{FS},(i)}$	
softGE 9.10	$\mathcal{M}_{\overline{\mathrm{Q}}\mathrm{FS}}^{\dagger}\mathcal{M}_{\mathrm{QFS}}$	$s_{v'1'}s_{v2}-s_{v2}-s_{v'1'}+1-\frac{1}{N_c^2}\left(Q_{v2v'1'}-s_{v2}-s_{v'1'}+1\right)$
9.10	$\mathcal{M}_{\mathrm{QFS}}^{\dagger}\mathcal{M}_{\overline{\mathrm{Q}}\mathrm{FS}}$	$s_{1v}s_{2'v'}-s_{2'v'}-s_{1v}+1-\frac{1}{N_c^2}\left(Q_{1v2'v'}-s_{2'v'}-s_{1v}+1\right)$
finite virtual 9.12	$\mathcal{M}_{\mathrm{LO}}^{\dagger}\mathcal{M}_{\mathrm{SESW,sub}}$	
9.14	$\mathcal{M}_{\mathrm{LO}}^{\dagger}\mathcal{M}_{\mathrm{GESW,sub}}$	$Q_{322'1'}s_{13}-s_{13}s_{32}-s_{2'1'}+1-\frac{1}{N_c^2}\left(Q_{122'1'}-s_{12}-s_{2'1'}+1\right)$
9.18	$\mathcal{M}_{\mathrm{LO}}^{\dagger}\mathcal{M}_{\mathrm{ISW,sub}}$	
9.13	$\mathcal{M}_{\mathrm{LO}}^{\dagger}\mathcal{M}_{\overline{\mathrm{SE}}\mathrm{SW,sub}}$	
9.16	$\mathcal{M}_{\mathrm{LO}}^{\dagger}\mathcal{M}_{\overline{\mathrm{GE}}\mathrm{SW,sub}}$	$Q_{132'1'}s_{32}-s_{13}s_{32}-s_{2'1'}+1-\frac{1}{N_c^2}\left(Q_{122'1'}-s_{12}-s_{2'1'}+1\right)$
9.20	$\mathcal{M}_{\mathrm{LO}}^{\dagger}\mathcal{M}_{\overline{\mathrm{I}}\mathrm{SW,sub}}$	
real terms 9.28	$\lvert\mathcal{M}_{\mathrm{QSW}}\rvert^2$	
9.29	$\lvert\mathcal{M}_{\overline{\mathrm{Q}}\mathrm{SW}}\rvert^2$	
9.30	$\mathcal{M}_{\overline{\mathrm{Q}}\mathrm{SW}}^{\dagger}\mathcal{M}_{\mathrm{QSW}}+\mathrm{c.c.}$	$s_{11'}s_{2'2}-s_{32}s_{13}-s_{31'}s_{2'3}+1-\frac{1}{N_c^2}\left(Q_{122'1'}-s_{12}-s_{2'1'}+1\right)$
9.33	$\lvert\mathcal{M}_{\mathrm{RI}}\rvert^2$	
9.35	$\mathcal{M}_{\mathrm{RI}}^{\dagger}\mathcal{M}_{\mathrm{QSW}}$	
9.37	$\mathcal{M}_{\mathrm{RI}}^{\dagger}\mathcal{M}_{\overline{\mathrm{Q}}\mathrm{SW}}$	
9.28	$\mathcal{M}_{\mathrm{QSW}}^{\dagger}\mathcal{M}_{\mathrm{QFS}}$	
9.30	$\mathcal{M}_{\overline{\mathrm{Q}}\mathrm{SW}}^{\dagger}\mathcal{M}_{\mathrm{QFS}}$	$Q_{v22'3}s_{31'}-s_{31'}s_{2'3}-s_{v2}+1-\frac{1}{N_c^2}\left(Q_{v22'1'}-s_{v2}-s_{2'1'}+1\right)$
9.35	$\mathcal{M}_{\mathrm{RI}}^{\dagger}\mathcal{M}_{\mathrm{QFS}}$	
9.28	$\mathcal{M}_{\mathrm{QFS}}^{\dagger}\mathcal{M}_{\mathrm{QSW}}$	$Q_{322'v'}s_{13}-s_{13}s_{32}-s_{2'v'}+1-\frac{1}{N_c^2}\left(Q_{122'v'}-s_{2'v'}-s_{12}+1\right)$
9.30	$\mathcal{M}_{\mathrm{QFS}}^{\dagger}\mathcal{M}_{\overline{\mathrm{Q}}\mathrm{SW}}$	
9.29	$\mathcal{M}_{\overline{\mathrm{Q}}\mathrm{SW}}^{\dagger}\mathcal{M}_{\overline{\mathrm{Q}}\mathrm{FS}}$	
9.30	$\mathcal{M}_{\mathrm{QSW}}^{\dagger}\mathcal{M}_{\overline{\mathrm{Q}}\mathrm{FS}}$	$Q_{31'1v}s_{2'3}-s_{2'3}s_{31'}-s_{1v}+1-\frac{1}{N_c^2}\left(Q_{2'1'1v}-s_{1v}-s_{2'1'}+1\right)$
9.37	$\mathcal{M}_{\mathrm{RI}}^{\dagger}\mathcal{M}_{\overline{\mathrm{Q}}\mathrm{FS}}$	
9.29	$\mathcal{M}_{\overline{\mathrm{Q}}\mathrm{FS}}^{\dagger}\mathcal{M}_{\overline{\mathrm{Q}}\mathrm{SW}}$	$Q_{v'1'13}s_{32}-s_{32}s_{13}-s_{v'1'}+1-\frac{1}{N_c^2}\left(Q_{v'1'12}-s_{v'1'}-s_{12}+1\right)$
9.30	$\mathcal{M}_{\overline{\mathrm{Q}}\mathrm{FS}}^{\dagger}\mathcal{M}_{\mathrm{QSW}}$	

Table 3. The different Wilson-line structures appearing in the NLO cross section.

JHEP10(2022)184

exchange of an instantaneous gluon:

$$
\begin{aligned}
&\mathcal{M}^{\dagger}_{\mathrm{LO}}\mathcal{M}_{\mathrm{GEFS},(ii)+\mathrm{IFS}} \\
&\quad= 64(2\pi)\alpha_{\mathrm{em}}e_f^2\alpha_s N_c^2 p_{j1}^+ p_{j2}^+ \int_{k_f^+}^{p_{j1}^+}\frac{\mathrm{d}k_3^+}{k_3^+}\frac{p_{j1}^+-k_3^+}{q^+}\left[(z^2+\bar{z}^2)+(1-2z)\frac{k_3^+}{q^+}\right] \\
&\qquad\times\int_{\mathbf{x}_{1'},\mathbf{x}_{2'},\mathbf{x}_1,\mathbf{x}_2} e^{-i\mathbf{p}_{j1}\cdot\mathbf{x}_{11'}}e^{-i\mathbf{p}_{j2}\cdot\mathbf{x}_{22'}}e^{i\frac{k_3^+}{p_{j1}^+}\mathbf{p}_{j1}\cdot\mathbf{x}_{12}}A^{\lambda}(\mathbf{x}_{1'2'})A^{\lambda}(\mathbf{x}_{12}) \\
&\qquad\times\int_{\mathbf{K}}\left(1+\frac{\mathbf{K}\cdot\mathbf{P}_\perp}{z\mathbf{K}^2}\right)\frac{e^{-i\mathbf{K}\cdot\mathbf{x}_{12}}}{(\mathbf{K}+\frac{p_{j1}^+-k_3^+}{p_{j1}^+}\mathbf{P}_\perp)^2-\frac{(p_{j2}^++k_3^+)(p_{j1}^+-k_3^+)}{p_{j1}^+p_{j2}^+}\mathbf{P}_\perp^2-i\epsilon} \\
&\qquad\times\left\langle s_{2'1'}s_{12}-s_{12}-s_{2'1'}+1-\frac{1}{N_c^2}\Big(Q_{2'1'12}-s_{12}-s_{2'1'}-1\Big)\right\rangle ,
\end{aligned}
\tag{9.7}
$$

where we used that:

$$
\mathrm{Tr}\Big(\mathrm{Dirac}^{\lambda'\dagger}_{\mathrm{LO}}\mathrm{Dirac}^{\bar{\lambda}\bar{\eta}\eta'}_{\bar{q}\to q,(ii)}\Big)=-64\frac{(p_{j1}^+p_{j2}^+)^2}{(k_3^+)^2}\delta^{\bar{\eta}\eta'}\delta^{\bar{\lambda}\lambda'}\left[(z^2+\bar{z}^2)+(1-2z)\frac{k_3^+}{q^+}\right] , \tag{9.8}
$$

and where z and $\bar{z}$ now denote + momentum fractions of the jets: $z\equiv p_{j1}^+/q^+$ and $\bar{z}\equiv p_{j2}^+/q^+$. Due to its simple Wilson-line structure, the $q\leftrightarrow\bar{q}$ conjugate contributions to the cross section can be simply obtained from the above result by exchanging the quark and antiquark indices:

$$
\begin{aligned}
\mathcal{M}^{\dagger}_{\mathrm{LO}}\mathcal{M}_{\overline{\mathrm{GEFS}},(ii)+\bar{\mathrm{I}}\mathrm{FS}} &= \mathcal{M}^{\dagger}_{\mathrm{LO}}\mathcal{M}_{\mathrm{GEFS},(ii)+\mathrm{IFS}}(1\leftrightarrow 2) , \\
\mathrm{Tr}\Big(\mathrm{Dirac}^{\lambda'\dagger}_{\mathrm{LO}}\mathrm{Dirac}^{\bar{\lambda}\bar{\eta}\eta'}_{q\to\bar{q}}\Big) &= \mathrm{Tr}\Big(\mathrm{Dirac}^{\lambda'\dagger}_{\mathrm{LO}}\mathrm{Dirac}^{\bar{\lambda}\bar{\eta}\eta'}_{\bar{q}\to q}\Big)(1\leftrightarrow 2) .
\end{aligned}
\tag{9.9}
$$

The terms due to interference between final-state emission from the quark and antiquark read:

$$
\begin{aligned}
&\int_{\mathbf{p}_3}\Big[\mathcal{M}^{\dagger}_{\overline{\mathrm{Q}}\mathrm{FS}}\mathcal{M}_{\mathrm{QFS}}+\mathcal{M}^{\dagger}_{\mathrm{QFS}}\mathcal{M}_{\overline{\mathrm{Q}}\mathrm{FS}}\Big] \\
&=-4(2\pi)^2\alpha_{\mathrm{em}}e_f^2\alpha_s\mathrm{Tr}\Big(\mathrm{Dirac}^{\eta'\lambda'\dagger}_{\overline{\mathrm{Q}}\mathrm{SW}}\mathrm{Dirac}^{\bar{\eta}\bar{\lambda}}_{\mathrm{QSW}}\Big)\frac{p_3^+}{p_{j1}^++p_3^+}\frac{p_3^+}{p_{j2}^++p_3^+} \\
&\quad\times\left\{\int_{\mathbf{v},\mathbf{v}'}\int_{\mathbf{x}_1,\mathbf{x}_{1'},\mathbf{x}_2,\mathbf{x}_{2'},\mathbf{x}_3} e^{-i\mathbf{p}_{j1}\cdot\mathbf{x}_{11'}}e^{-i\mathbf{p}_{j2}\cdot\mathbf{x}_{22'}}\right. \\
&\quad\times\delta^{(2)}\Big(\mathbf{v}-\frac{p_{j1}^+}{p_{j1}^++p_3^+}\mathbf{x}_1-\frac{p_3^+}{p_{j1}^++p_3^+}\mathbf{x}_3\Big)\delta^{(2)}\Big(\mathbf{v}'-\frac{p_{j2}^+}{p_{j2}^++p_3^+}\mathbf{x}_{2'}-\frac{p_3^+}{p_{j2}^++p_3^+}\mathbf{x}_3\Big) \\
&\quad\times A^{\bar{\eta}}(\mathbf{x}_{13})A^{\eta'}(\mathbf{x}_{2'3})A^{\bar{\lambda}}(\mathbf{v}-\mathbf{x}_2)A^{\lambda'}(\mathbf{v}'-\mathbf{x}_{1'}) \\
&\quad\times\left.\left\langle s_{v'1'}s_{v2}-s_{v2}-s_{v'1'}+1-\frac{1}{N_c^2}\Big(Q_{v2v'1'}-s_{v2}-s_{v'1'}+1\Big)\right\rangle+\mathrm{c.c.}\right\} ,
\end{aligned}
\tag{9.10}
$$

JHEP10(2022)184

with the Dirac trace, calculated with the help of identity (A.8):

$$\begin{aligned}
&\mathrm{Tr}\Big(\mathrm{Dirac}^{\eta'\lambda'\dagger}_{\overline{\mathrm{QSW}}}\mathrm{Dirac}^{\bar\eta\bar\lambda}_{\mathrm{QSW}}\Big)\\
&=-32\frac{p^+_{j1}p^+_{j2}}{q^+p^+_3}\Bigg[\frac{(2p^+_{j1}p^+_{j2}+(p^+_{j1}+p^+_{j2})p^+_3)\big((p^+_{j1})^2+(p^+_{j2})^2+(p^+_{j1}+p^+_{j2})p^+_3\big)}{q^+p^+_3}\delta^{\bar\lambda\lambda'}\delta^{\bar\eta\eta'}\\
&\qquad\qquad-(p^+_{j1}-p^+_{j2})^2\epsilon^{\bar\lambda\lambda'}\epsilon^{\bar\eta\eta'}\Bigg].
\end{aligned}\tag{9.11}$$

9.2 Finite virtual

SESW. The virtual contributions to the cross section due to the gluon self-energy correction scattering off the shockwave read, after having subtracted the UV divergence:

$$\begin{aligned}
&\mathcal{M}^\dagger_{\mathrm{LO}}\mathcal{M}_{\mathrm{SESW,sub}}=-32(2\pi)\alpha_{\mathrm{em}}e_f^2\alpha_s N_c^2p^+_{j1}p^+_{j2}(z^2+\bar z^2)\\
&\times\int_{k_f^+}^{p^+_{j1}}\frac{\mathrm{d}k^+_3}{k^+_3}\Big[1+\Big(1-\frac{k^+_3}{p^+_{j1}}\Big)^2\Big]\int_{\mathbf{x}_{1'},\mathbf{x}_{2'},\mathbf{x}_1,\mathbf{x}_2,\mathbf{x}_3}e^{-i\mathbf{p}_{j1}\cdot\mathbf{x}_{11'}}e^{-i\mathbf{p}_{j2}\cdot\mathbf{x}_{22'}}A^{\bar\lambda}(\mathbf{x}_{1'2'})A^{\bar\eta}(\mathbf{x}_{13})\\
&\times\Bigg\{e^{i\frac{k^+_3}{p^+_{j1}}\mathbf{p}_{j1}\cdot\mathbf{x}_{13}}A^{\bar\eta}(\mathbf{x}_{13})\mathcal{A}^{\bar\lambda}\Big(\frac{k^+_3}{p^+_{j1}}\mathbf{x}_{13}+\mathbf{x}_{21},\frac{k^+_3}{p^+_{j1}}\mathbf{x}_{13};\frac{q^+(p^+_{j1}-k^+_3)}{k^+_3p^+_{j2}}\Big)\\
&\quad\times\Big\langle Q_{322'1'}s_{13}-s_{13}s_{32}-s_{2'1'}+1-\frac{1}{N_c^2}\Big(Q_{122'1'}-s_{12}-s_{2'1'}+1\Big)\Big\rangle\\
&\quad-\Big(A^{\bar\eta}(\mathbf{x}_{13})-A^{\bar\eta}(\mathbf{x}_{23})\Big)A^{\bar\lambda}(\mathbf{x}_{21})\Big(1-\frac{1}{N_c^2}\Big)\Big\langle Q_{122'1'}-s_{12}-s_{2'1'}+1\Big\rangle\Bigg\},
\end{aligned}\tag{9.12}$$

and:

$$\begin{aligned}
&\mathcal{M}^\dagger_{\mathrm{LO}}\mathcal{M}_{\overline{\mathrm{SE}}\mathrm{SW,sub}}=+32(2\pi)\alpha_{\mathrm{em}}e_f^2\alpha_s N_c^2p^+_{j1}p^+_{j2}(z^2+\bar z^2)\\
&\times\int_{k_f^+}^{p^+_{j2}}\frac{\mathrm{d}k^+_3}{k^+_3}\Big[1+\Big(1-\frac{k^+_3}{p^+_{j2}}\Big)^2\Big]\int_{\mathbf{x}_{1'},\mathbf{x}_{2'},\mathbf{x}_1,\mathbf{x}_2,\mathbf{x}_3}e^{-i\mathbf{p}_{j1}\cdot\mathbf{x}_{11'}}e^{-i\mathbf{p}_{j2}\cdot\mathbf{x}_{22'}}A^{\bar\lambda}(\mathbf{x}_{1'2'})A^{\bar\eta}(\mathbf{x}_{23})\\
&\times\Bigg\{e^{i\frac{k^+_3}{p^+_{j2}}\mathbf{p}_{j2}\cdot\mathbf{x}_{23}}A^{\bar\eta}(\mathbf{x}_{23})\mathcal{A}^{\bar\lambda}\Big(\frac{k^+_3}{p^+_{j2}}\mathbf{x}_{23}+\mathbf{x}_{12},\frac{k^+_3}{p^+_{j2}}\mathbf{x}_{23};\frac{q^+(p^+_{j2}-k^+_3)}{k^+_3p^+_{j1}}\Big)\\
&\quad\times\Big\langle Q_{132'1'}s_{32}-s_{13}s_{32}-s_{2'1'}+1-\frac{1}{N_c^2}\Big(Q_{122'1'}-s_{12}-s_{2'1'}+1\Big)\Big\rangle\\
&\quad-\Big(A^{\bar\eta}(\mathbf{x}_{23})-A^{\bar\eta}(\mathbf{x}_{13})\Big)A^{\bar\lambda}(\mathbf{x}_{12})\Big(1-\frac{1}{N_c^2}\Big)\Big\langle Q_{122'1'}-s_{12}-s_{2'1'}+1\Big\rangle\Bigg\}.
\end{aligned}\tag{9.13}$$

JHEP10(2022)184

GESW. We find for the contributions due to a gluon being exchanged between the antiquark and quark, traveling through the shockwave:

$$\begin{aligned}\mathcal{M}^{\dagger}_{\mathrm{LO}}\mathcal{M}_{\mathrm{GESW}} = 2\pi\alpha_{\mathrm{em}}e_f^2\alpha_s N_c^2\int_{k_f^+}^{p_{j1}^+}\frac{\mathrm{d}k_3^+}{k_3^+}\frac{(k_3^+)^2}{p_{j1}^+(p_{j2}^+ + k_3^+)}\mathrm{Tr}\Big(\mathrm{Dirac}^{\lambda'\dagger}_{\mathrm{LO}}\mathrm{Dirac}^{\bar\lambda\bar\eta\eta'}_{\bar q\to q}\Big)\\ \times\int_{\mathbf{x}_{1'},\mathbf{x}_{2'},\mathbf{x}_1,\mathbf{x}_2,\mathbf{x}_3} e^{-i\mathbf{p}_{j1}\cdot\mathbf{x}_{11'}}e^{-i\mathbf{p}_{j2}\cdot\mathbf{x}_{22'}}e^{i\frac{k_3^+}{p_{j1}^+}\mathbf{p}_{j1}\cdot\mathbf{x}_{13}}A^{\lambda'}(\mathbf{x}_{1'2'})\\ \times A^{\eta'}(\mathbf{x}_{13})A^{\bar\eta}(\mathbf{x}_{23})\mathcal{A}^{\bar\lambda}\Big(\frac{p_{j2}^+\mathbf{x}_{12}+k_3^+\mathbf{x}_{13}}{p_{j2}^+ + k_3^+},\frac{k_3^+}{p_{j2}^+ + k_3^+}\mathbf{x}_{32};\frac{q^+p_{j2}^+}{k_3^+(p_{j1}^+ - k_3^+)}\Big)\\ \times\Big\langle Q_{322'1'}s_{13} - s_{13}s_{32} - s_{2'1'} + 1 - \frac{1}{N_c^2}\Big(Q_{122'1'} - s_{12} - s_{2'1'} + 1\Big)\Big\rangle\,,\end{aligned}\tag{9.14}$$

where the Dirac trace is easily calculated applying identity (A.8), with the following result:

$$\begin{aligned}\mathrm{Tr}\Big(\mathrm{Dirac}^{\lambda'\dagger}_{\mathrm{LO}}\mathrm{Dirac}^{\bar\lambda\bar\eta\eta'}_{\bar q\to q}\Big) = 32\frac{p_{j1}^+p_{j2}^+}{(q^+k_3^+)^2}\Big[\Big((k_3^+)^2 + k_3^+(p_{j2}^+ - p_{j1}^+) - 2p_{j1}^+p_{j2}^+\Big)\\ \times\Big((p_{j1}^+)^2 + (p_{j2}^+)^2 + k_3^+(p_{j2}^+ - p_{j1}^+)\Big)\delta^{\bar\lambda\lambda'}\delta^{\bar\eta\eta'}\\ + q^+k_3^+(k_3^+ + p_{j2}^+ - p_{j1}^+)^2\epsilon^{\bar\lambda\lambda'}\epsilon^{\bar\eta\eta'}\Big]\,.\end{aligned}\tag{9.15}$$

The $q\leftrightarrow\bar q$ conjugate, where the gluon is emitted from the quark and, after interaction with the shockwave, absorbed by the antiquark, is given by:

$$\begin{aligned}\mathcal{M}^{\dagger}_{\mathrm{LO}}\mathcal{M}_{\overline{\mathrm{GESW}}} = 2\pi\alpha_{\mathrm{em}}e_f^2\alpha_s N_c^2\int_{k_f^+}^{p_{j2}^+}\frac{\mathrm{d}k_3^+}{k_3^+}\frac{(k_3^+)^2}{p_{j2}^+(p_{j1}^+ + k_3^+)}\mathrm{Tr}\Big(\mathrm{Dirac}^{\lambda'\dagger}_{\mathrm{LO}}\mathrm{Dirac}^{\bar\lambda\bar\eta\eta'}_{q\to\bar q}\Big)\\ \times\int_{\mathbf{x}_{1'},\mathbf{x}_{2'},\mathbf{x}_1,\mathbf{x}_2,\mathbf{x}_3} e^{-i\mathbf{p}_{j1}\cdot\mathbf{x}_{11'}}e^{-i\mathbf{p}_{j2}\cdot\mathbf{x}_{22'}}e^{i\frac{k_3^+}{p_{j2}^+}\mathbf{p}_{j2}\cdot\mathbf{x}_{23}}A^{\lambda'}(\mathbf{x}_{1'2'})\\ \times A^{\eta'}(\mathbf{x}_{32})A^{\bar\eta}(\mathbf{x}_{31})\mathcal{A}^{\bar\lambda}\Big(\frac{p_{j1}^+\mathbf{x}_{21}+k_3^+\mathbf{x}_{23}}{p_{j1}^+ + k_3^+},\frac{k_3^+}{p_{j1}^+ + k_3^+}\mathbf{x}_{31};\frac{q^+p_{j1}^+}{k_3^+(p_{j2}^+ - k_3^+)}\Big)\\ \times\Big\langle Q_{132'1'}s_{32} - s_{13}s_{32} - s_{2'1'} + 1 - \frac{1}{N_c^2}\Big(Q_{122'1'} - s_{12} - s_{2'1'} + 1\Big)\Big\rangle\,,\end{aligned}\tag{9.16}$$

and the Dirac trace yields:

$$\begin{aligned}&\mathrm{Tr}\Big(\mathrm{Dirac}^{\lambda'\dagger}_{\mathrm{LO}}\mathrm{Dirac}^{\bar\lambda\bar\eta\eta'}_{q\to\bar q}\Big)\\ &= -32\frac{p_{j1}^+p_{j2}^+}{(q^+k_3^+)^2}\Big[\Big(k_3^+(p_{j1}^+ - p_{j2}^+) - 2p_{j1}^+p_{j2}^+\Big)\Big((k_3^+)^2 + k_3^+(p_{j1}^+ - p_{j2}^+) - 2p_{j1}^+p_{j2}^+\Big)\delta^{\bar\lambda\lambda'}\delta^{\bar\eta\eta'}\\ &\qquad - q^+(k_3^+)^2(k_3^+ + p_{j1}^+ - p_{j2}^+)\epsilon^{\bar\lambda\lambda'}\epsilon^{\bar\eta\eta'}\Big]\,.\end{aligned}\tag{9.17}$$

JHEP10(2022)184

ISW. The following contributions are due to the instantaneous splitting of the photon into a gluon, quark and antiquark where, after traveling through the shockwave, the gluon is absorbed by the quark:

$$\begin{aligned}
&\mathcal{M}_{\rm LO}^{\dagger}\mathcal{M}_{\rm ISW}\\
&\quad= -32(2\pi)\alpha_{\rm em}e_f^2\alpha_s N_c^2 p_{j1}^+p_{j2}^+\int_{k_f^+}^{p_{j1}^+}\mathrm{d}k_3^+\frac{p_{j1}^+-k_3^+}{q^+p_{j1}^+}\Big(\frac{p_{j1}^+}{p_{j2}^++k_3^+}+\frac{p_{j2}^+(p_{j1}^+-k_3^+)}{(p_{j1}^+)^2}\Big)\\
&\qquad\times\int_{\mathbf{x}_{1'},\mathbf{x}_{2'},\mathbf{x}_1,\mathbf{x}_2,\mathbf{x}_3}e^{-i\mathbf{p}_{j1}\cdot\mathbf{x}_{11'}}e^{-i\mathbf{p}_{j2}\cdot\mathbf{x}_{22'}}e^{i\mathbf{p}_{j1}\cdot\frac{k_3^+}{p_{j1}^+}\mathbf{x}_{13}}\\
&\qquad\times A^{\lambda'}(\mathbf{x}_{1'2'})A^{\lambda'}(\mathbf{x}_{31})\mathcal{C}\Big(\frac{k_3^+}{p_{j1}^+}\mathbf{x}_{13}+\mathbf{x}_{21},\frac{k_3^+}{p_{j1}^+}\mathbf{x}_{13};\frac{q^+(p_{j1}^+-k_3^+)}{p_{j2}^+k_3^+}\Big)\\
&\qquad\times\Big\langle Q_{322'1's_{13}}-s_{13}s_{32}-s_{2'1'}+1-\frac{1}{N_c^2}\Big(Q_{122'1'}-s_{12}-s_{2'1'}+1\Big)\Big\rangle\,.
\end{aligned}\tag{9.18}$$

In the above, we used the following result for the Dirac trace:

$$\mathrm{Tr}\Big(\mathrm{Dirac}_{\rm LO}^{\lambda'\dagger}\mathrm{Dirac}_{\rm ISW}^{\eta'}\Big)=32p_{j1}^+p_{j2}^+\delta^{\lambda'\eta'}\frac{(p_{j1}^+)^3+p_{j2}^+(p_{j1}^+-k_3^+)(p_{j2}^++k_3^+)}{k_3^+q^+(k_3^++p_{j2}^+-p_{j1}^+)}\,.\tag{9.19}$$

Likewise, when the gluon is absorbed by the antiquark, one obtains:

$$\begin{aligned}
&\mathcal{M}_{\rm LO}^{\dagger}\mathcal{M}_{\bar{\rm I}\rm SW}\\
&\quad= 32(2\pi)\alpha_{\rm em}e_f^2\alpha_s N_c^2 p_{j1}^+p_{j2}^+\int_{k_f^+}^{p_{j2}^+}\mathrm{d}k_3^+\frac{p_{j2}^+-k_3^+}{q^+p_{j2}^+}\Big(\frac{p_{j2}^+}{p_{j1}^++k_3^+}+\frac{p_{j1}^+(p_{j2}^+-k_3^+)}{(p_{j2}^+)^2}\Big)\\
&\qquad\times\int_{\mathbf{x}_{1'},\mathbf{x}_{2'},\mathbf{x}_1,\mathbf{x}_2,\mathbf{x}_3}e^{-i\mathbf{p}_{j1}\cdot\mathbf{x}_{11'}}e^{-i\mathbf{p}_{j2}\cdot\mathbf{x}_{22'}}e^{i\mathbf{p}_{j2}\cdot\frac{k_3^+}{p_{j2}^+}\mathbf{x}_{23}}\\
&\qquad\times A^{\lambda'}(\mathbf{x}_{1'2'})A^{\lambda'}(\mathbf{x}_{32})\mathcal{C}\Big(\frac{k_3^+}{p_{j2}^+}\mathbf{x}_{23}+\mathbf{x}_{12},\frac{k_3^+}{p_{j2}^+}\mathbf{x}_{23};\frac{q^+(p_{j2}^+-k_3^+)}{p_{j1}^+k_3^+}\Big)\\
&\qquad\times\Big\langle Q_{132'1's_{32}}-s_{13}s_{32}-s_{2'1'}+1-\frac{1}{N_c^2}\Big(Q_{122'1'}-s_{12}-s_{2'1'}+1\Big)\Big\rangle\,,
\end{aligned}\tag{9.20}$$

where we used that:

$$\mathrm{Tr}\Big(\mathrm{Dirac}_{\rm LO}^{\lambda'\dagger}\mathrm{Dirac}_{\bar{\rm I}\rm SW}^{\eta'}\Big)=-32p_{j1}^+p_{j2}^+\delta^{\lambda'\eta'}\frac{(p_{j2}^+)^3+p_{j1}^+(p_{j2}^+-k_3^+)(p_{j1}^++k_3^+)}{k_3^+q^+(k_3^++p_{j1}^+-p_{j2}^+)}\,.\tag{9.21}$$

GEFS, (i). The following contribution is what is left after subtracting $\mathcal{M}_{\mathrm{GEFS},(ii)}$ from the amplitude due to final-state gluon exchange:

$$\begin{aligned}
\mathcal{M}_{\rm LO}^{\dagger}\mathcal{M}_{\mathrm{GEFS},(i)}&=(2\pi)\alpha_{\rm em}e_f^2\alpha_s N_c^2\int_{k_f^+}^{p_{j1}^+}\mathrm{d}k_3^+\frac{p_{j1}^+-k_3^+}{q^+p_{j1}^+}\mathrm{Tr}\Big(\mathrm{Dirac}_{\rm LO}^{\lambda'\dagger}\mathrm{Dirac}_{\bar{q}\to q,(i)}^{\bar{\lambda}\bar{\eta}\eta'}\Big)\\
&\quad\times\int_{\mathbf{x}_{1'},\mathbf{x}_{2'},\mathbf{x}_1,\mathbf{x}_2}e^{-i\mathbf{p}_{j1}\cdot\mathbf{x}_{11'}}e^{-i\mathbf{p}_{j2}\cdot\mathbf{x}_{22'}}e^{i\frac{k_3^+}{p_{j1}^+}\mathbf{p}_{j1}\cdot\mathbf{x}_{12}}\\
&\quad\times A^{\lambda'}(\mathbf{x}_{1'2'})A^{\bar{\lambda}}(\mathbf{x}_{12})J^{\eta'\bar{\eta}}(k_3,\mathbf{x}_{12})\\
&\quad\times\Big\langle s_{2'1'}s_{12}-s_{12}-s_{2'1'}+1-\frac{1}{N_c^2}\Big(Q_{2'1'12}-s_{12}-s_{2'1'}-1\Big)\Big\rangle\,,
\end{aligned}\tag{9.22}$$

JHEP10(2022)184

with the Dirac trace:

$$\begin{aligned}\mathrm{Tr}\Big(\mathrm{Dirac}^{\lambda'\dagger}_{\mathrm{LO}}\mathrm{Dirac}^{\bar\lambda\bar\eta\eta'}_{\bar q\to q,(i)}\Big) = 32\frac{p^+_{j1}p^+_{j2}}{(q^+k^+_3)^2}\Bigg[&\Big((k^+_3)^2+k^+_3(p^+_{j2}-p^+_{j1})\Big)\\ &\times\Big((p^+_{j1})^2+(p^+_{j2})^2+k^+_3(p^+_{j2}-p^+_{j1})\Big)\delta^{\bar\lambda\lambda'}\delta^{\bar\eta\eta'}\\ &+q^+k^+_3(k^+_3+p^+_{j2}-p^+_{j1})^2\epsilon^{\bar\lambda\lambda'}\epsilon^{\bar\eta\eta'}\Bigg]\,.\end{aligned}\tag{9.23}$$

The $q\leftrightarrow\bar q$ conjugate contributions to the cross section can be simply obtained from the above result by exchanging the quark and antiquark indices:

$$\begin{aligned}\mathcal{M}^\dagger_{\mathrm{LO}}\mathcal{M}_{\overline{\mathrm{GEFS}},(i)} &= \mathcal{M}^\dagger_{\mathrm{LO}}\mathcal{M}_{\mathrm{GEFS},(i)}(1\leftrightarrow 2)\,,\\ \mathrm{Tr}\Big(\mathrm{Dirac}^{\lambda'\dagger}_{\mathrm{LO}}\mathrm{Dirac}^{\bar\lambda\bar\eta\eta'}_{q\to\bar q}\Big) &= \mathrm{Tr}\Big(\mathrm{Dirac}^{\lambda'\dagger}_{\mathrm{LO}}\mathrm{Dirac}^{\bar\lambda\bar\eta\eta'}_{\bar q\to q}\Big)(1\leftrightarrow 2)\,.\end{aligned}\tag{9.24}$$

IS+UV+FSUV. Finally, the contributions due to the initial-state corrections, ultraviolet counterterms, and ultraviolet part of the self-energy corrections to the asymptotic final states read:

$$\mathcal{M}^\dagger_{\mathrm{LO}}\mathcal{M}_{\mathrm{IS+UV+FSUV}} = |\mathcal{M}_{\mathrm{LO}}|^2\frac{\alpha_s C_F}{2\pi}\left(\frac{1}{2}\ln^2\frac{p^+_{j1}}{p^+_{j2}}-\frac{\pi^2}{6}+2\right)\,.\tag{9.25}$$

9.3 Real terms

Final-state gluon radiation outside jet. The two terms in the first line of eq. (9.6) are due to what we call the regular parts of $|\mathrm{QFS}|^2$ and $|\overline{\mathrm{Q}}\mathrm{FS}|^2$ (see section 8), where the gluon is emitted outside the jet (with $\xi=p^+_3/p^+_{j1}$):

$$\begin{aligned}\frac{\mathrm{d}\sigma^{|\mathrm{QFS}|^2;\,\mathrm{out};\,\mathrm{reg}}_{\mathrm{dijet}}}{\mathrm{d}p^+_{j1}\mathrm{d}^2\mathbf{p}_{j1}\mathrm{d}p^+_{j2}\mathrm{d}^2\mathbf{p}_{j2}} = &\frac{\theta(p^+_{j1})}{(2\pi)^3 2p^+_{j1}}\frac{\theta(p^+_{j2})}{(2\pi)^3 2p^+_{j2}}\frac{1}{2q^+}\frac{1}{2}|\mathcal{M}_{\mathrm{LO}}|^2_{\vec p_{1,2}\to\vec p_{j1,j2}}\\ &\times\frac{\alpha_s C_F}{2\pi}\int_0^{+\infty}\frac{\mathrm{d}\xi}{\xi}e^{-i\xi\mathbf{p}_{j1}\cdot\mathbf{x}_{11'}}\left[-2\ln R-\ln\left(\frac{\mathbf{p}^2_{j1}\mathbf{x}^2_{11'}}{c_0^2}\right)-2\ln\xi\right]\\ &\times\Bigg\{2\pi\delta(q^+-(1+\xi)p^+_{j1}-p^+_{j2})\left[1+\frac{(2\xi+\xi^2)(p^+_{j1})^2}{(p^+_{j1})^2+(p^+_{j2})^2}\right](1+(1+\xi)^2)\\ &-4\pi\delta(q^+-p^+_{j1}-p^+_{j2})\theta(1-\xi)\Bigg\}\,.\end{aligned}\tag{9.26}$$

JHEP10(2022)184

and

$$\frac{\mathrm{d}\sigma_{\mathrm{dijet}}^{|\overline{\mathrm{Q}}\mathrm{FS}|^2;\,\mathrm{out};\,\mathrm{reg}}}{\mathrm{d}p_{j1}^+\mathrm{d}^2\mathbf{p}_{j1}\mathrm{d}p_{j2}^+\mathrm{d}^2\mathbf{p}_{j2}} = \frac{\theta(p_{j1}^+)}{(2\pi)^3 2p_{j1}^+}\frac{\theta(p_{j2}^+)}{(2\pi)^3 2p_{j2}^+}\frac{1}{2q^+}\frac{1}{2}|\mathcal{M}_{\mathrm{LO}}|^2_{\vec{p}_{1,2}\to\vec{p}_{j1,j2}}$$
$$\times\frac{\alpha_s C_F}{2\pi}\int_0^{+\infty}\frac{\mathrm{d}\xi}{\xi}e^{-i\xi\mathbf{p}_{j2}\cdot\mathbf{x}_{22'}}\left[-2\ln R-\ln\left(\frac{\mathbf{p}_{j2}^2\mathbf{x}_{22'}^2}{c_0^2}\right)-2\ln\xi\right]$$
$$\times\left\{2\pi\delta(q^+-p_{j1}^+-(1+\xi)p_{j2}^+)\left[1+\frac{(2\xi+\xi^2)(p_{j2}^+)^2}{(p_{j1}^+)^2+(p_{j2}^+)^2}\right](1+(1+\xi)^2)\right.$$
$$\left.-4\pi\delta(q^+-p_{j1}^+-p_{j2}^+)\theta(1-\xi)\right\}. \tag{9.27}$$

QFS and QSW. The next terms are due to gluon emission before the shockwave and the interference with the final-state emission:

$$\begin{aligned}
&\int_{\mathbf{p}_3}\left[|\mathcal{M}_{\mathrm{QSW}}|^2+\mathcal{M}_{\mathrm{QSW}}^\dagger\mathcal{M}_{\mathrm{QFS}}+\mathcal{M}_{\mathrm{QFS}}^\dagger\mathcal{M}_{\mathrm{QSW}}\right]\\
&=2(2\pi)^2\alpha_{\mathrm{em}}e_f^2\alpha_s N_c^2\mathrm{Tr}\Big(\mathrm{Dirac}_{\mathrm{QSW}}^{\bar\eta\bar\lambda}\mathrm{Dirac}_{\mathrm{QSW}}^{\eta'\lambda'\dagger}\Big)\left(\frac{p_3^+}{p_{j1}^++p_3^+}\right)^2\\
&\times\int_{\mathbf{v},\mathbf{v}'}\int_{\mathbf{x}_1,\mathbf{x}_{1'},\mathbf{x}_2,\mathbf{x}_{2'},\mathbf{x}_3}e^{-i\mathbf{p}_{j1}\cdot\mathbf{x}_{11'}}e^{-i\mathbf{p}_{j2}\cdot\mathbf{x}_{22'}}\delta^{(2)}\left(\mathbf{v}-\frac{p_{j1}^+}{p_{j1}^++p_3^+}\mathbf{x}_1-\frac{p_3^+}{p_{j1}^++p_3^+}\mathbf{x}_3\right)\\
&\times\delta^{(2)}\left(\mathbf{v}'-\frac{p_{j1}^+}{p_{j1}^++p_3^+}\mathbf{x}_{1'}-\frac{p_3^+}{p_{j1}^++p_3^+}\mathbf{x}_3\right)A^{\bar\eta}(\mathbf{x}_{13})A^{\eta'}(\mathbf{x}_{1'3})\\
&\times\left\{\mathcal{A}^{\lambda'}\left(\mathbf{v}'-\mathbf{x}_{2'},\mathbf{x}_{31'},\frac{p_{j1}^+p_3^+q^+}{p_{j2}^+(p_{j1}^++p_3^+)^2}\right)\mathcal{A}^{\bar\lambda}\left(\mathbf{v}-\mathbf{x}_2,\mathbf{x}_{31},\frac{p_{j1}^+p_3^+q^+}{p_{j2}^+(p_{j1}^++p_3^+)^2}\right)\right.\\
&\quad\times\left\langle s_{11'}s_{2'2}-s_{32}s_{13}-s_{31'}s_{2'3}+1-\frac{1}{N_c^2}\Big(Q_{122'1'}-s_{12}-s_{2'1'}+1\Big)\right\rangle\\
&\quad-\mathcal{A}^{\lambda'}\left(\mathbf{v}'-\mathbf{x}_{2'},\mathbf{x}_{31'},\frac{p_{j1}^+p_3^+q^+}{p_{j2}^+(p_{j1}^++p_3^+)^2}\right)A^{\bar\lambda}(\mathbf{v}-\mathbf{x}_2)\\
&\quad\times\left.\left\langle Q_{v22'3}s_{31'}-s_{31'}s_{2'3}-s_{v2}+1-\frac{1}{N_c^2}\Big(Q_{v22'1'}-s_{v2}-s_{2'1'}+1\Big)\right\rangle+\mathrm{c.c.}\right\}.
\end{aligned}\tag{9.28}$$

Likewise, when the gluon is radiated from the antiquark:

$$\begin{aligned}
&\int_{\mathbf{p}_3}\left[|\mathcal{M}_{\overline{\mathrm{Q}}\mathrm{SW}}|^2+\mathcal{M}_{\overline{\mathrm{Q}}\mathrm{SW}}^\dagger\mathcal{M}_{\overline{\mathrm{Q}}\mathrm{FS}}+\mathcal{M}_{\overline{\mathrm{Q}}\mathrm{FS}}^\dagger\mathcal{M}_{\overline{\mathrm{Q}}\mathrm{SW}}\right]\\
&=2(2\pi)^2\alpha_{\mathrm{em}}e_f^2\alpha_s N_c^2\mathrm{Tr}\Big(\mathrm{Dirac}_{\overline{\mathrm{Q}}\mathrm{SW}}^{\eta'\lambda'\dagger}\mathrm{Dirac}_{\overline{\mathrm{Q}}\mathrm{SW}}^{\bar\eta\bar\lambda}\Big)\left(\frac{p_3^+}{p_{j2}^++p_3^+}\right)^2\\
&\times\int_{\mathbf{v},\mathbf{v}'}\int_{\mathbf{x}_1,\mathbf{x}_{1'},\mathbf{x}_2,\mathbf{x}_{2'},\mathbf{x}_3}e^{-i\mathbf{p}_{j1}\cdot\mathbf{x}_{11'}}e^{-i\mathbf{p}_{j2}\cdot\mathbf{x}_{22'}}\delta^{(2)}\left(\mathbf{v}-\frac{p_{j2}^+}{p_{j2}^++p_3^+}\mathbf{x}_2-\frac{p_3^+}{p_{j2}^++p_3^+}\mathbf{x}_3\right)\\
&\times\delta^{(2)}\left(\mathbf{v}'-\frac{p_{j2}^+}{p_{j2}^++p_3^+}\mathbf{x}_{2'}-\frac{p_3^+}{p_{j2}^++p_3^+}\mathbf{x}_3\right)A^{\bar\eta}(\mathbf{x}_{23})A^{\eta'}(\mathbf{x}_{2'3})
\end{aligned}\tag{9.29}$$

JHEP10(2022)184

$$
\times\Bigg\{\mathcal{A}^{\lambda'}\Big(\mathbf{v}'-\mathbf{x}_{1'},\mathbf{x}_{32'},\frac{p_{j2}^+p_3^+q^+}{p_{j1}^+(p_{j2}^++p_3^+)^2}\Big)\mathcal{A}^{\bar\lambda}\Big(\mathbf{v}-\mathbf{x}_1,\mathbf{x}_{32},\frac{p_{j2}^+p_3^+q^+}{p_{j1}^+(p_{j2}^++p_3^+)^2}\Big)
$$
$$
\times\Big\langle s_{11'}s_{2'2}-s_{2'3}s_{31'}-s_{13}s_{32}+1-\frac{1}{N_c^2}(Q_{122'1'}-s_{12}-s_{2'1'}+1)\Big\rangle
$$
$$
-\mathcal{A}^{\lambda'}\Big(\mathbf{v}'-\mathbf{x}_{1'},\mathbf{x}_{32'},\frac{p_{j2}^+p_3^+q^+}{p_{j1}^+(p_{j2}^++p_3^+)^2}\Big)A^{\bar\lambda}(\mathbf{v}-\mathbf{x}_1)
$$
$$
\times\Big\langle Q_{31'1v}s_{2'3}-s_{2'3}s_{31'}-s_{1v}+1-\frac{1}{N_c^2}(Q_{2'1'1v}-s_{1v}-s_{2'1'}+1)\Big\rangle+\text{c.c.}\Bigg\}.
$$

The contributions to the cross section due to the interference between gluon radiation from the quark and from the antiquark read:

$$
\begin{aligned}
&\int_{\mathbf{p}_3}\Big[\mathcal{M}^\dagger_{\overline{\text{Q}}\text{SW}}\mathcal{M}_{\text{QSW}}+\mathcal{M}^\dagger_{\overline{\text{Q}}\text{SW}}\mathcal{M}_{\text{QFS}}+\mathcal{M}^\dagger_{\overline{\text{Q}}\text{FS}}\mathcal{M}_{\text{QSW}}+\text{c.c.}\Big]\\
&=-2(2\pi)^2\alpha_{\text{em}}e_f^2\alpha_sN_c^2\text{Tr}\Big(\text{Dirac}^{\eta'\lambda'\dagger}_{\overline{\text{Q}}\text{SW}}\text{Dirac}^{\bar\eta\bar\lambda}_{\text{QSW}}\Big)\frac{p_3^+}{p_{j1}^++p_3^+}\frac{p_3^+}{p_{j2}^++p_3^+}\\
&\quad\times\int_{\mathbf{v},\mathbf{v}'}\int_{\mathbf{x}_1,\mathbf{x}_{1'},\mathbf{x}_2,\mathbf{x}_{2'},\mathbf{x}_3}e^{-i\mathbf{p}_{j1}\cdot\mathbf{x}_{11'}}e^{-i\mathbf{p}_{j2}\cdot\mathbf{x}_{22'}}\delta^{(2)}\Big(\mathbf{v}'-\frac{p_{j2}^+}{p_{j2}^++p_3^+}\mathbf{x}_{2'}-\frac{p_3^+}{p_{j2}^++p_3^+}\mathbf{x}_3\Big)\\
&\quad\times\delta^{(2)}\Big(\mathbf{v}-\frac{p_{j1}^+}{p_{j1}^++p_3^+}\mathbf{x}_1-\frac{p_3^+}{p_{j1}^++p_3^+}\mathbf{x}_3\Big)A^{\eta'}(\mathbf{x}_{2'3})A^{\bar\eta}(\mathbf{x}_{13})\\
&\quad\times\Bigg\{\mathcal{A}^{\lambda'}\Big(\mathbf{v}'-\mathbf{x}_{1'},\mathbf{x}_{32'},\frac{p_{j2}^+p_3^+q^+}{p_{j1}^+(p_{j2}^++p_3^+)^2}\Big)\mathcal{A}^{\bar\lambda}\Big(\mathbf{v}-\mathbf{x}_2,\mathbf{x}_{31},\frac{p_{j1}^+p_3^+q^+}{p_{j2}^+(p_{j1}^++p_3^+)^2}\Big)\\
&\qquad\times\Big\langle s_{11'}s_{2'2}-s_{2'3}s_{31'}-s_{13}s_{32}+1-\frac{1}{N_c^2}(Q_{122'1'}-s_{12}-s_{2'1'}+1)\Big\rangle\\
&\qquad-\mathcal{A}^{\lambda'}\Big(\mathbf{v}'-\mathbf{x}_{1'},\mathbf{x}_{32'},\frac{p_{j2}^+p_3^+q^+}{p_{j1}^+(p_{j2}^++p_3^+)^2}\Big)A^{\bar\lambda}(\mathbf{v}-\mathbf{x}_2)\\
&\qquad\times\Big\langle Q_{v22'3}s_{31'}-s_{v2}-s_{2'3}s_{31'}+1-\frac{1}{N_c^2}\Big(Q_{v22'1'}-s_{v2}-s_{2'1'}+1\Big)\Big\rangle\\
&\qquad-A^{\lambda'}(\mathbf{v}'-\mathbf{x}_{1'})\mathcal{A}^{\bar\lambda}\Big(\mathbf{v}-\mathbf{x}_2,\mathbf{x}_{31},\frac{p_{j1}^+p_3^+q^+}{p_{j2}^+(p_{j1}^++p_3^+)^2}\Big)\\
&\qquad\times\Big\langle Q_{v'1'13}s_{32}-s_{13}s_{32}-s_{v'1'}+1-\frac{1}{N_c^2}\Big(Q_{v'1'12}-s_{12}-s_{v'1'}+1\Big)\Big\rangle\\
&\qquad+\text{c.c.}\Bigg\}.
\end{aligned}
\tag{9.30}
$$

JHEP10(2022)184

The Dirac traces appearing in the above two expressions are easily calculated using the identities (A.5) and (A.7), and read:

$$\mathrm{Tr}\Big(\mathrm{Dirac}^{\eta'\lambda'\dagger}_{\mathrm{QSW}}\mathrm{Dirac}^{\bar\eta\bar\lambda}_{\mathrm{QSW}}\Big) = 32p^+_{j1}p^+_{j2}\Bigg[\frac{(p^+_{j1})^2+(p^+_{j1}+p^+_3)^2}{(p^+_3)^2}\frac{(p^+_{j2})^2+(p^+_{j1}+p^+_3)^2}{(q^+)^2}\delta^{\bar\lambda\lambda'}\delta^{\bar\eta\eta'} + \frac{(2p^+_{j1}+p^+_3)(p^+_{j1}-p^+_{j2}+p^+_3)}{p^+_3q^+}\epsilon^{\bar\lambda\lambda'}\epsilon^{\bar\eta\eta'}\Bigg], \tag{9.31}$$

$$\mathrm{Tr}\Big(\mathrm{Dirac}^{\eta'\lambda'\dagger}_{\overline{\mathrm{QSW}}}\mathrm{Dirac}^{\bar\eta\bar\lambda}_{\overline{\mathrm{QSW}}}\Big) = \mathrm{Tr}\Big(\mathrm{Dirac}^{\eta'\lambda'\dagger}_{\mathrm{QSW}}\mathrm{Dirac}^{\bar\eta\bar\lambda}_{\mathrm{QSW}}\Big)(1\leftrightarrow 2)\,. \tag{9.32}$$

RI: instantaneous gluon emission. We find for the contribution due to the instantaneous emission of a gluon:

$$\begin{aligned}\int_{\mathbf{p}_3}|\mathcal{M}_{\mathrm{RI}}|^2 &= 4(2\pi)^2\alpha_{\mathrm{em}}e_f^2\alpha_s\frac{p_1^{+2}p_3^{+2}(p^+_{j1}+p^+_3)^2}{(q^+)^6}\\ &\times\mathrm{Tr}|\mathrm{Dirac}_{\mathrm{RI}}|^2\int_{\mathbf{x}_{1'},\mathbf{x}_{2'},\mathbf{x}_1,\mathbf{x}_2,\mathbf{x}_3}e^{-i\mathbf{p}_{j1}\cdot\mathbf{x}_{11'}}e^{-i\mathbf{p}_{j2}\cdot\mathbf{x}_{22'}}\\ &\times\mathcal{C}\Big(\frac{p^+_{j1}}{q^+}\mathbf{x}_{21}+\frac{p^+_3}{q^+}\mathbf{x}_{23},\mathbf{x}_{31},\frac{p^+_{j1}p^+_3}{q^+p^+_{j2}}\Big)\mathcal{C}\Big(\frac{p^+_{j1}}{q^+}\mathbf{x}_{2'1'}+\frac{p^+_3}{q^+}\mathbf{x}_{2'3},\mathbf{x}_{31'},\frac{p^+_{j1}p^+_3}{q^+p^+_{j2}}\Big)\\ &\times\Big\langle s_{11'}s_{2'2}-s_{2'3}s_{31'}-s_{13}s_{32}+1-\frac{1}{N_c^2}(Q_{122'1'}-s_{12}-s_{2'1'}+1)\Big\rangle\,,\end{aligned} \tag{9.33}$$

with the Dirac trace:

$$\mathrm{Tr}|\mathrm{Dirac}_{\mathrm{RI}}|^2 = \frac{16(q^+)^2p^+_{j1}p^+_{j2}}{(p^+_{j1}+p^+_3)^2(p^+_{j2}+p^+_3)^2}\Big((p^+_{j1}-p^+_{j2})^2+(p^+_{j1}+p^+_{j2}+2p^+_3)^2\Big)\,. \tag{9.34}$$

Interference terms. Finally, the interference terms due to instantaneous gluon emission in the complex conjugate amplitude and radiation from a quark in the amplitude read:

$$\begin{aligned}&\int_{\mathbf{p}_3}\mathcal{M}^\dagger_{\mathrm{RI}}\Big(\mathcal{M}_{\mathrm{QSW}}+\mathcal{M}_{\mathrm{QFS}}\Big) = 2(2\pi)^2\alpha_{\mathrm{em}}e_f^2\alpha_sN_c^2\frac{p^+_{j1}(p^+_3)^2}{(q^+)^3}\mathrm{Tr}\Big(\mathrm{Dirac}^\dagger_{\mathrm{RI}}\mathrm{Dirac}^{\bar\eta\bar\lambda}_{\mathrm{QSW}}\Big)\\ &\times\int_{\mathbf{x}_{1'},\mathbf{x}_{2'},\mathbf{x}_1,\mathbf{x}_2,\mathbf{x}_3,\mathbf{v}}e^{-i\mathbf{p}_{j1}\cdot\mathbf{x}_{11'}}e^{-i\mathbf{p}_{j2}\cdot\mathbf{x}_{22'}}\delta^{(2)}\Big(\mathbf{v}-\frac{p^+_{j1}}{p^+_{j1}+p^+_3}\mathbf{x}_1-\frac{p^+_3}{p^+_{j1}+p^+_3}\mathbf{x}_3\Big)\\ &\times\mathcal{C}\Big(\frac{p^+_{j1}}{q^+}\mathbf{x}_{2'1'}+\frac{p^+_3}{q^+}\mathbf{x}_{2'3},\mathbf{x}_{31'},\frac{p^+_{j1}p^+_3}{q^+p^+_{j2}}\Big)A^{\bar\eta}(\mathbf{x}_{13})\\ &\times\Bigg\{-\mathcal{A}^{\bar\lambda}\Big(\mathbf{v}-\mathbf{x}_2,\mathbf{x}_{31},\frac{p^+_{j1}p^+_3q^+}{p^+_{j2}(p^+_{j1}+p^+_3)^2}\Big)\\ &\quad\times\Big\langle s_{11'}s_{2'2}-s_{32}s_{13}-s_{31'}s_{2'3}+1-\frac{1}{N_c^2}\Big(Q_{122'1'}-s_{12}-s_{2'1'}+1\Big)\Big\rangle\\ &\quad+A^{\bar\lambda}(\mathbf{v}-\mathbf{x}_2)\Big\langle Q_{v22'3}s_{31'}-s_{v2}-s_{31'}s_{2'3}+1-\frac{1}{N_c^2}\Big(Q_{v22'1'}-s_{v2}-s_{2'1'}+1\Big)\Big\rangle\Bigg\}\,,\end{aligned} \tag{9.35}$$

with the Dirac trace:

$$\mathrm{Tr}\Big(\mathrm{Dirac}^\dagger_{\mathrm{RI}}\mathrm{Dirac}^{\bar\eta\bar\lambda}_{\mathrm{QSW}}\Big) = -32p^+_{j1}p^+_{j2}\delta^{\bar\lambda\bar\eta}\frac{1}{p^+_3}\Big(\frac{(p^+_{j1}+p^+_3)^2}{p^+_{j2}+p^+_3}+\frac{p^+_{j1}p^+_{j2}}{p^+_{j1}+p^+_3}\Big)\,. \tag{9.36}$$

JHEP10(2022)184

Likewise, for the interference between instantaneous emission with gluon radiation from the antiquark, we find:

$$
\begin{aligned}
&\int_{\mathbf{p}_3} \mathcal{M}^{\dagger}_{\mathrm{RI}}\Big(\mathcal{M}_{\overline{\mathrm{Q}}\mathrm{SW}}+\mathcal{M}_{\overline{\mathrm{Q}}\mathrm{FS}}\Big)\\
&=-2(2\pi)\alpha_{\mathrm{em}}e_f^2\alpha_s N_c^2\frac{p_{j1}^+(p_3^+)^2(p_{j1}^++p_3^+)}{(q^+)^3(p_{j2}^++p_3^+)}\mathrm{Dirac}^{\dagger}_{\mathrm{RI}}\mathrm{Dirac}^{\bar\eta\bar\lambda}_{\overline{\mathrm{Q}}\mathrm{SW}}\\
&\quad\times\int_{\mathbf{x}_{1'},\mathbf{x}_{2'},\mathbf{x}_1,\mathbf{x}_2,\mathbf{x}_3,\mathbf{v}} e^{-i\mathbf{p}_{j1}\cdot\mathbf{x}_{11'}}e^{-i\mathbf{p}_{j2}\cdot\mathbf{x}_{22'}}\delta^{(2)}\left(\mathbf{v}-\frac{p_{j2}^+}{p_{j2}^++p_3^+}\mathbf{x}_2-\frac{p_3^+}{p_{j2}^++p_3^+}\mathbf{x}_3\right)\\
&\quad\times\mathcal{C}\left(\frac{p_{j1}^+}{q^+}\mathbf{x}_{2'1'}+\frac{p_3^+}{q^+}\mathbf{x}_{2'3'},\mathbf{x}_{3'1'},\frac{p_{j1}^+p_3^+}{q^+p_{j2}^+}\right)A^{\bar\eta}(\mathbf{x}_{23})\\
&\quad\times\Bigg\{-\mathcal{A}^{\bar\lambda}\left(\mathbf{v}-\mathbf{x}_1,\mathbf{x}_{32},\frac{p_{j2}^+p_3^+q^+}{p_{j1}^+(p_{j2}^++p_3^+)^2}\right)\\
&\qquad\times\left\langle s_{2'2}s_{11'}-s_{13}s_{32}-s_{2'3}s_{31'}+1-\frac{1}{N_c^2}\Big(Q_{122'1'}-s_{12}-s_{2'1'}+1\Big)\right\rangle\\
&\qquad+A^{\bar\lambda}(\mathbf{v}-\mathbf{x}_1)\left\langle Q_{31'1v}s_{2'3}-s_{1v}-s_{2'3}s_{31'}+1-\frac{1}{N_c^2}\Big(Q_{2'1'1v}-s_{1v}-s_{2'1'}+1\Big)\right\rangle\Bigg\},
\end{aligned}
\tag{9.37}
$$

with the Dirac trace:

$$
\mathrm{Tr}\Big(\mathrm{Dirac}^{\dagger}_{\mathrm{RI}}\mathrm{Dirac}^{\bar\eta\bar\lambda}_{\overline{\mathrm{Q}}\mathrm{SW}}\Big)=32p_{j1}^+p_{j2}^+\delta^{\bar\lambda\bar\eta}\frac{1}{p_3^+}\left(\frac{(p_{j2}^++p_3^+)^2}{p_{j1}^++p_3^+}+\frac{p_{j1}^+p_{j2}^+}{p_{j2}^++p_3^+}\right). \tag{9.38}
$$

10 Correlation limit

In the so-called 'correlation limit' (refs. [59, 60]), the two outgoing jets are back-to-back in the transverse plane. In this kinematic configuration, we recover a scale $\mathbf{k}_\perp=\mathbf{p}_{j1}+\mathbf{p}_{j2}$ set by the vector sum of the transverse jet momenta, which is small with respect to the center-of-mass energy $\sqrt{s}$ and the large transverse momentum of the jets $\mathbf{P}_\perp^2\sim\mathbf{p}_{j1}^2\sim\mathbf{p}_{j2}^2$. $\mathbf{k}_\perp^2$ is typically of the order of the saturation scale Q_s^2 but can in principle even become nonperturbative:

$$
s\gg\mathbf{P}_\perp^2\gg\mathbf{k}_\perp^2\sim Q_s^2\,. \tag{10.1}
$$

The emergence of the large ratio $\mathbf{P}_\perp^2/\mathbf{k}_\perp^2\gg1$ implies the appearance of large 'Sudakov' logarithms, which need to be resummed on top of the rapidity logarithms $Y_f^+\propto\ln s$. Sudakov resummation is governed by the Collins-Soper-Sterman (CSS [27, 28]) evolution equations, which are embedded in the framework of transverse momentum dependent (TMD) factorization (refs. [29, 31]). Cross sections in TMD factorization can be written as the convolution of a hard part with TMD parton distribution functions and/or fragmentation functions (TMD PDFs and TMD FFs), which evolve according to CSS.

It has been known since a long time [60] that, in the correlation limit, the leading-order CGC cross section (2.24) can be written as the product of a hard part with a gluon TMD PDF, consistent with what one would find in TMD factorization at tree level. One part

JHEP10(2022)184

of the proof that this correspondence holds at higher orders, is to demonstrate that the Sudakov logarithms in our NLO cross section have the right form and can be absorbed into CSS. It turns out that this first step is already highly non-trivial, and we will limit ourselves in this work to the Sudakov double logarithms at large N_c.

At double leading logarithmic (DLL) accuracy, the TMD factorization formula for our process $\gamma A \to \text{dijet} + X$ is:

$$\frac{\mathrm{d}\sigma^{\mathrm{TMD}}_{\mathrm{DLL}}}{\mathrm{d}z\mathrm{d}\bar{z}\mathrm{d}^2\mathbf{P}_\perp\mathrm{d}^2\mathbf{k}_\perp} = \frac{\mathrm{d}\sigma^{\mathrm{TMD}}_{\mathrm{LO}}}{\mathrm{d}z\mathrm{d}\bar{z}\mathrm{d}^2\mathbf{P}_\perp\mathrm{d}^2\mathbf{k}_\perp} \times e^{-\frac{1}{2}S_A(\mathbf{b}-\mathbf{b}',\mathbf{P}_\perp)} \,, \tag{10.2}$$

with some slight abuse of notation, since the product is really at the integrand level, and where S_A is the perturbative Sudakov factor which reads at LO and in the DLL approximation:

$$S_A(\mathbf{b}-\mathbf{b}',\mathbf{P}_\perp) = \frac{\alpha_s N_c}{2\pi}\ln^2\frac{\mathbf{P}_\perp^2(\mathbf{b}-\mathbf{b}')^2}{c_0^2} \,. \tag{10.3}$$

In the above formulas, $\mathbf{b}-\mathbf{b}'$ is the transverse coordinate conjugate to $\mathbf{k}_\perp$.

We will show in this section that the NLO cross section, in the correlation limit, takes the form

$$\begin{aligned}\mathrm{d}\sigma^{\mathrm{NLO}}_{\gamma A\to\text{dijet}+X} \overset{\text{corr. lim.}}{=} \mathrm{d}\sigma^{\mathrm{TMD}}_{\mathrm{LO}}\left(1-\frac{\alpha_s N_c}{4\pi}\ln^2\frac{\mathbf{P}_\perp^2(\mathbf{b}-\mathbf{b}')^2}{c_0^2}+\mathcal{O}(\text{single logs})\right)\\ +\mathcal{O}(\text{finite terms}) \,,\end{aligned} \tag{10.4}$$

hence proving agreement between the CGC and the TMD calculations, at least to DLL accuracy. The Sudakov double logarithm comes, at least at leading N_c, from soft-collinear gluon radiation just outside the jet, i.e. from the contribution $\mathcal{V}^{\text{out; phase}}_{|\mathrm{QFS}|^2}$ (eqs. (8.20) and (8.21)) and its $q \leftrightarrow \bar{q}$ counterpart. However, as was remarked very recently in [120], taken at face value the double logarithm in this contribution comes with the wrong sign (see section 10.2). We will demonstrate in subsection 10.3 that this wrong sign is compensated for by the mismatch between naive and kinematically-improved low-x resummation.

Finally, we should remark that in the seminal paper ref. [49], eq. (10.4) was already inferred from an analysis of Higgs hadroproduction combined with kinematical arguments. While physically insightful, the approach to the dijet case in [49] has some limitations. The calculation presented in this section relies on the complete NLO dijet calculation instead, which requires a systematic treatment of the low-x resummation. As such, our treatment constitutes an important step towards reaching full NLO accuracy in the back-to-back limit.

10.1 Leading order

Introducing the vector sum of the transverse momenta of the outgoing (anti)quark:

$$\mathbf{k}_\perp = \mathbf{p}_1 + \mathbf{p}_2 \,, \tag{10.5}$$

one can rewrite the transverse coordinates in function of $\mathbf{b}$ and $\mathbf{r}$ which are conjugate to $\mathbf{k}_\perp$ and to $\mathbf{P}_\perp$, respectively (remember that $z = p_1^+/q^+$ and $\bar{z} = p_2^+/q^+$):

$$\mathbf{x}_1 = \mathbf{b} + \bar{z}\mathbf{r}, \quad \mathbf{x}_2 = \mathbf{b} - z\mathbf{r} \,. \tag{10.6}$$

JHEP10(2022)184

After this coordinate transform, the squared of the LO amplitude (2.23) becomes:

$$\begin{aligned}\left|\mathcal{M}_{\rm LO}\right|^2 &= 16(4\pi)\alpha_{\rm em}e_f^2 p_1^+ p_2^+ (z^2+\bar{z}^2)N_c \\ &\times \int_{\mathbf{r},\mathbf{r}',\mathbf{b},\mathbf{b}'} e^{-i\mathbf{P}_\perp\cdot(\mathbf{r}-\mathbf{r}')} e^{-i\mathbf{k}_\perp\cdot(\mathbf{b}-\mathbf{b}')} A^{\lambda'}(\mathbf{r})A^{\lambda'}(\mathbf{r}') \\ &\times {\rm Tr}\Big\langle Q_{122'1'} - s_{12} - s_{2'1'} + 1\Big\rangle \,.\end{aligned} \tag{10.7}$$

Taking the correlation limit $\mathbf{P}_\perp \gg \mathbf{k}_\perp$ then implies $\mathbf{b},\mathbf{b}' \gg \mathbf{r},\mathbf{r}'$, which we will use to perform a Taylor expansion of the Wilson lines. At the lowest non-trivial order, the only nonzero contribution will come from the quadrupole operator since all $\mathcal{O}(\mathbf{r})$ corrections on dipoles evaluated in either two unprimed or two primed coordinates disappear:

$${\rm Tr}\Big[\partial^i_{\mathbf{r}}(U_{\mathbf{x}_i})U^\dagger_{\mathbf{b}}\Big]\Big|_{\mathbf{r}=0} = {\rm Tr}\Big[\partial^i_{\mathbf{r}}\partial^j_{\mathbf{r}}(U_{\mathbf{x}_i})U^\dagger_{\mathbf{b}}\Big]\Big|_{\mathbf{r}=0} = 0\,. \tag{10.8}$$

It is then easy to see that:

$${\rm Tr}\Big\langle Q_{122'1'} - s_{12} - s_{2'1'} + 1\Big\rangle \simeq \mathbf{r}^i\mathbf{r}'^j \frac{\rm Tr}{N_c}\Big\langle U_{\mathbf{b}}(\partial^i U^\dagger_{\mathbf{b}})(\partial^j U_{\mathbf{b}'})U^\dagger_{\mathbf{b}'}\Big\rangle \tag{10.9}$$

up to higher orders in the Taylor expansion. Eq. (10.7) then simplifies to:

$$\begin{aligned}\left|\mathcal{M}_{\rm LO}\right|^2 &\overset{\rm TMD}{=} 16\frac{\alpha_{\rm em}e_f^2}{\pi}p_1^+p_2^+(z^2+\bar{z}^2)\int_{\mathbf{r},\mathbf{r}'} e^{-i\mathbf{P}_\perp\cdot(\mathbf{r}-\mathbf{r}')}\frac{\mathbf{r}\cdot\mathbf{r}'}{\mathbf{r}^2\mathbf{r}'^2}\mathbf{r}^i\mathbf{r}'^j \\ &\times \int_{\mathbf{b},\mathbf{b}'} e^{-i\mathbf{k}_\perp\cdot(\mathbf{b}-\mathbf{b}')}{\rm Tr}\Big\langle U_{\mathbf{b}}(\partial^i U^\dagger_{\mathbf{b}})(\partial^j U_{\mathbf{b}'})U^\dagger_{\mathbf{b}'}\Big\rangle\,.\end{aligned} \tag{10.10}$$

In the thus obtained Wilson-line structure, one can recognize the so-called 'hadron correlator' which is parameterized by the unpolarized $\mathcal{F}_{\rm WW}$ and linearly-polarized $\mathcal{H}_{\rm WW}$ Weizsäcker-Williams gluon TMD [61]:

$$\begin{aligned}&\int_{\mathbf{b},\mathbf{b}'} e^{-i\mathbf{k}_\perp\cdot(\mathbf{b}-\mathbf{b}')}{\rm Tr}\Big\langle U_{\mathbf{b}}(\partial^i U^\dagger_{\mathbf{b}})(\partial^j U_{\mathbf{b}'})U^\dagger_{\mathbf{b}'}\Big\rangle \\ &= g_s^2(2\pi)^3\frac{1}{4}\left[\frac{\delta^{ij}}{2}\mathcal{F}_{\rm WW}(x_A,\mathbf{k}_\perp) + \left(\frac{\mathbf{k}^i_\perp\mathbf{k}^j_\perp}{\mathbf{k}^2_\perp} - \frac{\delta^{ij}}{2}\right)\mathcal{H}_{\rm WW}(x_A,\mathbf{k}_\perp)\right]\,.\end{aligned} \tag{10.11}$$

Finally, using eq. (2.1), we end up with (note that at LO and at the level of the cross section, the parton momenta can be identified with jet momenta):

$$\begin{aligned}\frac{{\rm d}\sigma^{\rm TMD}_{\rm LO}}{{\rm d}z{\rm d}\bar{z}{\rm d}^2\mathbf{P}_\perp{\rm d}^2\mathbf{k}_\perp} &= \frac{2\alpha_{\rm em}e_f^2}{(2\pi)^7}(z^2+\bar{z}^2)2\pi\delta(z+\bar{z}-1)\int_{\mathbf{r},\mathbf{r}'} e^{-i\mathbf{P}_\perp\cdot(\mathbf{r}-\mathbf{r}')}\frac{\mathbf{r}\cdot\mathbf{r}'}{\mathbf{r}^2\mathbf{r}'^2}\mathbf{r}^i\mathbf{r}'^j \\ &\times \int_{\mathbf{b},\mathbf{b}'} e^{-i\mathbf{k}_\perp\cdot(\mathbf{b}-\mathbf{b}')}{\rm Tr}\Big\langle U_{\mathbf{b}}(\partial^i U^\dagger_{\mathbf{b}})(\partial^j U_{\mathbf{b}'})U^\dagger_{\mathbf{b}'}\Big\rangle\,, \\ &= \frac{\alpha_{\rm em}e_f^2\alpha_s}{\mathbf{P}^4_\perp}(z^2+\bar{z}^2)\delta(1-z-\bar{z})\mathcal{F}_{\rm WW}(x_A,\mathbf{k}_\perp)\,,\end{aligned} \tag{10.12}$$

which is the same expression as one would find in a leading-order TMD factorization approach [60]. Note that, at the present lowest perturbative order, one needs an extra scale, such as a nonzero photon virtuality Q^2 or heavy-quark mass, to be sensitive to the linearly-polarized gluon TMD $\mathcal{H}_{\rm WW}$ [63, 64, 67].

JHEP10(2022)184

10.2 Sudakov double logs in the NLO cross section

The contributions $\mathcal{V}^{\text{out; phase}}_{|\text{QFS}|^2}$ and $\mathcal{V}^{\text{out; phase}}_{|\overline{\text{Q}}\text{FS}|^2}$ (see eqs. (8.20), (8.21) and (8.25)) factorize from the LO cross section (at integrand level), and can produce double large logarithms. In the correlation limit, since $\mathbf{p}_{j1} \to \mathbf{P}_\perp$ and $\mathbf{x}_{11'} \to \mathbf{b} - \mathbf{b}'$, $\mathcal{V}^{\text{out; phase}}_{|\text{QFS}|^2}$ becomes

$$\begin{aligned}\mathcal{V}^{\text{out; phase}}_{|\text{QFS}|^2} \underset{\text{corr. lim.}}{=} 2\int_0^1 \frac{\mathrm{d}\xi}{\xi}\Big[e^{-i\xi\mathbf{P}_\perp\cdot(\mathbf{b}-\mathbf{b}')} - 1\Big] \\ \times\left[-2\ln R - \ln\left(\frac{\mathbf{P}_\perp^2(\mathbf{b}-\mathbf{b}')^2}{c_0^2}\right) - 2\ln\xi\right] ,\end{aligned} \tag{10.13}$$

and $\mathcal{V}^{\text{out; phase}}_{|\overline{\text{Q}}\text{FS}|^2}$ has the same expression in the correlation limit. For simplicity let us restrict ourselves to the case in which the azimuthal angle of $\mathbf{P}_\perp$ is integrated over. Then, we have

$$\begin{aligned}\mathcal{V}^{\text{out; phase}}_{|\text{QFS}|^2} &\underset{\text{corr. lim.}}{=} 2\int_0^1 \frac{\mathrm{d}\xi}{\xi}\Big[\mathrm{J}_0(\xi|\mathbf{P}_\perp|\,|\mathbf{b}-\mathbf{b}'|) - 1\Big]\left[-2\ln R - \ln\left(\frac{\xi^2\,\mathbf{P}_\perp^2(\mathbf{b}-\mathbf{b}')^2}{c_0^2}\right)\right] \\ &= \frac{1}{2}\left(\ln\left(\frac{\mathbf{P}_\perp^2(\mathbf{b}-\mathbf{b}')^2}{c_0^2}\right)\right)^2 + 2\ln R\,\ln\left(\frac{\mathbf{P}_\perp^2(\mathbf{b}-\mathbf{b}')^2}{c_0^2}\right) \\ &\quad + \mathcal{O}\left(\frac{1}{\sqrt{|\mathbf{P}_\perp|\,|\mathbf{b}-\mathbf{b}'|}}\right) .\end{aligned} \tag{10.14}$$

Hence, in the correlation limit, the NLO corrections from eqs. (8.20) and (8.25) reduce to:

$$\begin{aligned}&\int_{\phi_{\mathbf{P}_\perp}} \frac{\mathrm{d}\sigma^{|\text{QFS}|^2+|\bar{\text{Q}}\text{FS}|^2;\ \text{out; phase}}_{\text{dijet}}}{\mathrm{d}p^+_{j1}\mathrm{d}^2\mathbf{p}_{j1}\mathrm{d}p^+_{j2}\mathrm{d}^2\mathbf{p}_{j2}} \\ &\quad= \int_{\phi_{\mathbf{P}_\perp}} \frac{\mathrm{d}\sigma^{\text{LO}}_{\text{dijet}}}{\mathrm{d}p^+_{j1}\mathrm{d}^2\mathbf{p}_{j1}\mathrm{d}p^+_{j2}\mathrm{d}^2\mathbf{p}_{j2}} \times \frac{\alpha_s C_F}{2\pi}\left[\mathcal{V}^{\text{out; phase}}_{|\text{QFS}|^2} + \mathcal{V}^{\text{out; phase}}_{|\overline{\text{Q}}\text{FS}|^2}\right] \\ &\quad\underset{\text{corr. lim.}}{=} \int_{\phi_{\mathbf{P}_\perp}} \frac{\mathrm{d}\sigma^{\text{TMD}}_{\text{LO}}}{\mathrm{d}z\mathrm{d}\bar{z}\mathrm{d}^2\mathbf{P}_\perp\mathrm{d}^2\mathbf{k}_\perp} \times \left[\frac{\alpha_s C_F}{2\pi}\left(\ln\left(\frac{\mathbf{P}_\perp^2(\mathbf{b}-\mathbf{b}')^2}{c_0^2}\right)\right)^2\right. \\ &\qquad\left. - \frac{2\alpha_s C_F}{\pi}\ln\left(\frac{1}{R}\right)\ln\left(\frac{\mathbf{P}_\perp^2(\mathbf{b}-\mathbf{b}')^2}{c_0^2}\right) + \mathcal{O}\left(\frac{\alpha_s C_F}{\sqrt{|\mathbf{P}_\perp|\,|\mathbf{b}-\mathbf{b}'|}}\right)\right] ,\end{aligned} \tag{10.15}$$

where once again the product takes place at the level of the integrand. These logarithms are indeed of the Sudakov type. However, the coefficient of the double log is positive, whereas the total Sudakov double log term should be negative.

Note that the only possible sources of Sudakov double logarithms are contributions to the cross section that exhibit soft divergences. In addition, since Sudakov logs exponentiate, they should have the same Wilson-line operator as at LO. In our calculation, apart from the contribution considered above, the only other possible sources of soft singularities are the ones discussed in section 5, i.e. the final-state exchange diagrams GEFS + IFS, and the real interference between QFS and $\overline{\text{Q}}$FS. However, there, only subleading-N_c terms are proportional to the LO color operator, while the leading-N_c operators do not include quadrupoles (and drop in the correlation limit). Due to the complexity of the diagrams

JHEP10(2022)184

in section 5, we are not attempting in this study to calculate their possible subleading-N_c contribution to Sudakov logarithms, and we stay instead at large N_c. Hence, we can actually replace C_F by $N_c/2$ in eq. (10.15) at this accuracy.

In our calculation of the NLO dijet cross section in the correlation limit, we thus obtain Sudakov double logarithms with the expected coefficient at large N_c but the wrong sign. We will now discuss the effect on this result from the kinematical improvement of the high-energy leading-log resummation.

10.3 Sudakov double logs from the mismatch of naive and kinematically consistent low-x resummation

In order to perform the subtraction and resummation of low-x (or high-energy) logs for the NLO dijet cross section, we have used the simplest scheme for JIMWLK resummation. As explained in section 6.1, in this scheme the evolution takes place along the p^+ axis, from a cutoff $k^+_{\rm min}$ to a factorization scale k^+_f. The JIMWLK evolution then resums multiple gluon emissions within this interval, which are strongly ordered in p^+ only.

However, such a simple scheme for the low-x resummation is known to fail beyond low-x leading logarithmic accuracy. Indeed, in a scheme like this, in order to simplify the kinematics, implicitly the approximation of infinite collision energy $\sqrt{s} \to \infty$ is made. This then leads to serious issues, like NLO cross sections which can become negative, and unstable low-x evolution equations at next-to-leading log accuracy. The main ingredient for a resolution of these issues is an improvement of the kinematics in the high-energy evolution equation [86–94], also known as a consistency- or kinematical constraint, which can be also understood as an all-order resummation of leading collinear logarithms within the high-energy evolution equation, either BFKL [86–90] or BK [90–93]. Due to its complexity, so far the case of the JIMWLK equation has been much less studied, although the same issue is present and can be addressed following a similar strategy [94].

For a large but finite collision energy $\sqrt{s}$, the strong p^+-ordering of successive emissions is necessary but not sufficient for large high-energy leading logs to arise in higher-order calculations. Instead, the necessary and sufficient condition is that successive emissions should be strongly ordered both in p^+ and in p^-, in opposite directions. The JIMWLK equation in the scheme that we have used thus leads to an oversubtraction of high-energy logarithms, in the domain satisfying the p^+-ordering but violating the p^--ordering. Note that the situation would have been similar if we had chosen a scheme for JIMWLK based on p^--ordering only, except that the oversubtraction would have happened in a different kinematic domain.

The contribution to be subtracted from the NLO correction and resummed into the LL evolution of the LO term should thus be defined with two conditions, which require two factorization scales. Schematically, in addition to the condition $p_3^+ < k_f^+$ for the gluon of momentum p_3 to participate to the high-energy evolution, one should also include a condition of the type $p_3^- > k_f^-$. Note that both factorization scales k_f^+ and k_f^- are used to specify the endpoint of the high-energy evolution of the target. They should thus be chosen in relation to the kinematics of the observable (the dijet in our case), and be independent of the kinematics of the target and of the collision energy $\sqrt{s}$. First, k_f^+ should be smaller

JHEP10(2022)184

or equal to the + momenta of both jets. A natural choice for k_f^+ is then:

$$k_f^+ = \frac{p_{j1}^+ p_{j2}^+}{q^+} \,. \tag{10.16}$$

The other factorization scale, k_f^-, should be a typical − momentum scale set by the dijet final state. Using the dijet mass squared

$$2p_{j1}^\mu p_{j2\,\mu} = \frac{\left(p_{j2}^+ \mathbf{p}_{j1} - p_{j1}^+ \mathbf{p}_{j2}\right)^2}{p_{j1}^+ p_{j2}^+} = \frac{(q^+)^2\,\mathbf{P}_\perp^2}{p_{j1}^+ p_{j2}^+} \tag{10.17}$$

and q^+, a natural choice for k_f^- can be written as:

$$k_f^- = \frac{2p_{j1}^\mu p_{j2\,\mu}}{2q^+} = \frac{q^+\,\mathbf{P}_\perp^2}{2p_{j1}^+ p_{j2}^+} = \frac{\mathbf{P}_\perp^2}{2k_f^+} \,. \tag{10.18}$$

The BK and JIMWLK evolution equations are usually written in mixed space, with + momenta and transverse positions. Hence, one has no direct access to the p^- of the gluon, which complicates imposing a condition of the type $p_3^- > k_f^-$. In practice, one is led to build a proxy for the p^- of the gluon out of the available mixed-space variables, so that k_f^- becomes a lower bound on a combination of + momenta and transverse positions involved in the gluon emission [90–94]. In the present section, we do not need to enter into such technicalities. We can stay at a quite schematic level in order to understand the interplay between Sudakov double logs and the kinematical improvement of the JIMWLK equation.

Sudakov logarithms are known to exponentiate, and thus to appear at higher orders in terms containing the same Wilson-line operator (or the same parton distribution) as the LO term. Hence, we will now focus on the part in the JIMWLK evolution that involves this same LO operator. It is not a surprise that this part is the one corresponding to the radiative corrections absorbed into the jet definition eq. (8.33). From the results of section 6, in our naive scheme for JIMWLK, at the cross section level this contribution amounts to multiplying the LO cross section with the factor

$$\begin{aligned} &2\alpha_s N_c \ln\left(\frac{k_f^+}{k_{\min}^+}\right) \int_{\mathbf{x}_3} \Big[A^\eta(\mathbf{x}_{1'3})A^\eta(\mathbf{x}_{13}) + A^\eta(\mathbf{x}_{2'3})A^\eta(\mathbf{x}_{23}) \\ &\qquad\qquad - A^\eta(\mathbf{x}_{13})A^\eta(\mathbf{x}_{23}) - A^\eta(\mathbf{x}_{1'3})A^\eta(\mathbf{x}_{2'3})\Big] \\ &= 2\alpha_s N_c \int_{k_{\min}^+}^{k_f^+} \frac{\mathrm{d}p_3^+}{p_3^+} \int_{\mathbf{P}_3} \frac{1}{\mathbf{P}_3^2}\Big[e^{i\mathbf{P}_3\cdot\mathbf{x}_{1'1}} + e^{i\mathbf{P}_3\cdot\mathbf{x}_{2'2}} - e^{i\mathbf{P}_3\cdot\mathbf{x}_{12}} - e^{i\mathbf{P}_3\cdot\mathbf{x}_{1'2'}}\Big] \,, \end{aligned} \tag{10.19}$$

using the momentum representation (2.16) of the Weizsäcker-Williams fields.

For the contribution (10.19), we can implement the extra condition $p_3^- > k_f^-$ corresponding to kinematical improvement directly in momentum space as

$$\frac{\mathbf{P}_3^2}{2p_3^+} > k_f^- = \frac{\mathbf{P}_\perp^2}{2k_f^+} \,. \tag{10.20}$$

JHEP10(2022)184

In other sections, we have obtained the NLO dijet cross section using a naive scheme for high-energy log subtraction (and resummation). Using instead a kinematically improved scheme for this subtraction, we would obtain the same result for the NLO cross section, plus an extra term: the difference between the naive and the kinematically improved integrated JIMWLK evolutions of the LO cross section. The contribution to this difference which is proportional to the LO operator would then be

$$2\alpha_s N_c \int_{k^+_{\min}}^{k^+_f} \frac{\mathrm{d}p^+_3}{p^+_3} \int_{\mathbf{P}_3} \frac{1}{\mathbf{P}_3^2} \Big[e^{i\mathbf{P}_3\cdot\mathbf{x}_{1'1}} + e^{i\mathbf{P}_3\cdot\mathbf{x}_{2'2}} - e^{i\mathbf{P}_3\cdot\mathbf{x}_{12}} - e^{i\mathbf{P}_3\cdot\mathbf{x}_{1'2'}} \Big] \times \left[1 - \theta\left(\frac{\mathbf{P}_3^2}{2p^+_3} - \frac{\mathbf{P}_\perp^2}{2k^+_f} \right) \right] , \tag{10.21}$$

with the term 1 in the bracket corresponding to the naive evolution with p^+ ordering only, whereas the theta function implements the condition (10.20), meaning imposing as well the p^- ordering of the gluons participating to the evolution with respect to the k^-_f scale set by the dijet kinematics. Making all the bounds explicit as theta functions, the expression (10.21) becomes:

$$2\alpha_s N_c \int_0^{+\infty} \frac{\mathrm{d}p^+_3}{p^+_3} \int_{\mathbf{P}_3} \frac{1}{\mathbf{P}_3^2} \Big[e^{i\mathbf{P}_3\cdot\mathbf{x}_{1'1}} + e^{i\mathbf{P}_3\cdot\mathbf{x}_{2'2}} - e^{i\mathbf{P}_3\cdot\mathbf{x}_{12}} - e^{i\mathbf{P}_3\cdot\mathbf{x}_{1'2'}} \Big] \times \theta\left(k^+_f - p^+_3\right) \theta\left(p^+_3 - k^+_{\min}\right) \theta\left(\frac{p^+_3}{k^+_f} \mathbf{P}_\perp^2 - \mathbf{P}_3^2 \right) . \tag{10.22}$$

There is one upper and two lower bounds for p^+_3. $k^+_{\min}$ was first introduced as a cutoff to regulate the p^+_3-integral. In the high-energy resummation, $k^+_{\min}$ also plays the role of the starting point of the evolution of the target, and allows us to implement the dependence of the cross section on the energy of the collision as $k^+_{\min} \propto 1/s$. According to both of these interpretations for $k^+_{\min}$, the lower bound $p^+_3 > k^+_{\min}$ is less restrictive than the other one in the expression (10.22), and can be dropped. Then, eq. (10.22) becomes

$$\begin{aligned} (10.22) &= 2\alpha_s N_c \int_{\mathbf{P}_3} \frac{1}{\mathbf{P}_3^2} \theta\left(\mathbf{P}_\perp^2 - \mathbf{P}_3^2\right) \ln\left(\frac{\mathbf{P}_\perp^2}{\mathbf{P}_3^2} \right) \\ &\quad \times \Big[e^{i\mathbf{P}_3\cdot\mathbf{x}_{1'1}} + e^{i\mathbf{P}_3\cdot\mathbf{x}_{2'2}} - e^{i\mathbf{P}_3\cdot\mathbf{x}_{12}} - e^{i\mathbf{P}_3\cdot\mathbf{x}_{1'2'}} \Big] \\ &= \frac{2\alpha_s N_c}{\pi} \int_0^{|\mathbf{P}_\perp|} \frac{\mathrm{d}|\mathbf{P}_3|}{|\mathbf{P}_3|} \ln\left(\frac{|\mathbf{P}_\perp|}{|\mathbf{P}_3|} \right) \\ &\quad \times \Big[\mathrm{J}_0\left(|\mathbf{P}_3|\,|\mathbf{x}_{1'1}|\right) + \mathrm{J}_0\left(|\mathbf{P}_3|\,|\mathbf{x}_{2'2}|\right) - \mathrm{J}_0\left(|\mathbf{P}_3|\,|\mathbf{x}_{12}|\right) - \mathrm{J}_0\left(|\mathbf{P}_3|\,|\mathbf{x}_{1'2'}|\right) \Big] . \end{aligned} \tag{10.23}$$

In the correlation limit, one has $\mathbf{x}_{12} \to 0$, $\mathbf{x}_{1'2'} \to 0$, $\mathbf{x}_{1'1} \to \mathbf{b}' - \mathbf{b}$ and $\mathbf{x}_{2'2} \to \mathbf{b}' - \mathbf{b}$, so that the expression (10.23) becomes

$$\begin{aligned} &\frac{4\alpha_s N_c}{\pi} \int_0^{|\mathbf{P}_\perp|\,|\mathbf{b}'-\mathbf{b}|} \frac{\mathrm{d}\tau}{\tau} \Big[\ln\left(|\mathbf{P}_\perp|\,|\mathbf{b}'-\mathbf{b}|\right) - \ln(\tau) \Big] \Big[\mathrm{J}_0(\tau) - 1 \Big] \\ &\qquad = -\frac{\alpha_s N_c}{2\pi} \left\{ \ln^2\left(\frac{\mathbf{P}_\perp^2\,(\mathbf{b}'-\mathbf{b})^2}{{c_0}^2} \right) + O\left(\frac{1}{\sqrt{|\mathbf{P}_\perp|\,|\mathbf{b}'-\mathbf{b}|}} \right) \right\} \end{aligned} \tag{10.24}$$

JHEP10(2022)184

for $|\mathbf{P}_\perp||\mathbf{b}'-\mathbf{b}| \gg 1$. This is a Sudakov double log type term, this time with the expected negative sign. Combining this contribution together with the leading-N_c term from eq. (10.15), one finally obtains the following total double logarithmic contribution

$$-\frac{\alpha_s N_c}{4\pi}\ln^2\left(\frac{\mathbf{P}_\perp^2\,(\mathbf{b}'-\mathbf{b})^2}{{c_0}^2}\right) \tag{10.25}$$

at leading N_c, which is indeed the expected Sudakov double log term from eq. (10.4).

Several remarks are in order:

- The calculation outlined in this subsection provides an extra motivation for the kinematical improvement of high-energy evolution equations like JIMWLK: it allows one to obtain the correct Sudakov double logarithms after including the leftover in the NLO cross section after high-energy resummation. The situation can be summarized as follows. In the naive scheme for JIMWLK resummation based on p^+-ordering only, any gluon radiation with smaller p^+ than the dijet scale k_f^+ is treated as part of the evolution of the target. By contrast, including kinematical improvement allows one to split such small-p^+ gluon radiation into two parts: the true contribution to the evolution of the target with smaller p^+ but larger p^- than the dijet, and the soft radiation with both p^+ and p^- smaller than the dijet. Sudakov logarithms originate from the soft regime only, which is thus distinct from the true regime contributing to the evolution of the target. But the naive scheme in p^+ without kinematical improvement for the target evolution misses this fact, and leads to oversubtracting high-energy logs out of the soft regime. This motivates future studies in order to understand the practical implementation of the proposal of ref. [94] for the kinematical improvement of JIMWLK, or to construct other prescriptions.

- We have focused on the leading-N_c contribution only. Subleading-N_c terms cancel in the naive version of the BK and JIMWLK equation, but this cancelation can be broken when kinematical improvement is included, as can be seen from ref. [91] in the BK case. Hence, at this stage, we have no control on a possible subleading-N_c correction to the coefficient of the Sudakov double log.

- If we had used a scheme for JIMWLK resummation based on p^--ordering only, the situation before kinematical improvement would have been more favorable. In that case, only gluon radiation with larger p^- than the dijet (and any p^+) would have been treated as part of the evolution of the target. This would not overlap with the soft regime characterized by both smaller p^+ and p^- than the dijet. Hence, Sudakov logs should be obtained correctly in this case even without kinematical improvement of JIMWLK, since the oversubtraction of high-energy logs happens in the regime of larger p^+ and larger p^- than the dijet, which is well separated from the soft regime. A formulation of the BK equation as evolution along p^- was proposed in ref. [93]. However, it is crucially based on specific properties of BK, and for the moment such a scheme does not exist for JIMWLK.

JHEP10(2022)184

10.4 Beyond the double leading logarithmic approximation

In principle, having obtained the full NLO cross section in general kinematics, one should be able to extend the notion of the correlation limit and write down a TMD-factorized NLO cross section for back-to-back dijets. All virtual diagrams would contribute since they preserve the leading-order kinematics. The most important real NLO corrections stem from gluon emissions inside or close to the jets, yielding Sudakov double- and single logarithms as well as finite terms.

A first step is to extend the calculation above to the Sudakov single logarithms, which is left for future work. In the second step, where all the virtual diagrams need to be analyzed to obtain the finite contributions to the NLO cross section, we immediately encounter some difficulties. Indeed, TMD factorization is obvious for all diagrams with initial- or final-state loop corrections (i.e. IS + UV + FSUV, GEFS, IFS), at least in the sense that up to power corrections one can write the Wilson lines as the WW gluon TMDs (10.11) which decouple from the hard part. Note that the rationale for this power expansion in our approach comes from the phases $e^{i\mathbf{P}_\perp\cdot\mathbf{r}}e^{i\mathbf{k}_\perp\cdot\mathbf{b}}$ which imply that $\mathbf{r}\ll\mathbf{b}$ when $\mathbf{P}_\perp\gg\mathbf{k}_\perp$. However, in all virtual graphs where the gluon scatters off the shockwave (SESW, GESW, ISW) this procedure is compromised due to the phase $e^{i\mathbf{P}_\perp\cdot(\mathbf{r}+\xi\mathbf{x}_{13})}e^{i\mathbf{k}_\perp\cdot\mathbf{b}}$, which now enforces $\mathbf{r}+\xi\mathbf{x}_{13}\ll\mathbf{b}$. With this condition, the Wilson-line structure

$$Q_{322'1'}s_{13}-s_{13}s_{32}-s_{2'1'}+1-\frac{1}{N_c^2}\Big(Q_{122'1'}-s_{12}-s_{2'1'}+1\Big) \tag{10.26}$$

cannot be cast in any form resembling a TMD. Such a form can only be established when one requires that $\mathbf{r}\ll\mathbf{b}$ and $\mathbf{x}_{13}\ll\mathbf{b}$ separately, which yields:

$$\begin{aligned}&\left\langle Q_{322'1'}s_{13}-s_{13}s_{32}-s_{2'1'}+1-\frac{1}{N_c^2}\Big(Q_{122'1'}-s_{12}-s_{2'1'}+1\Big)\right\rangle\\&\quad\simeq\left(\frac{2C_F}{N_c}\mathbf{r}^i\mathbf{r}'^j-\mathbf{x}_{13}^i\mathbf{r}'^j\right)\frac{\mathrm{Tr}}{N_c}\Big\langle U_{\mathbf{b}}(\partial^iU_{\mathbf{b}}^\dagger)(\partial^jU_{\mathbf{b}'})U_{\mathbf{b}'}^\dagger\Big\rangle\,,\end{aligned} \tag{10.27}$$

and would bring the virtual NLO contributions in a TMD-factorized form. Unfortunately, it is not clear to us whether such an expansion can be justified.

11 Conclusions

Making use of the dipole picture of the CGC effective theory and of LCPT, we have calculated the cross section for the inclusive production of two jets in the scattering of a real photon with a target proton or nucleus at low x. The computation was performed at next-to-leading order in α_s, while resumming the multiple rescatterings of the partons off the semiclassical gluon fields in the target to all orders in the eikonal approximation. Using dimensional regularization, we explicitly showed the cancellation of ultraviolet singularities between different virtual NLO corrections on the amplitude level. Likewise, we demonstrated how both soft and collinear divergences, which appear in final-state radiation, cancel through an intricate interplay between the jet definition and certain virtual diagrams. Moreover, we regularized rapidity divergences with the standard cutoff method

JHEP10(2022)184

and absorbed the resulting large logarithms into the JIMWLK equations. This hybrid scheme, i.e. the dimensional regularization of UV and soft-collinear divergences combined with a cutoff for rapidity divergences, is commonly used in higher-order CGC calculations. However, it has the drawback that it obfuscates the distinction between 'genuine' soft divergences on the one hand, and rapidity divergences on the other. The former are typically associated with initial- and final state radiation, while the latter are the hallmark of low-x physics and related to the highly boosted target. The fact that, as we show in section 8, not only all soft and collinear singularities cancel in the final-state, but the only large high-energy logarithms left are those removed by JIMWLK, is a powerful confirmation of the consistency of this scheme.

After having obtained the NLO dijet cross section, we have explored the back-to-back limit to investigate whether our result could be cast in a form consistent with TMD factorization. At leading order, the overlap of the CGC and the TMD frameworks for processes such as this has been demonstrated already some time ago [59, 60]. However, a full next-to-leading order matching is much more involved, since it constitutes an analysis of all Sudakov double and single logarithms as well as finite NLO contributions. A first demonstration that Sudakov double logarithms arise in the hadroproduction of a Higgs boson at low-x was performed in [49], where also the precise form of these double logs in dijet production was inferred based on kinematical arguments. In this work, we revisited the analysis of the Sudakov double logarithms in the dijet case, this time based on the full NLO calculation. We argue that a kinematical improvement of the JIMWLK resummation is crucial to obtain the correct result for the Sudakov double logarithms. We have also identified a class of virtual contributions that, at least at first sight, break TMD factorization on the finite or potentially single-logarithmic level. Before drawing definite conclusions a more thorough study of the correlation limit of our process is needed, which is left for future work. The inclusive dijet electroproduction process has been studied within TMD factorization in refs. [121, 122].

While this work was in progress, the NLO calculation of the inclusive dijet *electro*production cross section appeared in ref. [83]. This calculation was performed in a covariant formulation of the CGC rather than in LCPT, and using a different UV subtraction scheme. In the photoproduction limit $Q^2 \to 0$, our cross section and the $\gamma_T^* + A \to \text{dijet} + X$ cross section in [83] should coincide. The largest difference between both results stems from the treatment of the jet. Indeed, the final result eq. 7.16 of [83] for the dijet cross section is still sensitive to both single- and double logarithms in the rapidity renormalization scale $z_f = k_f^+/q^+$ (or in the rapidity cutoff k_{min}^+ if the JIMWLK subtraction is performed after the application of the jet algorithm.) Since these logarithms cannot be absorbed into JIMWLK and have a soft origin, not a rapidity one, they are unphysical and still need to cancel with soft gluon emission outside the jet, as demonstrated in section 8. Other differences between our results are relatively minor and mainly related to the precise + momentum due to the Dirac traces. In appendix B, we cast our partonic cross section in the same notations and conventions as [83] to facilitate a detailed comparison.

JHEP10(2022)184

Acknowledgments

The work of PT is supported by a postdoctoral fellowship fundamental research of the Research Foundation — Flanders (FWO) no. 1233422N. PT thanks Daniël Boer, Francesco G. Celiberto, Miguel Echevarría, and Cristian Pisano for numerous stimulating discussions. TA is supported in part by the National Science Centre (Poland) under the research grant no. 2018/31/D/ST2/00666 (SONATA 14). GB is supported in part by the National Science Centre (Poland) under the research grant no. 2020/38/E/ST2/00122 (SONATA BIS 10). The work of TA and GB has been performed in the framework of MSCA RISE 823947 "Heavy ion collisions: collectivity and precision in saturation physics" (HIEIC). This work has received funding from the European Union's Horizon 2020 research and innovation program under grant agreement No. 824093.

A Gamma matrices in dimensional regularization

In this appendix, we establish the gamma matrix identities in $D-2$ transverse Euclidean dimensions.

From the definition $\{\gamma^\mu, \gamma^\nu\} = 2g^{\mu\nu}$, we immediately obtain:

$$\{\gamma^i, \gamma^j\} = -2\delta^{ij} \,, \tag{A.1}$$

from which the following identity trivially follows:

$$\gamma^i\gamma^i = -(D-2) \,. \tag{A.2}$$

Repeatedly applying identity (A.1) allows us to write:

$$\gamma^i\gamma^j\gamma^k\gamma^l = \gamma^k\gamma^l\gamma^i\gamma^j + 2\delta^{il}\gamma^k\gamma^j - 2\delta^{ik}\gamma^l\gamma^j + 2\delta^{jl}\gamma^i\gamma^k - 2\delta^{jk}\gamma^i\gamma^l \,. \tag{A.3}$$

With the help of the above relation, it is straightforward to work out the commutation relation for the Dirac sigma, defined as $\sigma^{ij} = (i/2)[\gamma^i, \gamma^j]$, in $D-2$ dimensions:

$$\left[\sigma^{ij}, \sigma^{kl}\right] = 2i\delta^{il}\sigma^{kj} - 2i\delta^{ik}\sigma^{lj} + 2i\delta^{jl}\sigma^{ik} - 2i\delta^{jk}\sigma^{il} \,, \tag{A.4}$$

as well as the contraction:

$$\sigma^{ij}\sigma^{il} = (D-3)\delta^{jl} + i(D-4)\sigma^{jl} \,. \tag{A.5}$$

When evaluating Dirac traces, one can use the fact that γ^+ (and γ^-) commute with the transverse gamma matrices and hence also with σ^{ij}, and then apply the completeness relation

$$u^s_G(q^+)\bar{u}^s_G(q^+)\gamma^+ = 2q^+\mathcal{P}_G \,, \tag{A.6}$$

where $\mathcal{P}_G = \gamma^-\gamma^+/2$ is the projector on good spinor states.

The above definitions allow one to easily demonstrate the following identities:

$$\begin{aligned}
\mathrm{Tr}(\mathcal{P}_G) &= 2 \,, \\
\mathrm{Tr}(\mathcal{P}_G\sigma^{ij}) &= 0 \,, \\
\mathrm{Tr}(\mathcal{P}_G\sigma^{ij}\sigma^{kl}) &= 2(g^{ik}g^{jl} - g^{il}g^{jk}) \overset{D\to4}{=} 2\epsilon^{ij}\epsilon^{kl} \,, \\
\mathrm{Tr}(\mathcal{P}_G\sigma^{ij}\sigma^{kl}\sigma^{im}\sigma^{kn}) &\overset{D\to4}{=} \mathrm{Tr}(\mathcal{P}_G\sigma^{kl}\sigma^{ij}\sigma^{im}\sigma^{kn}) \overset{D\to4}{=} 2\delta^{jm}\delta^{ln} \,.
\end{aligned} \tag{A.7}$$

JHEP10(2022)184

Moreover, using the above relations as well as the commutation relation (A.4), it is straightforward to prove the following relation:

$$\begin{aligned}&\mathrm{Tr}\Big\{\mathcal{P}_G(A\delta^{\lambda\lambda'}+i\sigma^{\lambda\lambda'})(B\delta^{\eta\eta'}+i\sigma^{\eta\eta'})(C\delta^{\lambda\bar{\lambda}}+i\sigma^{\lambda\bar{\lambda}})(D\delta^{\eta\bar{\eta}}+i\sigma^{\eta\bar{\eta}})\Big\}\\ &\quad\overset{D\to 4}{=} 2\Big[(AC-1)(BD-1)\delta^{\bar{\eta}\eta'}\delta^{\bar{\lambda}\lambda'}+(A-C)(D-B)\sigma^{\bar{\eta}\eta'}\sigma^{\bar{\lambda}\lambda'}\Big]\,.\end{aligned} \tag{A.8}$$

B Cross section in the notation of Caucal-Salazar-Venugopalan

In this appendix, we provide our cross section (section 9) cast in the notations and conventions of ref. [83], to facilitate comparison with the results in that paper for the $\gamma_T^*+A\to q+\bar{q}+X$ and $\gamma_T^*+A\to q+\bar{q}+g+X$ NLO impact factors in the limit of vanishing photon virtuality $Q^2\to 0$.

In [83], the indices x, y, and z are used instead of 1, 2, and 3 for the coordinates of the quark, antiquark, and gluon, respectively, such that e.g. $\mathbf{r}_{xy}=\mathbf{x}_{12}$. Plus momenta are always written as fractions with the photon + momentum q^+, i.e. $z_q\equiv p_1^+/q^+$, $z_{\bar{q}}\equiv p_2^+/q^+$, and $z_g\equiv k_3^+/q^+$ (or $z_g\equiv p_3^+/q^+$ in real diagrams). The coordinate vectors

$$\begin{aligned}\mathbf{R}_{\mathrm{SE}}&\equiv -\frac{k_3^+}{p_1^+}\mathbf{x}_{13}+\mathbf{x}_{12}\,,\\ \mathbf{R}_{\mathrm{V}}&\equiv \frac{k_3^+}{p_2^++k_3^+}\mathbf{x}_{23}+\mathbf{x}_{12}=\frac{p_2^+\mathbf{x}_{12}+k_3^+\mathbf{x}_{13}}{p_2^++k_3^+}\,,\end{aligned} \tag{B.1}$$

and

$$X_V^2\equiv\frac{p_2^+}{q^+}\frac{p_1^+-k_3^+}{q^+}\mathbf{x}_{12}^2+\frac{k_3^+}{q^+}\frac{p_1^+-k_3^+}{q^+}\mathbf{x}_{31}^2+\frac{k_3^+p_2^+}{(q^+)^2}\mathbf{x}_{32}^2\,, \tag{B.2}$$

appear in the virtual diagrams SESW, GESW and ISW. The following short-hand notations are used for the Wilson-line structures:

$$\begin{aligned}\Xi_{\mathrm{LO}}&\equiv\Big\langle Q_{2'1'12}-s_{12}-s_{2'1'}+1\Big\rangle\,,\\ \frac{2}{N_c}\Xi_{\mathrm{NLO},1}&\equiv\Big\langle Q_{322'1'}s_{13}-s_{13}s_{32}-s_{2'1'}+1-\frac{1}{N_c^2}\Big(Q_{122'1'}-s_{12}-s_{2'1'}+1\Big)\Big\rangle\,,\\ \frac{2}{N_c}\Xi_{\mathrm{NLO},3}&\equiv\Big\langle s_{2'1'}s_{12}-s_{12}-s_{2'1'}+1-\frac{1}{N_c^2}\Big(Q_{122'1'}-s_{12}-s_{2'1'}+1\Big)\Big\rangle\,,\end{aligned} \tag{B.3}$$

while the compact notation

$$\int \mathrm{d}\Pi_{\mathrm{LO}}\equiv\int_{\mathbf{x}_{1'},\mathbf{x}_{2'},\mathbf{x}_1,\mathbf{x}_2} e^{-i\mathbf{p}_1\cdot\mathbf{x}_{11'}}e^{-i\mathbf{p}_2\cdot\mathbf{x}_{22'}} \tag{B.4}$$

is used for the transverse integral.

With the above notations, it is easy to show that the modified Weizsäcker-Williams- and Coulomb fields that appear in SESW, GESW, and ISW can be cast in the following form:

$$\begin{aligned}\mathcal{A}^{\bar{\lambda}}\Big(\frac{k_3^+}{p_1^+}\mathbf{x}_{13}+\mathbf{x}_{21},\frac{k_3^+}{p_1^+}\mathbf{x}_{13};\frac{q^+(p_1^+-k_3^+)}{k_3^+p_2^+}\Big)&=\frac{1}{2\pi}z_qz_{\bar{q}}\frac{\mathbf{R}_{\mathrm{SE}}^{\bar{\lambda}}}{X_V^2}\\ \mathcal{A}^{\bar{\lambda}}\Big(\frac{p_2^+\mathbf{x}_{12}+k_3^+\mathbf{x}_{13}}{p_2^++k_3^+},\frac{k_3^+}{p_2^++k_3^+}\mathbf{x}_{32};\frac{q^+p_2^+}{k_3^+(p_1^+-k_3^+)}\Big)&=-\frac{1}{2\pi}(z_q-z_g)(z_{\bar{q}}+z_g)^2\frac{\mathbf{R}_{\mathrm{V}}^{\bar{\lambda}}}{X_V^2}\,,\\ \mathcal{C}\Big(\frac{k_3^+}{p_1^+}\mathbf{x}_{13}+\mathbf{x}_{21},\frac{k_3^+}{p_1^+}\mathbf{x}_{13};\frac{q^+(p_1^+-k_3^+)}{p_2^+k_3^+}\Big)&=\frac{1}{(2\pi)^2}z_qz_{\bar{q}}\frac{1}{X_V^2}\,.\end{aligned} \tag{B.5}$$

JHEP10(2022)184

Finally, with the indices $J \equiv j1$ and $K \equiv j2$ for the jet initiated by the quark resp. antiquark, we can write the contribution to the cross section due to SESW, sub as follows:

$$\begin{aligned}\frac{\mathrm{d}\sigma_{\mathrm{SESW,sub}}}{\mathrm{d}\eta_J \mathrm{d}\eta_K \mathrm{d}^2\mathbf{p}_J \mathrm{d}^2\mathbf{p}_K} &= \frac{\alpha_{\mathrm{em}} e_f^2 N_c}{(2\pi)^6}\delta(1-z_J-z_K)\int \mathrm{d}\Pi_{\mathrm{LO}} 2 z_J^2 z_K^2 \frac{1}{\mathbf{r}_{x'y'}^2} \\ &\times \frac{\alpha_s}{\pi}\int_{z_{\min}}^{z_J}\frac{\mathrm{d}z_g}{z_g}\int\frac{\mathrm{d}^2\mathbf{z}_\perp}{\pi}(z_J^2+z_K^2)\left(1-\frac{z_g}{z_J}+\frac{z_g^2}{2z_J^2}\right) \\ &\times \left\{ e^{-i\frac{z_g}{z_J}\mathbf{p}_J\cdot\mathbf{r}_{zx}}\frac{1}{\mathbf{r}_{xz}^2}\frac{\mathbf{R}_{\mathrm{SE}}\cdot\mathbf{r}_{x'y'}}{X_V^2}\Xi_{\mathrm{NLO},1}\right. \\ &\quad \left. + \frac{1}{z_J z_K}\left(\frac{1}{\mathbf{r}_{xz}^2}-\frac{\mathbf{r}_{xz}\cdot\mathbf{r}_{yz}}{\mathbf{r}_{xz}^2\mathbf{r}_{yz}^2}\right)\frac{\mathbf{r}_{xy}\cdot\mathbf{r}_{x'y'}}{\mathbf{r}_{xy}^2}C_F\Xi_{\mathrm{LO}}\right\},\end{aligned} \tag{B.6}$$

in complete agreement with eq. B.1 in [83] up to the replacements $\frac{z_g}{2z_J^2} \to \frac{z_g^2}{2z_J^2}$ and $\mathbf{r}_{xy} \to \mathbf{r}_{x'y'}$ in the third line, which are likely typos.

Likewise, for the contribution due to GESW:

$$\begin{aligned}&\frac{\mathrm{d}\sigma_{\mathrm{GESW}}}{\mathrm{d}\eta_J \mathrm{d}\eta_K \mathrm{d}^2\mathbf{p}_J \mathrm{d}^2\mathbf{p}_K} = \frac{\alpha_{\mathrm{em}} e_f^2 N_c}{(2\pi)^6}\delta(1-z_J-z_K)\int \mathrm{d}\Pi_{\mathrm{LO}} 2 z_J^2 z_K^2 \frac{1}{\mathbf{r}_{x'y'}^2} \\ &\times \frac{\alpha_s}{\pi}\int_{z_{\min}}^{z_J}\frac{\mathrm{d}z_g}{z_g}\int\frac{\mathrm{d}^2\mathbf{z}_\perp}{\pi}e^{-i\frac{z_g}{z_J}\mathbf{p}_J\cdot\mathbf{r}_{zx}}\frac{(z_J-z_g)(z_K+z_g)}{2z_J^2 z_K} \\ &\times \left[\Big(z_g^2+z_g(z_K-z_J)-2z_J z_K\Big)\Big(z_J^2+z_K^2+z_g(z_K-z_J)\Big)\frac{\mathbf{r}_{zx}\cdot\mathbf{r}_{zy}}{\mathbf{r}_{zx}^2\mathbf{r}_{zy}^2}\frac{\mathbf{R}_{\mathrm{V}}\cdot\mathbf{r}_{x'y'}}{X_V^2}\right. \\ &\quad \left. - z_g(z_g+z_K-z_J)^2\frac{\mathbf{r}_{zx}\times\mathbf{r}_{zy}}{\mathbf{r}_{zx}^2\mathbf{r}_{zy}^2}\frac{\mathbf{R}_{\mathrm{V}}\times\mathbf{r}_{x'y'}}{X_V^2}\right]\Xi_{\mathrm{NLO},1}\,.\end{aligned} \tag{B.7}$$

The term $\mathbf{R}_{\mathrm{V}}\cdot\mathbf{r}_{x'y'}$ is equal to a factor z_K+z_g times the one in eq. B.1, assuming the Bessel function in the fourth line should read $K_1(QX_{\mathrm{V}})$. With the same assumption, for the term $\mathbf{R}_{\mathrm{V}}\times\mathbf{r}_{x'y'}$, the discrepancy is bigger with a prefactor:

$$\mathrm{term}^{\mathrm{TABM}}_{\mathbf{R}_{\mathrm{V}}\times\mathbf{r}_{x'y'}} = \frac{(z_K+z_g)(z_g+z_K-z_J)}{1+z_g-2z_J(z_K+z_g)}\mathrm{term}^{\mathrm{CSV}}_{\mathbf{R}_{\mathrm{V}}\times\mathbf{r}_{x'y'}}\,. \tag{B.8}$$

Finally, for ISW:

$$\begin{aligned}\frac{\mathrm{d}\sigma_{\mathrm{ISW}}}{\mathrm{d}\eta_J \mathrm{d}\eta_K \mathrm{d}^2\mathbf{p}_J \mathrm{d}^2\mathbf{p}_K} &= \frac{\alpha_{\mathrm{em}} e_f^2 N_c}{(2\pi)^6}\delta(1-z_J-z_K)\int \mathrm{d}\Pi_{\mathrm{LO}} 2 z_J^2 z_K^2 \frac{1}{\mathbf{r}_{x'y'}^2} \\ &\times \frac{\alpha_s}{\pi}\int_{z_{\min}}^{z_J}\frac{\mathrm{d}z_g}{z_g}\int\frac{\mathrm{d}^2\mathbf{z}_\perp}{\pi}e^{-i\frac{z_g}{z_J}\mathbf{p}_J\cdot\mathbf{r}_{zx}}\Xi_{\mathrm{NLO},1} \\ &\times -\frac{z_g(z_J-z_g)}{2z_J}\left(\frac{z_J}{z_K+z_g}+\frac{z_K(z_J-z_g)}{z_J^2}\right)\frac{\mathbf{r}_{zx}\cdot\mathbf{r}_{x'y'}}{\mathbf{r}_{zx}^2\mathbf{r}_{x'y'}^2}\frac{1}{X_V^2}\,,\end{aligned} \tag{B.9}$$

which is a factor $1/2$ times the result in eq. B.1 if we assume that a factor -1 was forgotten in front of the term $z_g(z_g-z_J)^2 z_K/z_J^3$ in the second line.

JHEP10(2022)184

Likewise, the notations $\mathbf{k}_\perp \equiv \mathbf{p}_1$, $\mathbf{p}_\perp \equiv \mathbf{p}_2$, and $\mathbf{k}_{g\perp} \equiv \mathbf{k}_3$ or $\mathbf{p}_3$ are employed for the transverse momentum of the quark, antiquark, and virtual resp. real gluon. The vector sum of the quark- and gluon momenta is written as $\boldsymbol{\Delta}_\perp \equiv \mathbf{p}_1 + \mathbf{p}_2$, while $\mathbf{P}_\perp$ denotes the same momentum combination as in our work. With the notation:

$$\boldsymbol{\Delta}^2_{\mathrm{V3}} \equiv -\frac{p_2^+ + k_3^+}{p_2^+}\frac{p_1^+ - k_3^+}{p_1^+}\mathbf{P}_\perp^2 \,, \tag{B.10}$$

and making use of the identity:

$$\int_{\mathbf{K}} \frac{e^{i\mathbf{K}\cdot\mathbf{x}}}{\mathbf{K}^2 + \mathbf{Q}^2} = \frac{1}{2\pi} K_0(|\mathbf{x}||\mathbf{Q}|) \,, \tag{B.11}$$

we can rewrite the integral J (3.18) as follows:

$$\begin{aligned}
\delta^{\eta'\bar{\eta}} J^{\eta'\bar{\eta}}(k_3^+, \mathbf{x}_{12}) &= e^{i(1-\frac{z_g}{z_q})\mathbf{P}_\perp\cdot\mathbf{r}_{xy}}\frac{1}{2\pi}K_0(r_{xy}\boldsymbol{\Delta}_{\mathrm{V3}}) \\
&\quad + \frac{z_g}{2z_K(z_J - z_g)}\frac{1}{2\pi}\mathcal{J}_\odot\Big(\mathbf{r}_{xy}, \Big(1 - \frac{z_g}{z_q}\Big)\mathbf{P}_\perp, \boldsymbol{\Delta}_{\mathrm{V3}}\Big) \,, \\
\epsilon^{\bar{\eta}\eta'} J^{\eta'\bar{\eta}}(k_3^+, \mathbf{x}_{12}) &= -i\frac{z_g}{(z_J - z_g)z_K}\frac{1}{2\pi}\mathcal{J}_\otimes\Big(\mathbf{r}_{xy}, \Big(1 - \frac{z_g}{z_q}\Big)\mathbf{P}_\perp, \boldsymbol{\Delta}_{\mathrm{V3}}\Big) \,.
\end{aligned} \tag{B.12}$$

The contributions to the cross section due to the virtual diagrams GEFS, (i) and GEFS, (ii) + IFS can then be written as follows:

$$\begin{aligned}
&\frac{\mathrm{d}\sigma_{\mathrm{GEFS},(i)}}{\mathrm{d}\eta_J \mathrm{d}\eta_K \mathrm{d}^2\mathbf{p}_J \mathrm{d}^2\mathbf{p}_K} = \frac{\alpha_{\mathrm{em}} e_f^2 N_c}{(2\pi)^6}\delta(1 - z_J - z_K)\int \mathrm{d}\Pi_{\mathrm{LO}} 2 z_J^2 z_K^2 \frac{1}{\mathbf{r}^2_{x'y'}} \\
&\times \frac{\alpha_s}{\pi}\int_{z_{\min}}^{z_J}\frac{\mathrm{d}z_g}{z_g}\frac{1}{\mathbf{r}^2_{xy}}\Xi_{\mathrm{NLO},3}\frac{1}{z_J z_K}\frac{z_J - z_g}{z_J z_g} \\
&\times \Big\{\Big(z_g^2 + z_g(z_K - z_J)\Big)\Big(z_J^2 + z_K^2 + z_g(z_K - z_J)\Big) \\
&\quad \times \Big(e^{i(\mathbf{P}_\perp + z_g\boldsymbol{\Delta}_\perp)\cdot\mathbf{r}_{xy}}(\mathbf{r}_{xy}\cdot\mathbf{r}_{x'y'})K_0(r_{xy}\boldsymbol{\Delta}_{\mathrm{V3}}) \\
&\qquad + \frac{z_g}{2z_K(z_J - z_g)}e^{i\frac{z_g}{z_J}\mathbf{p}_J\cdot\mathbf{r}_{xy}}(\mathbf{r}_{xy}\cdot\mathbf{r}_{x'y'})\mathcal{J}_\odot\Big(\mathbf{r}_{xy}, \Big(1 - \frac{z_g}{z_q}\Big)\mathbf{P}_\perp, \boldsymbol{\Delta}_{\mathrm{V3}}\Big)\Big) \\
&\quad - i\frac{z_g^2(z_g + z_K - z_J)^2}{(z_J - z_g)z_K}e^{i\frac{z_g}{z_J}\mathbf{p}_J\cdot\mathbf{r}_{xy}}(\mathbf{r}_{xy}\times\mathbf{r}_{x'y'})\mathcal{J}_\otimes\Big(\mathbf{r}_{xy}, \Big(1 - \frac{z_g}{z_q}\Big)\mathbf{P}_\perp, \boldsymbol{\Delta}_{\mathrm{V3}}\Big)\Big\} \,,
\end{aligned} \tag{B.13}$$

and:

$$\begin{aligned}
&\frac{\mathrm{d}\sigma_{\mathrm{GEFS},(ii)+\mathrm{IFS}}}{\mathrm{d}\eta_J \mathrm{d}\eta_K \mathrm{d}^2\mathbf{p}_J \mathrm{d}^2\mathbf{p}_K} = \frac{\alpha_{\mathrm{em}} e_f^2 N_c}{(2\pi)^6}\delta(1 - z_J - z_K)\int \mathrm{d}\Pi_{\mathrm{LO}} 2 z_J^2 z_K^2 \frac{1}{\mathbf{r}^2_{x'y'}} \\
&\times \frac{\alpha_s}{\pi}\int_{z_{\min}}^{z_J}\frac{\mathrm{d}z_g}{z_g}\frac{1}{\mathbf{r}^2_{xy}}\Xi_{\mathrm{NLO},3} 2\frac{z_J - z_g}{z_J z_K}\Big(z_J^2 + z_K^2 + z_g(z_K - z_J)\Big) \\
&\times \Big\{e^{i(\mathbf{P}_\perp + z_g\boldsymbol{\Delta}_\perp)\cdot\mathbf{r}_{xy}}(\mathbf{r}_{xy}\cdot\mathbf{r}_{x'y'})K_0(r_{xy}\boldsymbol{\Delta}_{\mathrm{V3}}) \\
&\quad - \frac{1}{2(z_J - z_g)}e^{i\frac{z_g}{z_J}\mathbf{p}_J\cdot\mathbf{r}_{xy}}(\mathbf{r}_{xy}\cdot\mathbf{r}_{x'y'})\mathcal{J}_\odot\Big(\mathbf{r}_{xy}, \Big(1 - \frac{z_g}{z_q}\Big)\mathbf{P}_\perp, \boldsymbol{\Delta}_{\mathrm{V3}}\Big)\Big\} \,.
\end{aligned} \tag{B.14}$$

JHEP10(2022)184

We completely agree with eq. B.4 in [83] for the terms involving K_0 and $\mathcal{J}_\odot$ (up to $-\frac{z_g}{2z_J z_K} \to -\frac{z_g^2}{2z_J z_K}$ which is likely a typo). However, we do not agree for the prefactor of $\mathcal{J}_\otimes$.

For the real partonic contribution due to $|\mathcal{M}_{\mathrm{QFS}}|^2$, we have:

$$\begin{aligned}\frac{\mathrm{d}\sigma_{\mathrm{QFS}^2}}{\mathrm{d}\eta_q \mathrm{d}\eta_{\bar{q}} \mathrm{d}\eta_g \mathrm{d}^2\mathbf{k}_\perp \mathrm{d}^2\mathbf{p}_\perp} &= \frac{\alpha_{\mathrm{em}} e_f^2 N_c}{(2\pi)^6} \delta(1-z_q-z_{\bar{q}}-z_g)\alpha_s \int \mathrm{d}\Pi_{\mathrm{LO}} \\ &\times C_F \Xi_{\mathrm{LO}} 8 z_q z_{\bar{q}} \Big(z_{\bar{q}}^2 - (1-z_{\bar{q}})^2\Big)\Big(1+\frac{z_g}{z_q}+\frac{z_g^2}{2z_q^2}\Big) \\ &\times \frac{\mathbf{r}_{xy}\cdot\mathbf{r}_{x'y'}}{\mathbf{r}_{xy}^2 \mathbf{r}_{x'y'}^2} \frac{e^{-i\mathbf{k}_{g\perp}\cdot\mathbf{r}_{xx'}}}{(\mathbf{k}_{g\perp} - z_g/z_q \mathbf{k}_\perp)^2}\,,\end{aligned} \tag{B.15}$$

which exactly corresponds to B.5, and for the interference term $\mathcal{M}_{\overline{\mathrm{QFS}}}^\dagger \mathcal{M}_{\mathrm{QFS}}$:

$$\begin{aligned}\frac{\mathrm{d}\sigma_{\overline{\mathrm{QFS}}^\dagger \mathrm{QFS}}}{\mathrm{d}\eta_q \mathrm{d}\eta_{\bar{q}} \mathrm{d}\eta_g \mathrm{d}^2\mathbf{k}_\perp \mathrm{d}^2\mathbf{p}_\perp \mathrm{d}^2\mathbf{k}_{g\perp}} &= \frac{\alpha_{\mathrm{em}} e_f^2 N_c}{(2\pi)^8} \delta(1-z_q-z_{\bar{q}}-z_g)\alpha_s \\ \times \int \mathrm{d}\Pi_{\mathrm{LO}} \Xi_{\mathrm{NLO},3} 8 z_q z_{\bar{q}} e^{-i\mathbf{k}_{g\perp}\cdot\mathbf{r}_{xx'}} &\Bigg\{ (z_q + z_{\bar{q}} - 2z_q z_{\bar{q}})\Big(1+\frac{z_g}{2z_q}+\frac{z_g}{2z_{\bar{q}}}\Big) \\ &\times \frac{-\mathbf{r}_{xy}\cdot\mathbf{r}_{x'y'}}{\mathbf{r}_{xy}^2\mathbf{r}_{x'y'}^2} \frac{(\mathbf{k}_{g\perp} - \frac{z_g}{z_q}\mathbf{k}_\perp)\cdot(\mathbf{k}_{g\perp} - \frac{z_g}{z_{\bar{q}}}\mathbf{p}_\perp)}{(\mathbf{k}_{g\perp} - \frac{z_g}{z_q}\mathbf{k}_\perp)^2 (\mathbf{k}_{g\perp} - \frac{z_g}{z_{\bar{q}}}\mathbf{p}_\perp)^2} \\ &- \frac{z_g(z_q - z_{\bar{q}})^2}{2z_q z_{\bar{q}}} \frac{-\mathbf{r}_{xy}\times\mathbf{r}_{x'y'}}{\mathbf{r}_{xy}^2\mathbf{r}_{x'y'}^2} \frac{(\mathbf{k}_{g\perp} - \frac{z_g}{z_q}\mathbf{k}_\perp)\times(\mathbf{k}_{g\perp} - \frac{z_g}{z_{\bar{q}}}\mathbf{p}_\perp)}{(\mathbf{k}_{g\perp} - \frac{z_g}{z_q}\mathbf{k}_\perp)^2 (\mathbf{k}_{g\perp} - \frac{z_g}{z_{\bar{q}}}\mathbf{p}_\perp)^2} \Bigg\},\end{aligned} \tag{B.16}$$

which agrees with B.7 up to the difference $1+\frac{z_g}{z_q}+\frac{z_g}{z_{\bar{q}}} \to 1+\frac{z_g}{2z_q}+\frac{z_g}{2z_{\bar{q}}}$ in the third line and obvious typos in the transverse momentum structures.

For the remaining real contributions, the authors of [83] do not provide an explicit evaluation of the Dirac traces hence we cannot compare further.

References

[1] V.N. Gribov and L.N. Lipatov, *Deep inelastic ep scattering in perturbation theory*, *Sov. J. Nucl. Phys.* **15** (1972) 438 [*Yad. Fiz.* **15** (1972) 781] [INSPIRE].

[2] Y.L. Dokshitzer, *Calculation of the structure functions for deep inelastic scattering and e^+e^- annihilation by perturbation theory in quantum chromodynamics*, *Sov. Phys. JETP* **46** (1977) 641 [*Zh. Eksp. Teor. Fiz.* **73** (1977) 1216] [INSPIRE].

[3] G. Altarelli and G. Parisi, *Asymptotic freedom in parton language*, *Nucl. Phys. B* **126** (1977) 298 [INSPIRE].

JHEP10(2022)184

[4] E.A. Kuraev, L.N. Lipatov and V.S. Fadin, *The Pomeranchuk singularity in non-Abelian gauge theories*, *Sov. Phys. JETP* **45** (1977) 199 [*Zh. Eksp. Teor. Fiz.* **72** (1977) 377] [INSPIRE].

[5] I.I. Balitsky and L.N. Lipatov, *The Pomeranchuk singularity in quantum chromodynamics*, *Sov. J. Nucl. Phys.* **28** (1978) 822 [*Yad. Fiz.* **28** (1978) 1597] [INSPIRE].

[6] S. Catani, M. Ciafaloni and F. Hautmann, *Gluon contributions to small x heavy flavor production*, *Phys. Lett. B* **242** (1990) 97 [INSPIRE].

[7] S. Catani, M. Ciafaloni and F. Hautmann, *High-energy factorization and small x heavy flavor production*, *Nucl. Phys. B* **366** (1991) 135 [INSPIRE].

[8] S. Catani and F. Hautmann, *High-energy factorization and small x deep inelastic scattering beyond leading order*, *Nucl. Phys. B* **427** (1994) 475 [hep-ph/9405388] [INSPIRE].

[9] M. Froissart, *Asymptotic behavior and subtractions in the Mandelstam representation*, *Phys. Rev.* **123** (1961) 1053 [INSPIRE].

[10] L.V. Gribov, E.M. Levin and M.G. Ryskin, *Semihard processes in QCD*, *Phys. Rept.* **100** (1983) 1 [INSPIRE].

[11] L.D. McLerran and R. Venugopalan, *Computing quark and gluon distribution functions for very large nuclei*, *Phys. Rev. D* **49** (1994) 2233 [hep-ph/9309289] [INSPIRE].

[12] L.D. McLerran and R. Venugopalan, *Gluon distribution functions for very large nuclei at small transverse momentum*, *Phys. Rev. D* **49** (1994) 3352 [hep-ph/9311205] [INSPIRE].

[13] L.D. McLerran and R. Venugopalan, *Green's functions in the color field of a large nucleus*, *Phys. Rev. D* **50** (1994) 2225 [hep-ph/9402335] [INSPIRE].

[14] J. Jalilian-Marian, A. Kovner, A. Leonidov and H. Weigert, *The BFKL equation from the Wilson renormalization group*, *Nucl. Phys. B* **504** (1997) 415 [hep-ph/9701284] [INSPIRE].

[15] J. Jalilian-Marian, A. Kovner, A. Leonidov and H. Weigert, *The Wilson renormalization group for low x physics: towards the high density regime*, *Phys. Rev. D* **59** (1998) 014014 [hep-ph/9706377] [INSPIRE].

[16] J. Jalilian-Marian, A. Kovner and H. Weigert, *The Wilson renormalization group for low x physics: gluon evolution at finite parton density*, *Phys. Rev. D* **59** (1998) 014015 [hep-ph/9709432] [INSPIRE].

[17] A. Kovner, J.G. Milhano and H. Weigert, *Relating different approaches to nonlinear QCD evolution at finite gluon density*, *Phys. Rev. D* **62** (2000) 114005 [hep-ph/0004014] [INSPIRE].

[18] H. Weigert, *Unitarity at small Bjorken x*, *Nucl. Phys. A* **703** (2002) 823 [hep-ph/0004044] [INSPIRE].

[19] E. Iancu, A. Leonidov and L.D. McLerran, *Nonlinear gluon evolution in the color glass condensate. 1*, *Nucl. Phys. A* **692** (2001) 583 [hep-ph/0011241] [INSPIRE].

[20] E. Iancu, A. Leonidov and L.D. McLerran, *The renormalization group equation for the color glass condensate*, *Phys. Lett. B* **510** (2001) 133 [hep-ph/0102009] [INSPIRE].

[21] E. Ferreiro, E. Iancu, A. Leonidov and L. McLerran, *Nonlinear gluon evolution in the color glass condensate. 2*, *Nucl. Phys. A* **703** (2002) 489 [hep-ph/0109115] [INSPIRE].

[22] I. Balitsky, *Operator expansion for high-energy scattering*, *Nucl. Phys. B* **463** (1996) 99 [hep-ph/9509348] [INSPIRE].

JHEP10(2022)184

[23] I. Balitsky, *Factorization for high-energy scattering*, *Phys. Rev. Lett.* **81** (1998) 2024 [hep-ph/9807434] [INSPIRE].

[24] I. Balitsky, *Factorization and high-energy effective action*, *Phys. Rev. D* **60** (1999) 014020 [hep-ph/9812311] [INSPIRE].

[25] Y.V. Kovchegov, *Small x F_2 structure function of a nucleus including multiple Pomeron exchanges*, *Phys. Rev. D* **60** (1999) 034008 [hep-ph/9901281] [INSPIRE].

[26] Y.L. Dokshitzer, D. Diakonov and S.I. Troian, *Hard processes in quantum chromodynamics*, *Phys. Rept.* **58** (1980) 269 [INSPIRE].

[27] J.C. Collins, D.E. Soper and G.F. Sterman, *Transverse momentum distribution in Drell-Yan pair and W and Z boson production*, *Nucl. Phys. B* **250** (1985) 199 [INSPIRE].

[28] J.C. Collins, D.E. Soper and G.F. Sterman, *Soft gluons and factorization*, *Nucl. Phys. B* **308** (1988) 833 [INSPIRE].

[29] J. Collins, *Foundations of perturbative QCD*, *Camb. Monogr. Part. Phys. Nucl. Phys. Cosmol.* **32** (2011) 1 [INSPIRE].

[30] M.G. Echevarria, A. Idilbi and I. Scimemi, *Factorization theorem for Drell-Yan at low q_T and transverse momentum distributions on-the-light-cone*, *JHEP* **07** (2012) 002 [arXiv:1111.4996] [INSPIRE].

[31] R. Angeles-Martinez et al., *Transverse Momentum Dependent (TMD) parton distribution functions: status and prospects*, *Acta Phys. Polon. B* **46** (2015) 2501 [arXiv:1507.05267] [INSPIRE].

[32] X.-D. Ji, J.-P. Ma and F. Yuan, *QCD factorization for semi-inclusive deep-inelastic scattering at low transverse momentum*, *Phys. Rev. D* **71** (2005) 034005 [hep-ph/0404183] [INSPIRE].

[33] F. Hautmann and H. Jung, *Angular correlations in multi-jet final states from k-perpendicular-dependent parton showers*, *JHEP* **10** (2008) 113 [arXiv:0805.1049] [INSPIRE].

[34] M. Deak, F. Hautmann, H. Jung and K. Kutak, *Forward jet production at the Large Hadron Collider*, *JHEP* **09** (2009) 121 [arXiv:0908.0538] [INSPIRE].

[35] H. Jung et al., *The CCFM Monte Carlo generator CASCADE version* 2.2.03, *Eur. Phys. J. C* **70** (2010) 1237 [arXiv:1008.0152] [INSPIRE].

[36] M. Deak, F. Hautmann, H. Jung and K. Kutak, *Forward jets and energy flow in hadronic collisions*, *Eur. Phys. J. C* **72** (2012) 1982 [arXiv:1112.6354] [INSPIRE].

[37] S. Dooling, F. Hautmann and H. Jung, *Hadroproduction of electroweak gauge boson plus jets and TMD parton density functions*, *Phys. Lett. B* **736** (2014) 293 [arXiv:1406.2994] [INSPIRE].

[38] M. Hentschinski, A. Kusina and K. Kutak, *Transverse momentum dependent splitting functions at work: quark-to-gluon splitting*, *Phys. Rev. D* **94** (2016) 114013 [arXiv:1607.01507] [INSPIRE].

[39] M. Bury, A. van Hameren, H. Jung, K. Kutak, S. Sapeta and M. Serino, *Calculations with off-shell matrix elements, TMD parton densities and TMD parton showers*, *Eur. Phys. J. C* **78** (2018) 137 [arXiv:1712.05932] [INSPIRE].

JHEP10(2022)184

[40] M. Hentschinski, A. Kusina, K. Kutak and M. Serino, *TMD splitting functions in k_T factorization: the real contribution to the gluon-to-gluon splitting*, *Eur. Phys. J. C* **78** (2018) 174 [arXiv:1711.04587] [INSPIRE].

[41] E. Blanco, A. van Hameren, H. Jung, A. Kusina and K. Kutak, *Z boson production in proton-lead collisions at the LHC accounting for transverse momenta of initial partons*, *Phys. Rev. D* **100** (2019) 054023 [arXiv:1905.07331] [INSPIRE].

[42] A. van Hameren, P. Kotko, K. Kutak and S. Sapeta, *Broadening and saturation effects in dijet azimuthal correlations in p-p and p-Pb collisions at $\sqrt{s} = 5.02$ TeV*, *Phys. Lett. B* **795** (2019) 511 [arXiv:1903.01361] [INSPIRE].

[43] A. van Hameren, P. Kotko, K. Kutak and S. Sapeta, *Sudakov effects in central-forward dijet production in high energy factorization*, *Phys. Lett. B* **814** (2021) 136078 [arXiv:2010.13066] [INSPIRE].

[44] M. Hentschinski, *Transverse momentum dependent gluon distribution within high energy factorization at next-to-leading order*, *Phys. Rev. D* **104** (2021) 054014 [arXiv:2107.06203] [INSPIRE].

[45] M. Nefedov, *Sudakov resummation from the BFKL evolution*, *Phys. Rev. D* **104** (2021) 054039 [arXiv:2105.13915] [INSPIRE].

[46] D.-X. Zheng and J. Zhou, *Sudakov suppression of the Balitsky-Kovchegov kernel*, *JHEP* **11** (2019) 177 [arXiv:1906.06825] [INSPIRE].

[47] P. Sun, B.-W. Xiao and F. Yuan, *Gluon distribution functions and Higgs boson production at moderate transverse momentum*, *Phys. Rev. D* **84** (2011) 094005 [arXiv:1109.1354] [INSPIRE].

[48] A.H. Mueller, B.-W. Xiao and F. Yuan, *Sudakov resummation in small-x saturation formalism*, *Phys. Rev. Lett.* **110** (2013) 082301 [arXiv:1210.5792] [INSPIRE].

[49] A.H. Mueller, B.-W. Xiao and F. Yuan, *Sudakov double logarithms resummation in hard processes in the small-x saturation formalism*, *Phys. Rev. D* **88** (2013) 114010 [arXiv:1308.2993] [INSPIRE].

[50] B.-W. Xiao, F. Yuan and J. Zhou, *Transverse momentum dependent parton distributions at small-x*, *Nucl. Phys. B* **921** (2017) 104 [arXiv:1703.06163] [INSPIRE].

[51] A. Stasto, S.-Y. Wei, B.-W. Xiao and F. Yuan, *On the dihadron angular correlations in forward pA collisions*, *Phys. Lett. B* **784** (2018) 301 [arXiv:1805.05712] [INSPIRE].

[52] C. Marquet, S.-Y. Wei and B.-W. Xiao, *Probing parton saturation with forward Z^0-boson production at small transverse momentum in p+p and p+A collisions*, *Phys. Lett. B* **802** (2020) 135253 [arXiv:1909.08572] [INSPIRE].

[53] D. Boer, P.J. Mulders, J. Zhou and Y.-J. Zhou, *Suppression of maximal linear gluon polarization in angular asymmetries*, *JHEP* **10** (2017) 196 [arXiv:1702.08195] [INSPIRE].

[54] J. Zhou, *Scale dependence of the small x transverse momentum dependent gluon distribution*, *Phys. Rev. D* **99** (2019) 054026 [arXiv:1807.00506] [INSPIRE].

[55] D. Boer, Y. Hagiwara, J. Zhou and Y.-J. Zhou, *Scale evolution of T-odd gluon TMDs at small x*, *Phys. Rev. D* **105** (2022) 096017 [arXiv:2203.00267] [INSPIRE].

[56] C.J. Bomhof, P.J. Mulders and F. Pijlman, *The construction of gauge-links in arbitrary hard processes*, *Eur. Phys. J. C* **47** (2006) 147 [hep-ph/0601171] [INSPIRE].

JHEP10(2022)184

[57] A. Metz and J. Zhou, *Distribution of linearly polarized gluons inside a large nucleus*, *Phys. Rev. D* **84** (2011) 051503 [arXiv:1105.1991] [INSPIRE].

[58] T. Altinoluk, C. Marquet and P. Taels, *Low-x improved TMD approach to the lepto- and hadroproduction of a heavy-quark pair*, *JHEP* **06** (2021) 085 [arXiv:2103.14495] [INSPIRE].

[59] F. Dominguez, B.-W. Xiao and F. Yuan, *k_t-factorization for hard processes in nuclei*, *Phys. Rev. Lett.* **106** (2011) 022301 [arXiv:1009.2141] [INSPIRE].

[60] F. Dominguez, C. Marquet, B.-W. Xiao and F. Yuan, *Universality of unintegrated gluon distributions at small x*, *Phys. Rev. D* **83** (2011) 105005 [arXiv:1101.0715] [INSPIRE].

[61] P.J. Mulders and J. Rodrigues, *Transverse momentum dependence in gluon distribution and fragmentation functions*, *Phys. Rev. D* **63** (2001) 094021 [hep-ph/0009343] [INSPIRE].

[62] S. Meissner, A. Metz and K. Goeke, *Relations between generalized and transverse momentum dependent parton distributions*, *Phys. Rev. D* **76** (2007) 034002 [hep-ph/0703176] [INSPIRE].

[63] F. Dominguez, J.-W. Qiu, B.-W. Xiao and F. Yuan, *On the linearly polarized gluon distributions in the color dipole model*, *Phys. Rev. D* **85** (2012) 045003 [arXiv:1109.6293] [INSPIRE].

[64] E. Akcakaya, A. Schäfer and J. Zhou, *Azimuthal asymmetries for quark pair production in pA collisions*, *Phys. Rev. D* **87** (2013) 054010 [arXiv:1208.4965] [INSPIRE].

[65] A. Dumitru, T. Lappi and V. Skokov, *Distribution of linearly polarized gluons and elliptic azimuthal anisotropy in deep inelastic scattering dijet production at high energy*, *Phys. Rev. Lett.* **115** (2015) 252301 [arXiv:1508.04438] [INSPIRE].

[66] C. Marquet, E. Petreska and C. Roiesnel, *Transverse-momentum-dependent gluon distributions from JIMWLK evolution*, *JHEP* **10** (2016) 065 [arXiv:1608.02577] [INSPIRE].

[67] C. Marquet, C. Roiesnel and P. Taels, *Linearly polarized small-x gluons in forward heavy-quark pair production*, *Phys. Rev. D* **97** (2018) 014004 [arXiv:1710.05698] [INSPIRE].

[68] T. Altinoluk, R. Boussarie, C. Marquet and P. Taels, *TMD factorization for dijets + photon production from the dilute-dense CGC framework*, *JHEP* **07** (2019) 079 [arXiv:1810.11273] [INSPIRE].

[69] T. Altinoluk, R. Boussarie, C. Marquet and P. Taels, *Photoproduction of three jets in the CGC: gluon TMDs and dilute limit*, *JHEP* **07** (2020) 143 [arXiv:2001.00765] [INSPIRE].

[70] M. Bury, P. Kotko and K. Kutak, *TMD gluon distributions for multiparton processes*, *Eur. Phys. J. C* **79** (2019) 152 [arXiv:1809.08968] [INSPIRE].

[71] P. Kotko, K. Kutak, C. Marquet, E. Petreska, S. Sapeta and A. van Hameren, *Improved TMD factorization for forward dijet production in dilute-dense hadronic collisions*, *JHEP* **09** (2015) 106 [arXiv:1503.03421] [INSPIRE].

[72] A. van Hameren, P. Kotko, K. Kutak, C. Marquet, E. Petreska and S. Sapeta, *Forward di-jet production in p+Pb collisions in the small-x improved TMD factorization framework*, *JHEP* **12** (2016) 034 [*Erratum ibid.* **02** (2019) 158] [arXiv:1607.03121] [INSPIRE].

[73] T. Altinoluk, R. Boussarie and P. Kotko, *Interplay of the CGC and TMD frameworks to all orders in kinematic twist*, *JHEP* **05** (2019) 156 [arXiv:1901.01175] [INSPIRE].

[74] T. Altinoluk and R. Boussarie, *Low x physics as an infinite twist (G)TMD framework: unravelling the origins of saturation*, *JHEP* **10** (2019) 208 [arXiv:1902.07930] [INSPIRE].

JHEP10(2022)184

[75] R. Boussarie and Y. Mehtar-Tani, *Gauge invariance of transverse momentum dependent distributions at small x*, *Phys. Rev. D* **103** (2021) 094012 [arXiv:2001.06449] [INSPIRE].

[76] A. van Hameren, P. Kotko, K. Kutak, S. Sapeta and E. Żarów, *Probing gluon number density with electron-dijet correlations at EIC*, *Eur. Phys. J. C* **81** (2021) 741 [arXiv:2106.13964] [INSPIRE].

[77] R. Boussarie, H. Mäntysaari, F. Salazar and B. Schenke, *The importance of kinematic twists and genuine saturation effects in dijet production at the Electron-Ion Collider*, *JHEP* **09** (2021) 178 [arXiv:2106.11301] [INSPIRE].

[78] J.B. Kogut and D.E. Soper, *Quantum electrodynamics in the infinite momentum frame*, *Phys. Rev. D* **1** (1970) 2901 [INSPIRE].

[79] J.D. Bjorken, J.B. Kogut and D.E. Soper, *Quantum electrodynamics at infinite momentum: scattering from an external field*, *Phys. Rev. D* **3** (1971) 1382 [INSPIRE].

[80] S.J. Brodsky, H.-C. Pauli and S.S. Pinsky, *Quantum chromodynamics and other field theories on the light cone*, *Phys. Rept.* **301** (1998) 299 [hep-ph/9705477] [INSPIRE].

[81] A. Accardi et al., *Electron Ion Collider: the next QCD frontier. Understanding the glue that binds us all*, *Eur. Phys. J. A* **52** (2016) 268 [arXiv:1212.1701] [INSPIRE].

[82] LHeC and FCC-he Study Group collaborations, *The Large Hadron-Electron Collider at the HL-LHC*, *J. Phys. G* **48** (2021) 110501 [arXiv:2007.14491] [INSPIRE].

[83] P. Caucal, F. Salazar and R. Venugopalan, *Dijet impact factor in DIS at next-to-leading order in the color glass condensate*, *JHEP* **11** (2021) 222 [arXiv:2108.06347] [INSPIRE].

[84] P. Sun, C.P. Yuan and F. Yuan, *Soft gluon resummations in dijet azimuthal angular correlations in hadronic collisions*, *Phys. Rev. Lett.* **113** (2014) 232001 [arXiv:1405.1105] [INSPIRE].

[85] P. Sun, C.P. Yuan and F. Yuan, *Transverse momentum resummation for dijet correlation in hadronic collisions*, *Phys. Rev. D* **92** (2015) 094007 [arXiv:1506.06170] [INSPIRE].

[86] M. Ciafaloni, *Coherence effects in initial jets at small Q^2/s*, *Nucl. Phys. B* **296** (1988) 49 [INSPIRE].

[87] B. Andersson, G. Gustafson and J. Samuelsson, *The linked dipole chain model for DIS*, *Nucl. Phys. B* **467** (1996) 443 [INSPIRE].

[88] J. Kwiecinski, A.D. Martin and P.J. Sutton, *Constraints on gluon evolution at small x*, *Z. Phys. C* **71** (1996) 585 [hep-ph/9602320] [INSPIRE].

[89] G.P. Salam, *A resummation of large subleading corrections at small x*, *JHEP* **07** (1998) 019 [hep-ph/9806482] [INSPIRE].

[90] L. Motyka and A.M. Stasto, *Exact kinematics in the small x evolution of the color dipole and gluon cascade*, *Phys. Rev. D* **79** (2009) 085016 [arXiv:0901.4949] [INSPIRE].

[91] G. Beuf, *Improving the kinematics for low-x QCD evolution equations in coordinate space*, *Phys. Rev. D* **89** (2014) 074039 [arXiv:1401.0313] [INSPIRE].

[92] E. Iancu, J.D. Madrigal, A.H. Mueller, G. Soyez and D.N. Triantafyllopoulos, *Resumming double logarithms in the QCD evolution of color dipoles*, *Phys. Lett. B* **744** (2015) 293 [arXiv:1502.05642] [INSPIRE].

JHEP10(2022)184

[93] B. Ducloué, E. Iancu, A.H. Mueller, G. Soyez and D.N. Triantafyllopoulos, *Non-linear evolution in QCD at high-energy beyond leading order*, *JHEP* **04** (2019) 081 [arXiv:1902.06637] [INSPIRE].

[94] Y. Hatta and E. Iancu, *Collinearly improved JIMWLK evolution in Langevin form*, *JHEP* **08** (2016) 083 [arXiv:1606.03269] [INSPIRE].

[95] G.A. Chirilli, B.-W. Xiao and F. Yuan, *One-loop factorization for inclusive hadron production in pA collisions in the saturation formalism*, *Phys. Rev. Lett.* **108** (2012) 122301 [arXiv:1112.1061] [INSPIRE].

[96] G.A. Chirilli, B.-W. Xiao and F. Yuan, *Inclusive hadron productions in pA collisions*, *Phys. Rev. D* **86** (2012) 054005 [arXiv:1203.6139] [INSPIRE].

[97] I. Balitsky and G.A. Chirilli, *Photon impact factor in the next-to-leading order*, *Phys. Rev. D* **83** (2011) 031502 [arXiv:1009.4729] [INSPIRE].

[98] I. Balitsky and G.A. Chirilli, *Photon impact factor and k_T-factorization for DIS in the next-to-leading order*, *Phys. Rev. D* **87** (2013) 014013 [arXiv:1207.3844] [INSPIRE].

[99] G. Beuf, *NLO corrections for the dipole factorization of DIS structure functions at low x*, *Phys. Rev. D* **85** (2012) 034039 [arXiv:1112.4501] [INSPIRE].

[100] G. Beuf, *Dipole factorization for DIS at NLO: loop correction to the $\gamma^*_{T,L} \to q\bar{q}$ light-front wave functions*, *Phys. Rev. D* **94** (2016) 054016 [arXiv:1606.00777] [INSPIRE].

[101] G. Beuf, *Dipole factorization for DIS at NLO: combining the $q\bar{q}$ and $q\bar{q}g$ contributions*, *Phys. Rev. D* **96** (2017) 074033 [arXiv:1708.06557] [INSPIRE].

[102] H. Hänninen, T. Lappi and R. Paatelainen, *One-loop corrections to light cone wave functions: the dipole picture DIS cross section*, *Annals Phys.* **393** (2018) 358 [arXiv:1711.08207] [INSPIRE].

[103] G. Beuf, T. Lappi and R. Paatelainen, *Massive quarks in NLO dipole factorization for DIS: longitudinal photon*, *Phys. Rev. D* **104** (2021) 056032 [arXiv:2103.14549] [INSPIRE].

[104] G. Beuf, T. Lappi and R. Paatelainen, *Massive quarks at one loop in the dipole picture of deep inelastic scattering*, *Phys. Rev. Lett.* **129** (2022) 072001 [arXiv:2112.03158] [INSPIRE].

[105] G. Beuf, T. Lappi and R. Paatelainen, *Massive quarks in NLO dipole factorization for DIS: transverse photon*, *Phys. Rev. D* **106** (2022) 034013 [arXiv:2204.02486] [INSPIRE].

[106] R. Boussarie, A.V. Grabovsky, D.Y. Ivanov, L. Szymanowski and S. Wallon, *Next-to-leading order computation of exclusive diffractive light vector meson production in a saturation framework*, *Phys. Rev. Lett.* **119** (2017) 072002 [arXiv:1612.08026] [INSPIRE].

[107] H. Mäntysaari and J. Penttala, *Exclusive production of light vector mesons at next-to-leading order in the dipole picture*, *Phys. Rev. D* **105** (2022) 114038 [arXiv:2203.16911] [INSPIRE].

[108] H. Mäntysaari and J. Penttala, *Exclusive heavy vector meson production at next-to-leading order in the dipole picture*, *Phys. Lett. B* **823** (2021) 136723 [arXiv:2104.02349] [INSPIRE].

[109] K. Roy and R. Venugopalan, *NLO impact factor for inclusive photon + dijet production in e+A DIS at small x*, *Phys. Rev. D* **101** (2020) 034028 [arXiv:1911.04530] [INSPIRE].

[110] R. Boussarie, A.V. Grabovsky, L. Szymanowski and S. Wallon, *On the one loop $\gamma^{(*)} \to q\bar{q}$ impact factor and the exclusive diffractive cross sections for the production of two or three jets*, *JHEP* **11** (2016) 149 [arXiv:1606.00419] [INSPIRE].

JHEP10(2022)184

[111] I. Balitsky and G.A. Chirilli, *Rapidity evolution of Wilson lines at the next-to-leading order*, *Phys. Rev. D* **88** (2013) 111501 [arXiv:1309.7644] [INSPIRE].

[112] A. Kovner, M. Lublinsky and Y. Mulian, *Jalilian-Marian, Iancu, McLerran, Weigert, Leonidov, Kovner evolution at next to leading order*, *Phys. Rev. D* **89** (2014) 061704 [arXiv:1310.0378] [INSPIRE].

[113] A. Kovner, M. Lublinsky and Y. Mulian, *NLO JIMWLK evolution unabridged*, *JHEP* **08** (2014) 114 [arXiv:1405.0418] [INSPIRE].

[114] M. Lublinsky and Y. Mulian, *High energy QCD at NLO: from light-cone wave function to JIMWLK evolution*, *JHEP* **05** (2017) 097 [arXiv:1610.03453] [INSPIRE].

[115] A.H. Mueller, *Small x behavior and parton saturation: a QCD model*, *Nucl. Phys. B* **335** (1990) 115 [INSPIRE].

[116] N.N. Nikolaev and B.G. Zakharov, *Color transparency and scaling properties of nuclear shadowing in deep inelastic scattering*, *Z. Phys. C* **49** (1991) 607 [INSPIRE].

[117] F. Dominguez, A.H. Mueller, S. Munier and B.-W. Xiao, *On the small-x evolution of the color quadrupole and the Weizsäcker-Williams gluon distribution*, *Phys. Lett. B* **705** (2011) 106 [arXiv:1108.1752] [INSPIRE].

[118] Y.L. Dokshitzer, G.D. Leder, S. Moretti and B.R. Webber, *Better jet clustering algorithms*, *JHEP* **08** (1997) 001 [hep-ph/9707323] [INSPIRE].

[119] M. Wobisch and T. Wengler, *Hadronization corrections to jet cross-sections in deep inelastic scattering*, in *Workshop on Monte Carlo generators for HERA physics (plenary starting meeting)*, (1998), p. 270 [hep-ph/9907280] [INSPIRE].

[120] F. Salazar, *Dijet production in DIS at one-loop in the CGC*, seminar at the University of Jyväskylä, https://indico.cern.ch/event/1121597/, Jyväskylä, Finland, March 2022.

[121] R.F. del Castillo, M.G. Echevarria, Y. Makris and I. Scimemi, *TMD factorization for dijet and heavy-meson pair in DIS*, *JHEP* **01** (2021) 088 [arXiv:2008.07531] [INSPIRE].

[122] R.F. del Castillo, M.G. Echevarria, Y. Makris and I. Scimemi, *Transverse momentum dependent distributions in dijet and heavy hadron pair production at EIC*, *JHEP* **03** (2022) 047 [arXiv:2111.03703] [INSPIRE].

JHEP10(2022)184